Vrije Universiteit Brussel

Multimodal Semiconductor Ring Lasers: An Analytical Study

Proefschrift ingediend tot het behalen van de academische graad van

Burgerlijk Elektrotechnisch Ingenieur

Lennert Appeltant

Promotor: Prof. Dr. Jan Danckaert

Advisors: Ir. Philippe Tassin, Dr. Ir. Guy Van der Sande

Faculteit Ingenieurswetenschappen
Vakgroep Toegepaste Natuurkunde en Fotonica

Juni 2008

Multimodal Semiconductor Ring Lasers:
An Analytical Study

Lennert Appeltant
Vrije Universiteit Brussel, Faculteit Ingenieurswetenschappen
Vakgroep Toegepaste Natuurkunde en Fotonica

Proefschrift ingediend tot het behalen van de academische graad van
Burgerlijk Elektrotechnisch Ingenieur

Promotor: Prof. Dr. Jan Danckaert
Advisors: Ir. Philippe Tassin, Dr. Ir. Guy Van der Sande
Jury members: Prof. Dr. Ir. Ronald Van Loon, Prof. Dr. Ir. Geert Morthier,
Prof. Dr. Ir. Johan Schoukens, Ir. Philippe Tassin, Ir. Lendert Gelens

This document was typeset with LaTeX 2_ε

Acknowledgments

Writing an acknowledgement. . . How can I fulfil this job without forgetting someone? So many interested people asked me again and again how my thesis work was progressing. It was not always easy to explain that once again the simulation did not work or that I had spent the entire academic year on studying one set of equations.

Although in this time of electronic highways, it should be possible to solve every problem from behind your PC, this thesis work especially taught me that real progress is made when someone directly speaks to you and explains what you have been doing wrong this time. Philippe, I would warmly like to thank you, not only for the detailed corrections of the texts, but also for your willingness to extensively answer my questions, again and again. Guy, I also really appreciate what you did, as well the reading of my preliminary versions, as guiding me through the mathematical challenges. Lendert, you too knew that whenever my simulations gave anything but the correct result, it would not take me long to hurry to your office to ask for help. Stefano Beri, I would like to thank you, not only for the scientific discussions, but also for lending me your chair countless times. Working in team on 'the ninth floor' has been very valuable on the educational level, but I especially appreciated the relaxed atmosphere. I thank you all for your enthusiasm, your support, especially when things were critical. I appreciated the humour with which you pointed out my photonic stupidities.

Thank you Kevin, my Photoshop-hero, for helping me with the cover of this work and also Michael Peeters, for letting me steal your latex code for the thesis template. David, you have earned a mentioning in this acknowledgment for providing me the raw materials for the production of multiple copies.

This moment also seems appropriate to thank all my fellow students of the past years for the contacts we had. They were not always scientifically inspired, but that does not imply I obtained less wisdom from them. Thank you Arnout, Stefaan and all the Erasmus Mundus people for keeping the spirit alive in the multimedia room, even when we worked there until late in the evening.

I want to express my gratitude to all my professors of the past years, who, by their different points of view, have led me to studying photonics. My sincerest thanks go to Prof. Dr. Irina Veretennicoff, who has made an important contribution to this process.

Finally, I would like to explicitly thank my promotor, Prof. Dr. Jan Danckaert, for supporting me with inspiration and feedback. He created the opportunities to realise this thesis work. In particular the freedom of choice and work have allowed me to accomplish what I had in mind.

Lennert Appeltant
Brussels, Belgium
June 2008

Summary

Semiconductor ring lasers (SRLs) are lasers with a cavity consisting of a circular waveguide. Due to their rotational symmetry, every mode propagating in the cavity has a counterpart propagating in the opposite direction. Because of nonlinear interaction, while one directional mode is lasing, the mode in the other direction can be largely suppressed. This regime shows a bistability between the directional modes and is therefore of great interest due to its potential use in optical information storage. This, combined with the planar structure of the device, renders SRLs very suitable for implementation in optical integrated circuits.

Here we pursue an analytical study of SRLs with two longitudinal modes, each consisting of two directional modes. First, we derive a set of rate equations from first principles, governing the dynamical behaviour. This model yields good results, but is very involved, making the interpretation not straightforward. We have solved this by reducing the original set of nine real equations to a new set of five expressions, using asymptotic methods. This reduction is based on the different time scales present in the laser system and eliminates the relatively fast relaxation oscillations.
We compare numerical solutions of the reduced model to those of the full model and in this way we validate the performed transformations and approximations. Subsequently, we determine analytically the steady-state solutions of the reduced model. These solutions describe which of the two longitudinal modes is lasing and whether these modes lase in one or both directions of propagation.

Since there are many stationary solutions, their stability determines the features of the output power as a function of the current. By performing a linear stability analysis, we calculate the bifurcation currents of the steady-state solutions. For simpler steady states, we are able to perform the stability analysis in an analytical way and we give the bifurcation currents as a function of the geometrical and dynamical parameters of the laser. The stability of the general solution is too involved to determine, but can be found numerically. By applying a parameter sweep we obtain a visual representation.

The approach followed in this master thesis provides a solid tool to explain and predict the dynamical behaviour of SRLs given their operating conditions.

Samenvatting

Halfgeleider ringlasers (HRL's) zijn lasers met een caviteit die bestaat uit een circulaire golfgeleider. Vanwege hun rotationele symmetrie heeft elke mode die zich voortplant in de caviteit een tegenhanger die zich voortplant in de tegengestelde richting. Door niet-lineaire interactie, kan terwijl een directionele mode aan het lasen is, de mode in de andere richting sterk onderdrukt worden. Dit regime vertoont een bistabiliteit tussen de directionele modes en is daarom van groot belang gezien het potentieel om dit te gebruiken voor optische informatie-opslag. Dit, gecombineerd met de planaire structuur van het toestel, maakt HRL's zeer geschikt voor implementatie in optische, geïntegreerde circuits.

Hier zullen we ons toeleggen op een analytische studie van HRL's met twee longitudinale modes, elk bestaande uit twee directionele modes. Eerst leiden we een stel vergelijkingen af, vertrekkende van basisprincipes, die het dynamische gedrag bepalen. Dit model levert goede resultaten, maar is zeer complex, wat de interpretatie niet voor de hand liggend maakt. We hebben dit verholpen door de originele set van negen reële vergelijkingen te reduceren tot vijf uitdrukkingen, gebruik makende van asymptotische methoden. Deze reductie is gebaseerd op de verschillende tijdsschalen die aanwezig zijn in het lasersysteem en elimineert de relatief snelle relaxatie oscillaties. We vergelijken de numerieke resultaten van het gereduceerde model met die van het volledige model en op deze manier valideren we de uitgevoerde transformaties en benaderingen. Vervolgens zullen we analytisch de stationaire oplossingen van het gereduceerde model bepalen. Deze oplossingen beschrijven welke van de twee longitudinale modes aan het lasen is en of deze modes lasen in een enkele of in beide voortplantingsrichtingen.

Aangezien er vele oplossingen zijn voor het model is het hun stabiliteit die de eigenschappen van het uitgaande vermogen als functie van de stroom bepaalt. Door een lineaire stabiliteitsanalyse uit te voeren, kunnen we de bifurcatiestromen berekenen van de gevonden stationaire oplossingen. Voor meer eenvoudige stationaire toestanden zijn we in staat om de stabiliteitsanalyse op een analytische manier uit te voeren en de bifurcatiestromen als functie van de geometrische en dynamische parameters te beschrijven. De stabiliteit van de algemene oplossing is te complex om bepaald te worden, maar kan

numeriek teruggevonden worden. Door een parametersweep toe te passen, verkrijgen we een visuele voorstelling.

De aanpak die gevolgd wordt in deze master thesis, levert ons een bruikbare manier op om het dynamische gedrag van HRL's te verklaren en te voorspellen indien de werkingscondities gegeven zijn.

Résumé

Des lasers annulaires semi-conducteurs (LASs) sont des lasers avec une cavité qui consiste en un guide d'onde circulaire. A cause de leur symétrie rotationnelle, chaque mode qui se reproduit dans la cavité a une contrepartie qui se reproduit dans la direction opposée. En raison de l' interaction non linéaire, pendant qu'un mode directionnel lase, le mode qui va dans l'autre direction peut être fortement réprimé. Ce régime présente une bistabilité entre les modes directionnels et est par conséquent d'une très grande importance vu la possibilité d'utiliser ce potentiel pour le stockage d'information optique. Ceci, en combinaison avec la structure planaire de cet appareil, rend les LASs très appropriés pour l'implémentation dans des circuits optiques intégrés.

Nous nous appliquerons ici à l'étude analytique des LASs avec deux modes longitudinaux, chacun consistant en deux modes directionnels. D'abord nous dérivons un ensemble d' équations déterminant le comportement dynamique en partant des principes de base. Ce modèle produit de bons résultats, mais il est très complexe, ce qui fait que l'interprétation n'est pas évidente. Nous avons remédié à ce problème en réduisant le set original de neuf équations réelles à un nouveau set de cinq expressions, en utilisant des méthodes asymptotiques. Cette réduction est basée sur différentes échelles temporelles présentes dans le système laser qui élimine les oscillations relaxantes relativement rapides. Nous comparons les résultats numériques du modèle réduit à ceux du modèle complet et de cette façon nous validons les transformations exécutées et les approximations. Ensuite nous déterminons d'une façon analytique les solutions stationnaires du modèle réduit. Ces solutions décrivent quel des deux modes longitudinaux lase et si ce mode lase dans une seule ou dans les deux directions de propagation.

Etant donné qu'il y a beaucoup de solutions stationnaires, c'est leur stabilité qui détermine les propriétés de la capacité sortante comme fonction du courant. En appliquant une analyse de stabilité linéaire nous pouvons calculer les courants de bifurcation des solutions stationnaires trouvées. Pour des 'steady states' plus simples nous pouvons exécuter l'analyse de stabilité d'une façon analytique et décrire les courants de bifurcation comme fonction des paramètres géométriques et dynamiques du laser. La stabilité de la solution générale est trop complexe à déterminer, mais peut être rétablie

numériquement. En utilisant un 'sweep' paramétrique nous obtenons une représentation visuelle.

L'approche utilisée dans cette thèse de master nous procure une procédure fiable afin d'expliquer et de prédire le comportement dynamique des LASs partant des conditions d'opération connues.

Contents

Chapter 1

Introduction

After a brief introduction on the history and basic principles of lasers, with special attention given to *semiconductor lasers*, we focus on those having a ring-shaped optical cavity. These devices have some interesting properties that render them very suitable as candidates for use in photonic integrated circuits. This first chapter will concentrate on the phenomenologic description of the construction and fabrication of semiconductor ring lasers. Furthermore, the operation of the single mode semiconductor ring laser will be reviewed.

1.1

Short History and Basic Principles of Lasers

The word "laser" is an acronym for Light Amplification by Stimulated Emission of Radiation. Typically, the light emitted by a laser is a narrow monochromatic beam with a well-defined wavelength. The coherence length of the light is significantly longer than for a conventional light source such as a light bulb. The first to describe the phenomenon of stimulated emission was Albert Einstein in 1917 [1, 2]. Besides absorption and spontaneous emission, he has shown that stimulated emission is a mechanism that takes place when light interacts with matter. Unfortunately, it took over 30 years for people to realise that this implied that coherent light amplification is made possible with population inversion. The first laser to work was a pulsing ruby laser, made by Theodore Maiman at Hughes Research Laboratories in June 1960. Since, many variations and improvements have been realised. Two essential ingredients have to be present in order to achieve laser action:

- Optical gain. This can be achieved in what is called an active medium. The gain medium is a material (gas, liquid, solid or free electrons) that allows for stimulated emission to occur. Electronic transitions must take place emitting photons with a specific frequency. Population inversion must be present to make stimulated emission dominant over absorption, i.e., more carriers have to be present at the

higher energy levels than at the lower ones. To achieve this, pumping of the gain medium is necessary. This can be done by optical injection with another laser or a flash lamp or by electrical injection.

- The generated light must be partially confined in an optical cavity. In its simplest form, the cavity consists of two mirrors arranged such that light bounces back and forth, each time passing again through the gain medium. To couple the light to the outside world, one of the two mirrors should be partially transparent.

The development of lasers started with the creation of the maser, which is an acronym for Microwave Amplification by Stimulated Emission of Radiation. Charles H. Townes was the first one to build such a maser in 1954. One of the biggest problems in this early design was the fact that continuous output could not be achieved. Indeed, we know now that a system with more than two energy levels is required in order to maintain population inversion. Nikolai Basov and Alexander Prokhorov from the USSR [3] first developed this idea and were rewarded for it with the 1964 Nobel Prize in Physics, together with Charles H. Townes. It was Townes who, along with Arthur Schawlow, [4] suggested in December 1958 the first design for an optical maser or, as it was renamed later, a laser. As mentioned before, Theodore Maiman realised the first real laser in 1960 [5]. Just before the end of 1960, the first gas laser, a He-Ne laser, was made by Ali Javan, William Bennet, and Donald Herriot.
Although Basov and Javan were the firsts to propose the concept of a semiconductor laser diode, it was first demonstrated by Robert N. Hall in 1962. Hall's device was made of gallium arsenide and emitted at 850 nm in the near-infrared region of the spectrum. Later, semiconductor lasers emitting in the visible spectrum were demonstrated by Nick Holonyak, Jr. It took many years, until 1970, when Zhores Alferov in the USSR and Izuo Hayashi and Morton Panish of Bell Telephone Laboratories in the USA independently developed laser diodes continuously operating at room temperature, using the hetero-junction structure. Alferov [6], together with Herbert Kroemer [7], were rewarded the 2000 Nobel Prize in Physics.
Lasers have become a multi-billion dollar industry. They are the vital components in telecommunications, optical storage devices such as compact disc and DVD players, but are also present in e.g., bar code readers, laser printers and laser pointers. Besides their use in industry for cutting steel and other metals and for inscribing patterns, lasers are also commonly used in various fields in science. Techniques such as spectroscopy are based on the fact that you have control or at least knowledge about a well-defined wavelength. Both military and medicine make use of lasers, respectively for target identification and illumination for weapons delivery and for surgery or cosmetic applications. Semiconductor lasers represent an important share of this laser industry and are omnipresent in daily life. They have been and are constructed in all kinds of shapes and dimensions and will undoubtedly continue to play an important role in further technological developments.

1.2 Semiconductor Lasers

1.2.1 Semiconductors as Optical Gain Medium

Generally, lasers are classified according to their active material. Examples are gas lasers, solid-state lasers, semiconductor lasers, dimer lasers... In semiconductor lasers, a p-n junction acts as a photon source. This system differs from the pure atomic system found in gas lasers, since the energy levels are closely spaced in bands, rather than well defined levels. The shape of the bands is determined by the material and the crystal lattice structure and can be represented in an E-k diagramma as in Figure 1.1. This graph gives the energy of the carriers as a function of their crystal wave number. The upper band represents the conduction band, while the lower one is called the valence band. These bands indicate the allowed energy states for the carriers. At room temperature, the lower states of the conduction band are occupied with electrons (denoted by circles in Figure 1.1) and the higher states of the valence band are occupied by holes (denoted by discs in Figure 1.1). The energies between the conduction and the valence band are forbidden and constitute the bandgap, which is defined as the energy difference between the minimum of the conduction band and the maximum of the valence band. In the case where minimum and maximum correspond to the same crystal wave number, we speak of a direct bandgap material, otherwise it is called indirect. Materials such as silicon are indirect, while gallium arsenide has a direct bandgap.

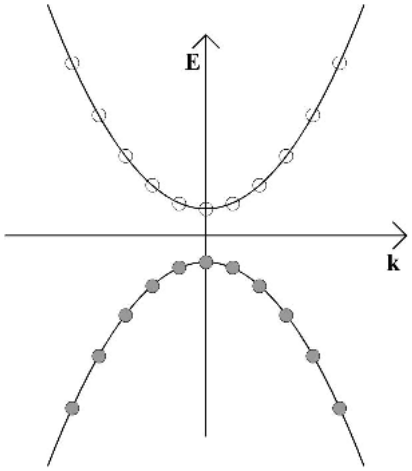

Figure 1.1: E-k diagramma of a semiconductor with direct bandgap. The upper band is called the conduction band and the lower one is called the valence band. Electrons are represented by circles and holes by discs. (Picture from Ref. [8])

1.2.2 Operation of a Semiconductor Laser

The most important structure in the semiconductor active material is the p-n junction, depicted in Figure 1.2. The junction consists of two doped semiconductors that are put next to each other. One of them is doped with impurities that lead to an excess of electrons and is referred to as the n-doped material. The other one, which is called the p-doped material, is doped with impurities that give rise to an excess of holes. In the p-region holes are the majority carriers and in the n-region electrons are the majority carriers. In the p-region, the Fermi level is at a different level than in the n-region. When the two differently doped materials are brought in contact with each other, the energy bands will bend, because, in Figure 1.2(a), the Fermi level must be constant all over the p-n junction. In Figure 1.2(a), the Fermi level is denoted by E_F. On the interface between both regions there is a neutral zone, which is called the depletion area. Without a bias voltage, the width of the depletion area is W_d. However, when a forward bias is applied across the junction, as in Figure 1.2(b), the density of the carriers, both n- and p-type, will increase around the junction. Holes from the p-doped zone will be injected into the depletion area and the same happens to the electrons from the n-doped zone. When an electron and a hole are present in the same region, they will annihilate each other or recombine. To obey the law of energy conservation, a phonon or photon must be emitted. Indirect bandgap materials have the property that the minimum of their

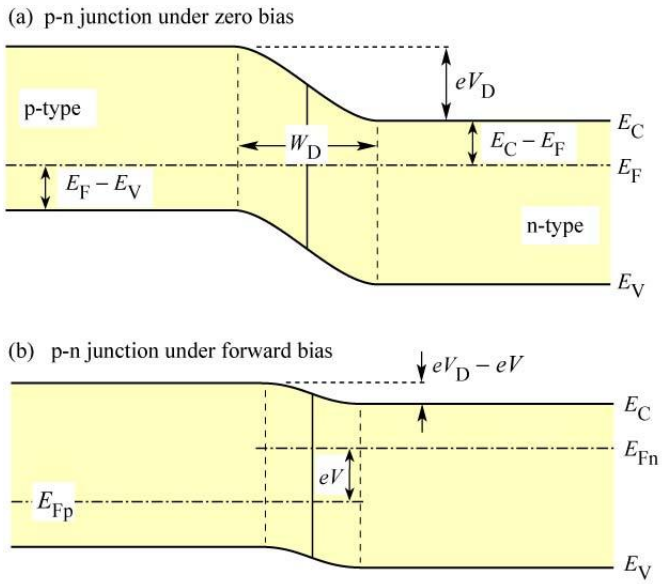

Figure 1.2: Schematic representation of a p-n junction, with indication of the different energy levels. E_F represents the Fermi level, E_C the conduction band and E_V the valence band. (a) depicts the situation when no bias voltage is applied, while in (b) a forward voltage is applied (Picture from Ref. [9]).

conduction band corresponds to another momentum than the maximum of the valence band. When an electron undergoes a transition from conduction to valence band, the recombination of electrons and holes leads to a change in momentum. A photon cannot compensate this large change in momentum, so the energy will be used for the creation of a phonon, leading to dissipation and heating. On the other hand, when the semiconductor's bandgap is direct (e.g., III-V materials), there is no change in momentum and the energy change can lead to the emission of a photon.
An electron at a certain position in the conduction band has a finite lifetime. There is a certain probability that it decays to the valence band with emission of a photon. This process is called spontaneous emission. However, this is not sufficient to make the semiconductor lase. To explain lasing we need to introduce another effect: stimulated emission. Many electrons find themselves at a certain energy level in the conduction band. These positions are metastable, the electrons reside there, but even the slightest perturbation could cause them to decay suddenly. A photon with the right energy, e.g., created by spontaneous emission, will make the electron oscillate and this can be enough to leave the metastable state. It can be shown that the newly created photon has the same frequency as the incident one and the light is therefore monochromatic. Also, it has the same direction and phase, so it is coherent. This photon can stimulate in turn other carriers to decay and emit a photon. If the number of carriers is larger in the conduction band than in the valence band (population inversion), this process will repeat itself many times and lasing action will occur. To keep the medium in population inversion, a pump current is needed. The material will consume current and emit photons.
The next step to build a useful semiconductor laser is making sure that the generated light is confined. To guide the light, an optical waveguide is constructed near the p-n interface. At both ends of the waveguide, one needs to make sure that a significant part of the light is fed back into the cavity, such that the same photons can cause stimulated emission several times. Of course, the structures that cause the feedback will still allow some light to escape from the cavity. If the gain equals the losses (absorption in the cavity and incomplete reflection at the edges), lasing will occur.
Although the approach described above is correct, in practice there are some techniques that significantly improve the performance of the semiconductor laser. A first configuration is the double heterostructure. In these devices, a layer of low bandgap material is sandwiched between two high bandgap layers. In this way, the diffusion current, away from the active region, is limited. Because of the higher index of refraction of this new layer, an optical waveguide is created. Now both the electric and optical energy density have increased, pushing down the threshold current for lasing action. If the middle layer is made thin enough, it will restrict motion of carriers in the vertical direction and act as a quantum well. The energy of the carriers becomes quantised and the carriers are concentrated in discrete energy states that contribute to the laser action.

1.3 Semiconductor Ring Lasers

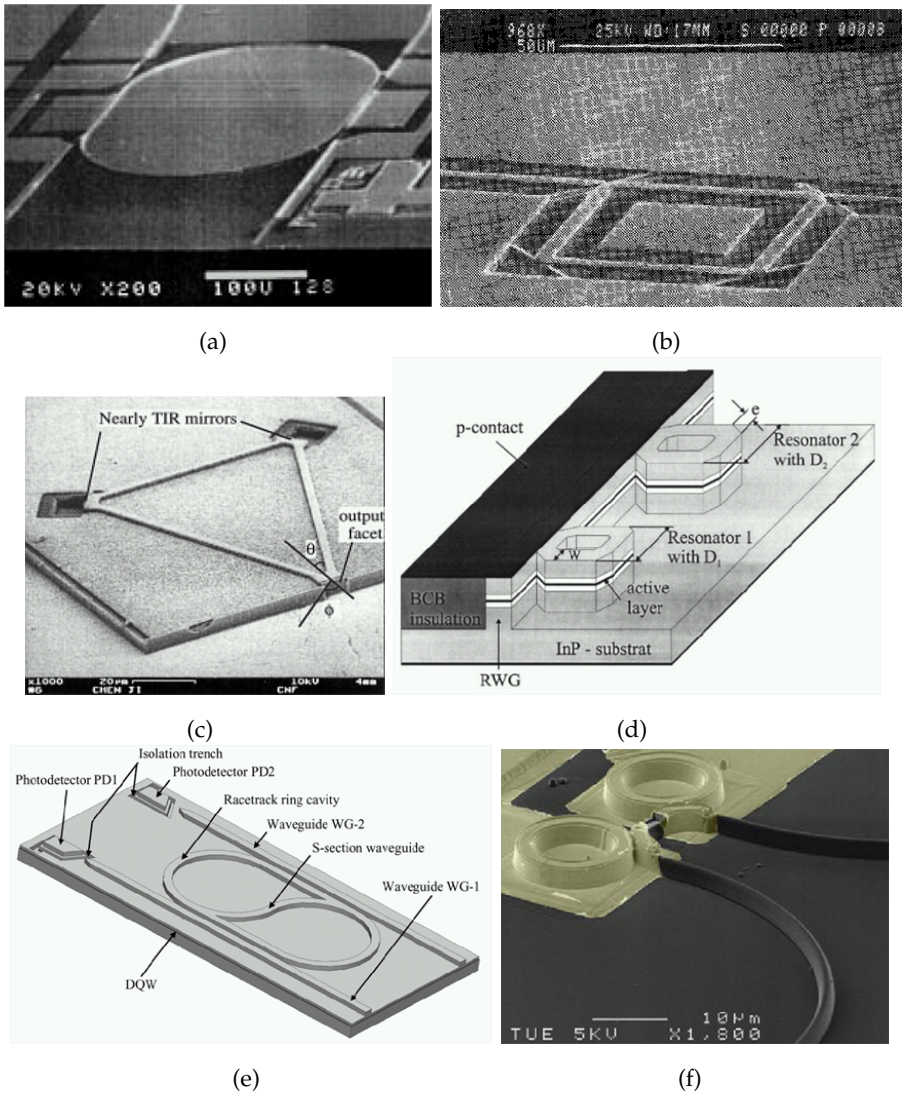

(a) (b) (c) (d) (e) (f)

Figure 1.3: Semiconductor ring laser are constructed in different shapes and configurations. (a) Racetrack [10], (b) Square [11], (c) Triangle [12], (d) Coupled microsquare [13], (e) S-shaped [14], (f) Coupled ring lasers [15]

This thesis work will concentrate on a specific kind of semiconductor lasers, namely semiconductor ring lasers, as the ones depicted in Figure 1.3. Such devices have first been demonstrated in 1980 by Andrew Shuh-Huei Liao and Shyh Wang [16]. Since, they have been in the centre of attention, because of their potential applications in

photonic integrated circuits. The basic structure of the ring laser includes a circular resonator and straight output waveguide. As a consequence of this structure there is no need for feedback reflectors, what makes it attractive for applications in integrated optics. Different cavity geometries can be used such as circular, race track, square or triangular, while making use of different waveguides [See Figure 1.3(a)-(f)]. One of their most important features is their high wavelength stability. In a ring-shaped cavity, the situation is totally different from the more common setup, the Fabry-Perot cavity. While in a Fabry-Perot cavity the light bounces back and forth between two mirrors, the light in a ring laser follows a closed trajectory. A very important consequence of this construction is the possibility for two counter-propagating modes to be present simultaneously. If the resonator is build by using only two mirrors, the light also travels in two directions, but both of them together form one mode. If there is a perturbation present in the forward traveling light it will move over to the backward traveling light after reflection. In a perfect ring resonator, there is in principle no direct coupling between the counter-propagating modes and they can coexist in the cavity. As we will explain later on in this chapter, there are multiple effects that do cause a coupling between counter-propagating modes, but still the situation is different from the Fabry-Perot case.

1.3.1 Geometry and Fabrication of Ring Lasers

The ring can be constructed in many ways. One possible way is by using a set of mirrors that guides the light around in a closed trajectory. This is true as long as there is somewhere in the setup an active medium to provide the gain. Another way is to use total internal reflection (TIR) [17]. Semiconductor ring laser dimensions can be fabricated at the sub-millimeter level. The ring lasers we are considering here are quantum well ring lasers. The schematic of the waveguide is given in Figure 1.4.

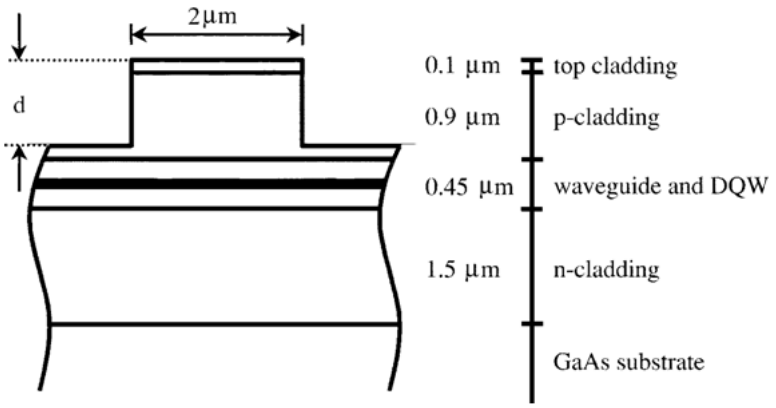

Figure 1.4: This figure depicts the profile of a heterostructure double quantum well semiconductor ring laser. The ring shape is etched into the upper two cladding layers (From Sorel *et al.* [18]).

Remember that the basic structure is a substrate with a p-n junction, so a p-cladding and an n-cladding on top of it. In Figure 1.4, a top cladding is present as well, to protect the entire structure from scratches, chemical substances, water... Between the p and n-cladding, one finds an extra waveguide layer, which is slightly differently doped in order to have another index of refraction. This layer is inserted for better confinement of the light that is generated at the interface of the p-n junction. A double quantum well layer is inserted to make sure that the energy states are concentrated around the desired levels. To define the ring shaped cavity it suffices to etch only into the top p-cladding layer (shallow etching [19]). This changes the index of refraction in that area sufficiently to assure guiding of the light. It is not necessary to etch all the way until the waveguide itself (deep etching [20]). Of course, the etching depth is a highly important factor that influences the characteristics of the laser. Another aspect is the radius of the ring cavity. A smaller radius of curvature leads to a smaller ring laser, with the obvious benefits for monolithic integration, but also requires new waveguide design. As the ring is smaller, there will be more bending losses.
Finally, we need to describe the output coupler, since some of the light inside the cavity needs to be coupled out of the cavity for external use. Because in a ring laser there is the possibility that two counter-propagating modes are present, the output coupler has two sides. One side will serve as a coupler for the clockwise mode and the other side will be a coupler to the outside world for the counter-clockwise mode. The coupler itself is basically a waveguide similar to the circular resonator, which is located in the near proximity of the resonator. Inside the ring, the waves are guided in the waveguide because of total internal reflection. This means that evanescent waves are present outside the circular waveguide. If the output coupler is close enough to the cavity, it will pick up the evanescent waves and couple light out of the ring laser to the outside world, e.g., a detector. However, the presence of the output coupler introduces an effect that influences the dynamics of the ring laser, backscattering. There are three kinds of backscattering. The first one is referred to as distributed backscattering. All over the cavity, parts of light are coupled into the counter-propagating mode, due to the imperfection of the waveguide. Second, a significant amount of light reflects at the output coupler itself. Finally, some light couples from the cavity into the output coupler. It propagates through the straight waveguide and reflects at the end facet. If this reflected light couples back into the cavity, it reinforces the counter-propagating mode. These effects signify that the output coupler can be a source of linear coupling between two modes. The best way to avoid this optical feedback through reflection is by slightly tilting the output coupler facets [18] as demonstrated in Figure 1.5.

1.3.2 Operation of a Single Mode Ring Laser

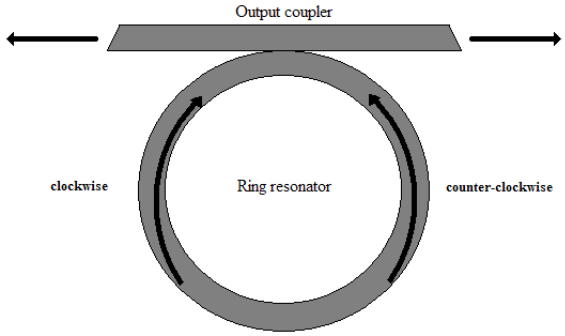

Figure 1.5: Representation of a semiconductor ring laser with circular cavity and straight output coupler. The end facets of the output coupler are tilted 5° to avoid optical feedback.

We now consider the case of a single mode semiconductor ring laser as depicted in Figure 1.5. When we speak of a single mode ring laser, the mode referred to is a longitudinal mode. In a single mode ring laser, two counter-propagating modes are present in the circular cavity, but both of them belong to the same longitudinal mode. So both modes have exactly the same frequency, but travel in opposite directions. The frequency of this light is determined by the fact that the phase difference that corresponds to one round trip in the cavity equals 2π. The modes interact with the active medium, but also with each other. There are two effects that couple the two modes with each other that we consider. First, there is the backscattering. As explained in the previous section, it provides a linear coupling between the two counter-propagating modes. Especially at low intensities this term will become important. Second, the process of gain saturation is responsible for nonlinear coupling. In any laser, and therefore also in a semiconductor ring laser, the carrier density increases with the pump current up to threshold, this is the point where the gain equals the losses. Once the threshold is reached and the device starts to lase, the carrier density remains constant. All extra carriers that are injected will recombine and emit photons. If the current is further increased, the amount of output power in the form of light will also increase linearly with the current. However, this relation between output power and pump current is not entirely correct, because gain saturation occurs. Not all extra carriers will instantly recombine and the carrier density will increase linearly with the pump current. The compression of the gain can be caused by spatial or spectral hole burning. The former is a result of the standing wave nature of the optical modes. Carriers are depleted faster at the crest of the wave, with a decrease in modal gain as a result. More important is spectral hole burning. This is due to the the fact that two modes with almost the same frequency will compete for the same carriers. Although these effects are small, they cause the slope of the P-I curve to change slightly, the higher the saturation, the

flatter the curve. At high intensities, saturation plays an important role. In ring lasers, an optical mode is not only saturated by itself, but also by the other mode, with the same frequency but a different direction of propagation. So the higher the intensity of one mode, the more its own gain as well as the gain of the other mode will be saturated.

1.3.3 Operating Regimes

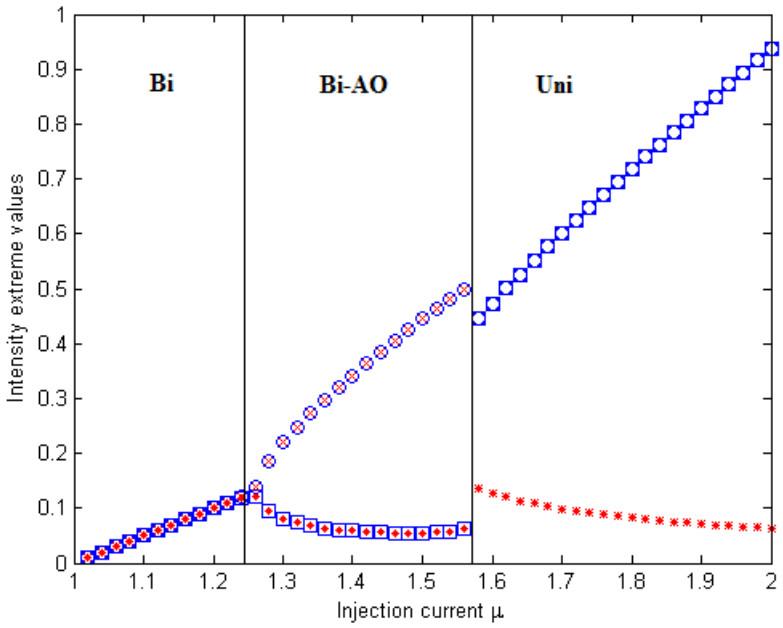

Figure 1.6: Simulated P-I curve of a single mode ring laser. The used model can be found in Eqs (2.104)-(2.106), with parameters defined in chapter 3: $K_d = 0.1631$, $K_c = 2.1939$, $S_0 = 2.5$, $C_0 = 5$ and $\alpha = 3.5$. In this plot, three distinct regimes are observed. The first (Bi), is called the bidirectional regime, next there is the bidirectional regime with alternate oscillations (Bi-AO) and finally there is the unidirectional regime (Uni). The maxima and minima of $|E_1|$ are denoted by open blue squares and circles, respectively. For the second mode, the maxima and minima of $|E_2|$ are denoted by red crosses and dots, respectively.

Later on in this work, a detailed study of the different regimes that can occur in a ring laser, will be presented. However, it is interesting to already mention them and give some explanations about their origin. We explained that there are two effects we should keep in mind, the backscattering and the gain saturation. In Figure 1.6, a simulated P-I curve is depicted, representing the behaviour of the modal intensities as a function of the pump current. The two counter-propagating modes are represented by two colours. For each mode both the minimum and the maximum values of the stationary output power

are plotted. One immediately notices the three regimes present in this current range. When the laser is at threshold (scaled pump current μ equals 1), the gain saturation is of almost no importance. Both modes begin to lase simultaneously and equal in strength. This is called the bidirectional regime. This situation seems logical, after all when one of the modes lases significantly stronger than the other, there will also be a greater amount of light that is coupled into the other direction, due to backscattering. When the current is further increased, the power of both modes also increases until a certain point, the first bifurcation point. A bifurcation occurs when a small, smooth change made to the parameter values (the bifurcation parameters) of a system, causes a sudden 'qualitative' or topological change in its dynamical behaviour [21]. When the pump current surpasses the first bifurcation current, the system is no longer in the bidirectional regime. Both the intensities will start to oscillate in time. The total output energy remains a constant for a certain current since both modes oscillate in perfect antiphase. When one mode has a maximum intensity, the other mode intensity reaches a minimum. If again the pump current is driven up, the oscillation frequency, which initially had a frequency of about 100MHz, decreases almost linearly [18]. This second regime is also called bidirectional, but with alternate oscillations. The same story continues until a new bifurcation point is reached. For currents beyond this second bifurcation point, the laser operates in the third regime, the unidirectional regime. There are no longer oscillations and one of the modes is partially or almost completely suppressed by the other. Yet, it is not a priori defined which of the two modes will be the dominant one and which will be suppressed. The situation is bistable and in case there is no external injection or asymmetry, noise will determine which mode dominates. The bistability can be exploited for optical switching, rendering ring lasers promising candidates for all-optical data processing. In Figures 1.7 and 1.8, time traces at certain currents in this P-I curve are depicted, one for the bidirectional regime and one for the bidirectional regime with alternate oscillations.

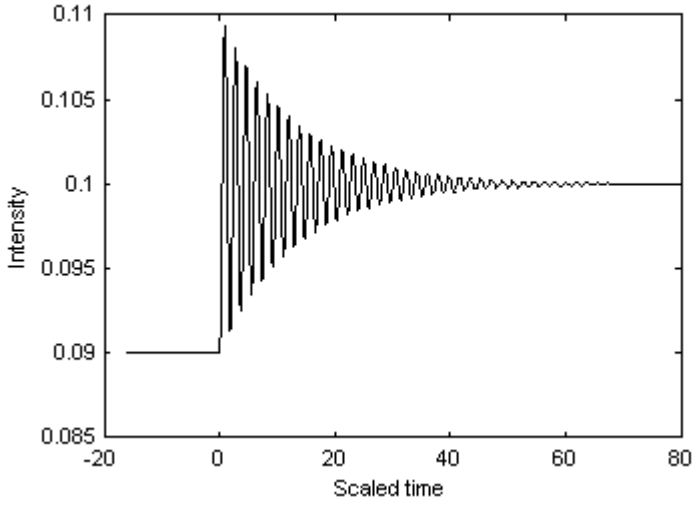

Figure 1.7: Timetrace at $\mu = 1.2$ for the intensity, considering the same parameters as the ones in Figure 1.6. This current is in the range of the bidirectional regime. The current for $t < 0$ equals 1.18. At $t = 0$, a current step is applied and the system starts to converge to a new steady-state value.

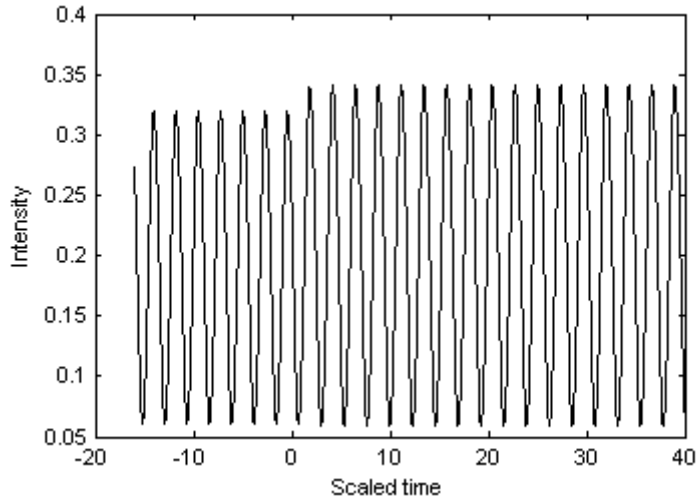

Figure 1.8: Timetrace at $\mu = 1.4$ for the intensity, considering the same parameters as the ones in Figure 1.6. This current is in the range of the bidirectional regime with alternate oscillations. The current for $t < 0$ equals 1.38. At $t = 0$, a current step is applied and the system starts to converge to a new steady-state value for the amplitude of the oscillations.

1.4 Contents of This Master Thesis

The following chapter will start from known physical laws and relations to deduce a rate equation model for the multimode operation of a semiconductor ring laser with two longitudinal modes, using various transformations and approximations. Some effects will be added phenomenologically, such as the saturation of the gain. Subsequently, this model will be nondimensionalised. The goal of chapter 3 is then to apply a reduction method on the obtained model, reducing the model from 9 real equations to 5. The new expressions will be far more suitable for interpretation and will even provide us some analytical expressions of the solutions. The most general solution is too complicated to be found analytically, but can be numerically represented by making use of a parameter sweep. In this model, fast dynamics will have been eliminated from the equations. Chapter 4 focuses on the study of the stability of the stationary solutions found in chapter 3. An in-depth linear stability analysis will supply us with enough information to be able to predict the appearance of certain areas of the P-I curve, once the parameters are given. The study of the multimode model and its stability will consist of both analytical and numerical calculations and the agreement between these two. Finally, some conclusions are drawn in chapter 5.

Chapter 2

Rate Equations for a Semiconductor Ring Laser with Two Longitudinal Modes

An exact description of the dynamical behaviour of semiconductor lasers requires a study of the electromagnetic fields in the laser cavity and of the gain medium using electromagnetics and quantum mechanics. To reduce the co;plexity of the problem, we will introduce rate equations, which describe the evolution in time of the optical field and the carrier density through a set of ordinary differential equations. They have proven to be successful in describing the steady-state behaviour and the dynamics of lasers on time scales slower than the cavity round trip time [22–24]. In order to derive the appropriate rate equations, we choose to apply a semiclassical approach by obtaining the field dynamics in a classical way and by describing the gain dynamics on a quantum mechanical level.

2.1 Cavity Configuration

A picture of a semiconductor ring cavity is depicted in Figure 2.1(a). A model of this cavity is given in Figure 2.1(b). Light waves are guided in a ring-shaped cavity and confined by total internal reflection. Part of the light is coupled into the output coupler, a straight waveguide in the near proximity of the ring cavity. At the two ends of this output coupler, small amounts of the light waves are reflected and coupled back into the cavity. For a bended waveguide, one should take into account the fact that bending losses appear in the cavity. The smaller the cavity dimensions, the smaller the radius of curvature and the higher the losses. However, in this study the bending losses are ignored since practical devices with extremely low bending losses can be achieved by well-designed ring shapes [25]. Therefore, we can model the cavity by the simplified

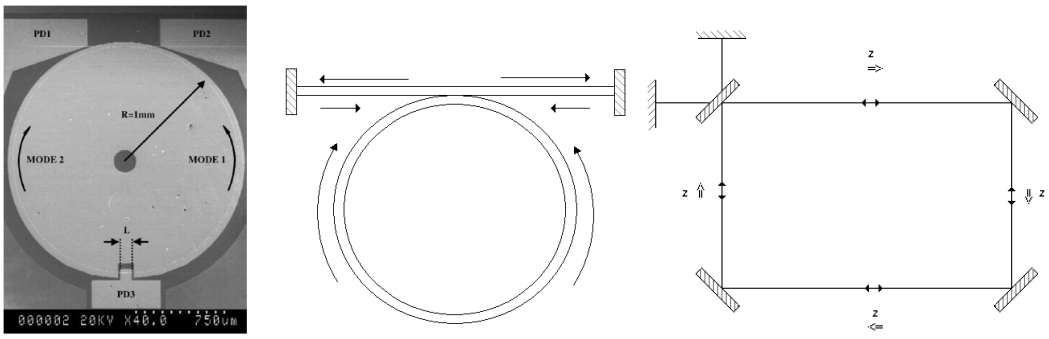

(a) (b) (c)

Figure 2.1: (a) A SEM micrograph of the semiconductor ring laser devices, with the layout of the ohmic contacts made to the structure. The radius of the ring cavity is 1 mm. Since the spacing between the ring cavity and the output coupler is about $1\mu m$, the evanescent coupling is 1% to 5% depending on the etching depth of the waveguides. The edges of the output waveguide are tilted at 5° to reduce the optical back reflection to 0.5% [18]. (b) Schematic representation of the ring laser, with two counter-propagating modes in the ring shape cavity. (c) Ring cavity with four mirrors. One mirror is partially reflective. The two mirrors outside of the ring allow for the linear coupling from a mode in one direction to a mode in the opposite direction. The total length of the cavity equals L.

scheme of Figure 2.1(c), which consists of a closed trajectory between four mirrors. The mirror at the top left corner is only partially reflective, while the other three are assumed perfect and will have no effect on the field dynamics. Because the top left mirror is only partially reflective, a part of the resonating light wave is coupled out of the cavity to the output coupler. The two additional mirrors have the role of the end facets of the coupler and will reflect a part of the escaped light wave and couple it back into the cavity. If one follows the path of a light ray that gets coupled out and then back in, it becomes clear that the light is coupled into the counter-propagating mode.

2.2 Modeling the Electromagnetic Field

2.2.1 The Wave Equation for the Electric Field in the Cavity Waveguide

The dynamical interaction between the electromagnetic field and the material is given by the Maxwell equations [26]. Let us consider the following formulation of these basic

laws:

$$\vec{\nabla} \cdot \vec{E} = \frac{\rho_{free}}{\epsilon_0} - \frac{1}{\epsilon_0}\vec{\nabla} \cdot \vec{P}, \tag{2.1}$$

$$\vec{\nabla} \cdot \vec{B} = 0, \tag{2.2}$$

$$\vec{\nabla} \times \vec{E} = -\frac{\partial \vec{B}}{\partial t}, \tag{2.3}$$

$$c^2\vec{\nabla} \times \vec{B} = \frac{1}{\epsilon_0}\vec{J}_{free} + \frac{1}{\epsilon_0}\frac{\partial \vec{P}}{\partial t} + \frac{\partial \vec{E}}{\partial t}, \tag{2.4}$$

where $\vec{E}$ en $\vec{B}$ are , respectively, the electric field and the magnetic induction field. $\vec{P}$ is the polarisation field, ϵ_0 is the permittivity of free space. ρ_{free}, which denotes the free charge carriers, is zero, because we assume charge neutrality. Eqs. (2.1)- (2.4) enable the derivation of the electromagnetic wave equation by applying some mathematical manipulations. We choose the z coordinate along the path in the cavity and assume the electric field and the polarisation field to be transversely polarised, in the x-direction, perpendicular on the direction of propagation, the z-direction. Because the transverse distribution of the wave is more or less constant due to the fact that the wave is strongly confined in the waveguide, we will only take the variations in the z-direction into account. As a consequence of these assumptions, the term $\vec{\nabla}\left(-\frac{1}{\epsilon_0}\vec{\nabla} \cdot \vec{P}\right) = 0$, because $\vec{P} = P\vec{1_x}$ and, since we assume only variations in the z-direction, $\vec{\nabla} = \frac{\partial}{\partial z}\vec{1_z}$. The wave equation becomes

$$\frac{\partial^2 \vec{E}}{\partial z^2} - \frac{1}{c^2}\frac{\partial^2 \vec{E}}{\partial t^2} - \frac{1}{\epsilon_0 c^2}\frac{\partial^2 \vec{P}}{\partial t^2} - \frac{1}{\epsilon_0 c^2}\frac{\partial \vec{J}_{free}}{\partial t} = 0. \tag{2.5}$$

Some of these terms can be rewritten in a more suitable form, using basic relations between physical quantities. The polarisation, $\vec{P}$, can be formulated as

$$\vec{P} = \epsilon_0 \chi_b \vec{E} + \vec{P}_p, \tag{2.6}$$

with χ_b being the background susceptibility and $\vec{P}_p$ being the polarisation originating from the the active material, which will provide the necessary gain. It is experimentally found that the current density $\vec{J}$ can be modeled by

$$\vec{J} = \epsilon_0 \sigma \vec{E}. \tag{2.7}$$

This will be one of the processes that cause losses in the cavity. Finally, the refractive index n can be defined as

$$n = \sqrt{1 + \chi_b}. \tag{2.8}$$

Substituting all this in Eq. (2.5) leads to

$$\frac{\partial^2 \vec{E}}{\partial z^2} - \frac{n^2}{c^2}\frac{\partial^2 \vec{E}}{\partial t^2} - \mu_0 \frac{\partial^2 \vec{P_p}}{\partial t^2} - \frac{\sigma}{c^2}\frac{\partial \vec{E}}{\partial t} = 0. \tag{2.9}$$

2.2.2 The Slowly Varying Envelope Approximation

In the absence of nonlinearities and backscattering, the eigenmodes of the system are forward and backward traveling waves. For this reason we expand the field as follows

$$\vec{E}(\vec{r},t) = E(z,t)\,\vec{1_x}, \tag{2.10}$$
$$E(z,t) = A_{cw}(z,t) + A_{ccw}(z,t) + c.c., \tag{2.11}$$

with

$$A_{cw}(z,t) = E_{cw}(z)e^{i(k_0 z-\omega_0 t)}, \tag{2.12}$$
$$A_{ccw}(z,t) = E_{ccw}(z)e^{-i(k_0 z+\omega_0 t)}. \tag{2.13}$$

And for the polarisation $\vec{P_p}$:

$$\vec{P_p}(\vec{r},t) = P_p(z,t)\,\vec{1_x}, \tag{2.14}$$
$$P_p(z,t) = B_{cw}(z,t) + B_{ccw}(z,t) + c.c., \tag{2.15}$$

with

$$B_{cw}(z,t) = P_{cw}(z)e^{i(k_0 z-\omega_0 t)}, \tag{2.16}$$
$$B_{ccw}(z,t) = P_{ccw}(z)e^{-i(k_0 z+\omega_0 t)}, \tag{2.17}$$

with E_{cw}, E_{ccw}, P_{cw} and P_{ccw} the complex slowly varying amplitudes. Now, we will invoke the so-called Slowly Varying Envelope Approximation (SVEA). Immediately, one can rewrite Eq. (2.9), using the fact that $e^{i(k_0 z-\omega_0 t)}$ and $e^{-i(k_0 z+\omega_0 t)}$ are orthogonal functions:

$$\frac{\partial^2 A_{cw}}{\partial z^2} - \frac{n^2}{c^2}\frac{\partial^2 A_{cw}}{\partial t^2} - \mu_0\frac{\partial^2 B_{cw}}{\partial t^2} - \frac{\sigma}{c^2}\frac{\partial A_{cw}}{\partial t} = 0, \tag{2.18}$$
$$\frac{\partial^2 A_{ccw}}{\partial z^2} - \frac{n^2}{c^2}\frac{\partial^2 A_{ccw}}{\partial t^2} - \mu_0\frac{\partial^2 B_{ccw}}{\partial t^2} - \frac{\sigma}{c^2}\frac{\partial A_{ccw}}{\partial t} = 0. \tag{2.19}$$

Similar equations hold for the complex conjugate. The fact that E_{cw}, E_{ccw}, P_{cw} and P_{ccw} are slowly varying functions of space and time can be mathematically expressed as

$$E_{cw}(z,t) = E_{cw}(Z_1, Z_2, ..., T), \tag{2.20}$$
$$E_{ccw}(z,t) = E_{ccw}(Z_1, Z_2, ..., T), \tag{2.21}$$
$$P_{cw}(z,t) = P_{cw}(Z_1, Z_2, ..., T), \tag{2.22}$$
$$P_{ccw}(z,t) = P_{ccw}(Z_1, Z_2, ..., T), \tag{2.23}$$

with every Z_i representing a longer and longer space scale, i.e., the function is far more slowly varying in Z_2 as it is in Z_1, etc. [27]. The fact that every Z_i represents a different

space scale means that the derivatives can be written as

$$\frac{\partial E_i}{\partial z} = \delta \frac{\partial E_i}{\partial Z_1} + \delta^2 \frac{\partial E_i}{\partial Z_2} + ..., \tag{2.24}$$

$$\frac{\partial E_i}{\partial t} = \delta \frac{\partial E_i}{\partial T}. \tag{2.25}$$

The δ-factor is introduced to indicate the order of a term. Before the terms in the wave equation can be grouped by order, we have to mention that the σ in Eq. (2.9) is of $O(\delta)$, because the losses are small, just as P_{cw} and P_{ccw} are of $O(\delta)$, because we consider a quantum well. That is why we will write

$$\sigma \to \delta\sigma, \tag{2.26}$$

$$P_{cw} \to \delta P_{cw}, \tag{2.27}$$

$$P_{ccw} \to \delta P_{ccw}. \tag{2.28}$$

Because the exponentials corresponding to the forward and backward traveling waves are orthogonal functions, we continue with the equations for the forward propagating wave. It now becomes possible to expand every term of Eq. (2.18):

$$\frac{\partial^2 A_{cw}}{\partial z^2} = \left(-k_0^2 E_{cw} + 2i\delta k_0 \frac{\partial E_{cw}}{\partial Z_1} + 2i\delta^2 k_0 \frac{\partial E_{cw}}{\partial Z_2} + \delta^2 \frac{\partial^2 E_{cw}}{\partial Z_1^2} + O(\delta^3) \right) e^{i(k_0 - \omega_0 t)}, \tag{2.29}$$

$$\frac{\partial A_{cw}}{\partial t} = \left(-i\omega_0 E_{cw} + \delta \frac{\partial E_{cw}}{\partial T} \right) e^{i(k_0 - \omega_0 t)}, \tag{2.30}$$

$$\frac{\partial^2 E_{cw}}{\partial t^2} = \left(-\omega_0^2 E_{cw} - 2\delta i\omega_0 \frac{\partial E_{cw}}{\partial T} + \delta^2 \frac{\partial^2 E_{cw}}{\partial T^2} \right) e^{i(k_0 - \omega_0 t)}, \tag{2.31}$$

$$\frac{\partial^2 B_{cw}}{\partial t^2} = \delta \left(-\omega_0^2 P_{cw} - 2\delta i\omega_0 \frac{\partial P_{cw}}{\partial T} + \delta^2 \frac{\partial^2 P_{cw}}{\partial T^2} \right) e^{i(k_0 - \omega_0 t)}. \tag{2.32}$$

Grouping all the terms in the wave equation by order gives:

- For the terms of $O(\delta^0)$

$$k_0^2 - \frac{n^2}{c^2}\omega_0^2 = 0. \tag{2.33}$$

  What we find is the dispersion relation of the material.

- For the terms of $O(\delta^1)$

$$2ik_0 \frac{\partial E_{cw}}{\partial Z_1} + 2i\frac{n^2}{c^2}\omega_0 \frac{\partial E_{cw}}{\partial T} + \mu_0 \omega_0^2 P_{cw} + i\frac{\sigma}{c^2}\omega_0 = 0 \tag{2.34}$$

$$\Leftrightarrow \frac{\partial E_{cw}}{\partial Z_1} + \frac{n}{c}\frac{\partial E_{cw}}{\partial T} - i\frac{\mu_0 \omega_0 c}{2n} P_{cw} + \frac{\sigma}{2cn} E_{cw} = 0 \tag{2.35}$$

Next, a new variable is introduced. The purpose of this transformation is to define a coordinate that travels along with the wave. It is obvious that different transformations are needed for the forward and backward propagating wave. The coordinate transformations for the forward wave are given by the Leibniz formulas

$$\xi_F = Z_1, \tag{2.36}$$

$$\tau = T - \frac{n}{c} Z_1. \tag{2.37}$$

Using the chain rule we find:

$$\frac{\partial}{\partial \xi_{cw}} = \frac{\partial}{\partial Z_1} \cdot \frac{\partial Z_1}{\partial \xi_{cw}} + \frac{\partial}{\partial T} \cdot \frac{\partial T}{\partial \xi_{cw}}, \tag{2.38}$$

$$= \frac{\partial}{\partial Z_1} + \frac{n}{c} \frac{\partial}{\partial T}. \tag{2.39}$$

This means that Eq. (2.35) reduces to

$$\frac{\partial E_{cw}}{\partial \xi_{cw}} = i \frac{\mu_0 \omega_0 c}{2n} P_{cw} - \frac{\sigma}{2cn} E_{cw} \tag{2.40}$$

$-\frac{\sigma}{2cn}$ represents a loss term, due to absorption in the medium. The gain term is hidden in P_{cw}, with the imaginary part leading to the gain term and the real part acting as propagation term.

2.3 Mean Field Model

To find an expression for E_{cw}, Eq. (2.40) has to be integrated over the cavity.

$$E_{cw}(\xi_{cw} = L) = E_{cw}(\xi_{cw} = 0) + \int_{u_{cw}=0}^{u_{cw}=L} \left(i \frac{\mu_0 \omega_0 c}{2n} P_{cw}(u_{cw}) - \frac{\sigma}{2cn} E_{cw}(u_{cw}) \right) du_{cw}. \tag{2.41}$$

We assume that $E_{cw}(u_{cw})$ and $P_{cw}(u_{cw})$ vary only slightly while traveling through the cavity. Therefore, we can take the integrand constant. Eq. (2.41) becomes

$$E_{cw}(L) = E_{cw}(0) + L \left(i \frac{\mu_0 \omega_0 c}{2n} P_{cw}(0) - \frac{\sigma}{2cn} E_{cw}(0) \right) \tag{2.42}$$

Now, we will consider the cavity effect by imposing the boundary conditions. We express that the amplitude of the electric field after one roundtrip equals the sum of the reflected part of E_{cw} and the part coupled in from E_{ccw} through the external mirrors. Here we return to the coordinate system with z and t:

$$E_{cw}(0, \frac{L}{v_g}) = \rho E_{cw}(L, 0) + k E_{ccw}(0, \frac{L}{v_g}), \tag{2.43}$$

with ρ the reflectivity of the mirror. Another way to write ρ is:

$$\rho = 1 - \Sigma, \tag{2.44}$$

with Σ the transmittance of the mirror. Substituting Eq. (2.42) in Eq. (2.43) and keeping in mind that the fields remain nearly constant for one cavity roundtrip gives:

$$E_{cw}(0, \frac{L}{v_g}) = (1 - \Sigma)\, E_{cw}(0,0) + \rho L \left(i\frac{\mu_0 \omega_0 c}{2n} P_{cw}(z,t) - \frac{\sigma}{2cn} E_{cw}(z,t) \right) + k E_{ccw}(0, \frac{L}{v_g}). \tag{2.45}$$

We define the roundtrip time

$$\tau_R = \frac{L}{v_g}. \tag{2.46}$$

Eq. (2.45) becomes

$$\begin{aligned}
\frac{dE_{cw}(t)}{dT} &= \lim_{\tau_R \to 0} \frac{E_{cw}(0,\tau_R) - E_{cw}(0,0)}{\tau_R} && (2.47)\\
&\approx \frac{E_{cw}(0,\tau_R) - E_{cw}(0,0)}{\tau_R} && (2.48)\\
&= -\frac{\Sigma}{\tau_R} E_{cw}(t) + \frac{\rho L}{\tau_R} \left(i\frac{\mu_0 \omega_0 c}{2n} P_{cw}(t) - \frac{\sigma}{2cn} E_{cw}(t) \right) + \frac{k}{\tau_R} E_{ccw}(t) && (2.49)\\
&= \left(-\frac{\Sigma}{\tau_R} - \frac{\rho L \sigma}{2cn\tau_R} \right) E_{cw}(t) + i\frac{\rho L \mu_0 \omega_0 c}{2n\tau_R} P_{cw}(t) + \frac{k}{\tau_R} E_{ccw}(t). && (2.50)
\end{aligned}$$

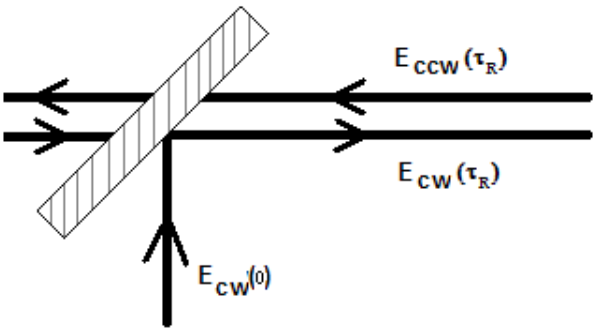

Figure 2.2: Close up from top left mirror. To formulate the boundary condition, one has to include both the clockwise and the counter-clockwise propagating field.

2.4 Modeling the Gain Medium

After deducing the electric field in a classical way, we will now use a semiclassical approach to find an expression for the evolution of the polarisation field and the carriers. This implies starting from the Schrödinger equation. For simplicity, we model the semiconductor by a Maxwell-Bloch two-level model [28–30]. Applying this approach means omitting all but two energy levels.

2.4.1 A Two Level Model of the Gain Medium

In a two-level model for a semiconductor, the light-matter interaction happens through transitions from the conduction to the valence band. Although in reality a whole range of transitions is possible, in this model only two energy levels are allowed to participate in the carrier transitions. Since we consider now quantum properties, we have to use the wavefunction of the electron, $\psi(\vec{r}, t)$. Its evolution is given by the Schrödinger equation:

$$i\hbar \frac{\partial}{\partial t}\psi(\vec{r}, t) = \hat{H}\psi(\vec{r}, t). \tag{2.51}$$

In the above equation, $\hat{H}$ represents the Hamiltonian of the system and $\hbar$ is Dirac's constant. The stationary solutions of Eq. (2.51) are given by:

$$\psi_n(\vec{r}, t) = u_n(\vec{r})e^{-i\frac{E_n}{\hbar}t}, \tag{2.52}$$

where $u_n(\vec{r})$ is an eigenfunction of the Hamiltonian and E_n is the corresponding eigenvalue. The wave function then becomes

$$\psi_n(\vec{r}, t) = C_a u_a(\vec{r})e^{-i\frac{E_a}{\hbar}t} + C_b u_b(\vec{r})e^{-i\frac{E_b}{\hbar}t}. \tag{2.53}$$

The coefficients C_a and C_b can be used to express the probabilities that the systems resides in the a^{th} or b^{th} energy state. To study the interaction between the system and an electric field present in the medium, we need to add an interaction energy operator to the Hamiltonian.

$$\hat{H} = \hat{H}_0 + \hat{\Theta}. \tag{2.54}$$

In Eq. (2.54), $\hat{H}_0$ represents the unperturbed Hamiltonian and $\hat{\Theta}$ serves as perturbation term. We expand the wavefunction in terms of the eigenstates of the unperturbed Hamiltonian and regard C_a and C_b to be time-dependent. When the wave function is substituted in the Schrödinger equation, it is possible to find the derivatives of C_a and C_b by multiplying with u_a^* or u_b^* and then integrating over the entire space.

$$\frac{d}{dt}C_a = -\frac{i}{\hbar}\hat{\Theta}_{aa}C_a - \frac{i}{\hbar}\hat{\Theta}_{ab}e^{i\frac{E_a - E_b}{\hbar}t}C_b, \tag{2.55}$$

$$\frac{d}{dt}C_b = -\frac{i}{\hbar}\hat{\Theta}_{bb}C_b - \frac{i}{\hbar}\hat{\Theta}_{ba}e^{-i\frac{E_a - E_b}{\hbar}t}C_a, \tag{2.56}$$

with

$$\hat{\Theta}_{mn} = \int u_m^*(\vec{r})\hat{\Theta}u_n(\vec{r})d^3\vec{r} \tag{2.57}$$

2.4.2 Dipole Approximation

The perturbation energy, $\hat{\Theta}$, is related to the electric dipole operator:

$$\hat{\Theta} = -e\hat{\vec{r}}\cdot\vec{E}(\vec{R},t), \tag{2.58}$$

with $\vec{R}$ the vector indicating the position of the center of mass of the dipole. It is assumed that the electric field remains constant over the dimensions of the dipole, what comes down to having a lower energy when the dipole is aligned along the electric field than when it is aligned against it. To find the polarisation, one has to multiply the expectation value of the electric dipole operator with the number of systems per unit volume. It is also known that $\left\|u_n(\vec{r})\right\|^2$ is a symmetrical function of $\vec{r}$ and $\vec{r}$ itself is antisymmetrical. The expectation value becomes

$$\left\langle e\hat{\vec{r}}\right\rangle = e\hat{\vec{r}}_{ba}C_a(t)C_b^*(t)e^{-i\frac{E_a-E_b}{\hbar}t} + c.c., \tag{2.59}$$

with $\vec{r}_{ab}$ the complex electric dipole matrix element

$$\hat{\vec{r}}_{ba} = \int u_a^*(\vec{r})\hat{\vec{r}}u_b(\vec{r})d^3\vec{r}. \tag{2.60}$$

Since only $C_a(t)C_b^*(t)$ is of importance, because $\hat{\Theta}_{aa}$ and $\hat{\Theta}_{bb}$ are zero, we write the electric dipole interaction energy matrix element as:

$$\hat{\Theta}_{ab} = -e\hat{\vec{r}}_{ab}\cdot\vec{E}(\vec{R},t) = -\hat{\vec{\mu}}\cdot\vec{E}(\vec{R},t) = \hat{\Theta}_{ba}^* \tag{2.61}$$

From now on, we will ignore the spatial dependence of the electric field and use $\vec{E}(t) = \vec{E}_0e^{-i\omega t}$. In the case $\omega = \frac{E_a-E_b}{\hbar}$, the exact resonance, we can substitute Eq. (2.61) in Eqs. (2.55)- (2.56) and find that

$$\frac{d^2}{dt^2}C_b = -\Omega_R^*C_b, \tag{2.62}$$

with Ω_R being the Rabi frequency, given by

$$\Omega_R = \frac{\left\|\vec{\mu}\cdot\vec{E}_0\right\|}{\hbar}. \tag{2.63}$$

Now, suppose that if $t = 0$, the system is in the lower state. Using the fact that C_a and C_b can be used to calculate the probabilities by taking $\| \|^2$ we understand that $C_b(0) = 1, C_a(0) = 0$. We find that

$$C_b(t) = \cos \Omega_R t. \tag{2.64}$$

If one now wants to know the probability of the system being in the lower state, it suffices to calculate

$$\|C_b(t)\|^2 = \frac{(1 + \cos 2\Omega_R t)}{2}. \tag{2.65}$$

The above equation implicates that the wave function oscillates between the lower and upper states sinusoidally at twice the Rabi frequency, a phenomenon known as Rabi flopping.

2.4.3 From One Atom to an Ensemble of Atoms: the Density Matrix

Our approach described above is correct in the case where only one dipole is present. However, in a real system such as the active medium, there are a countless number of dipoles present. To take this into account $\langle e\vec{r} \rangle$ should be averaged over all dipoles present. The second averaging will be denoted with an overbar. For convenience, we define a density matrix with the elements:

$$\rho_{nm} = \overline{C_n C_m^*} e^{-i\frac{E_n - E_m}{\hbar}t}. \tag{2.66}$$

We know that

$$\overline{\left\langle \hat{\Theta} \right\rangle} = Tr\left(\hat{\rho} \cdot \hat{\theta}\right), \tag{2.67}$$

with $\hat{\rho}$ the density matrix and the operator $\hat{\theta}$ taken in its matrix form. The evolution of the density matrix is given by

$$\frac{d}{dt}\hat{\rho} = -\frac{i}{\hbar}\left[\hat{H}, \hat{\rho}\right]. \tag{2.68}$$

More specific, for a laser system, it is found that

$$\frac{d}{dt}\rho_{ab} = -\gamma_\perp \rho_{ab} - i\frac{E_a - E_b}{\hbar}\rho_{ab} - \frac{i}{\hbar}\vec{\mu} \cdot \vec{E} n_{ab}, \tag{2.69}$$

$$\frac{d}{dt}n_{ab} = \Lambda - \frac{2i}{\hbar}\left(\vec{\mu}^* \cdot \vec{E}^* \rho_{ab} - \vec{\mu} \cdot \vec{E} \rho_{ab}^*\right) + \left.\frac{dn_{ab}}{dt}\right|_{decay}, \tag{2.70}$$

with $n_{ab} = \rho_{aa} - \rho_{bb}$, representing the microscopic population difference. In Eqs. (2.69)-(2.70), some terms have been added phenomenologically. Whenever the electric field is turned off, ρ_{ab} will relax back to its equilibrium value. Indeed, if we suppose that we

have a single two level system, with ρ_{ab} a complex number, then this system has a certain phase. But, as already mentioned, there are many dipoles, so many systems, each with their own phase. The phase will vary from system to system, with the average phase of the ensemble being zero. We call the dephasing rate of the microscopic dipoles, $\gamma_\perp$. Because of a similar reasoning, ρ_{aa} and ρ_{bb} should relax to their initial values, resulting in n_{ab} relaxing to zero. Because the population is also pumped, some atoms will be taken from the b-state and put into the a-state. Λ is called the pump parameter.

2.4.4 Macroscopic Model

To describe the system on a macroscopic scale, we have to find a relation between the microscopic expressions for the polarisation and carrier density and the macroscopic ones. These relations are given by

$$P_p = \frac{\aleph}{V}\vec{\mu}^* \rho_{ab}, \tag{2.71}$$

$$N = \frac{\aleph}{V} n_{ab}, \tag{2.72}$$

with $\aleph$ the number of systems in the ensemble and V the volume of the quantum well. In this quantum well the evolution of the carrier density is determined by four processes:

- The first one is the fact that the active medium is pumped electrically because of the current injection. This directly results in an increase in the carrier number, N. The pump rate equals $J/el = \aleph\Lambda/V$, with J being the injected ring current density, e the electron charge, l the active layer thickness and.
- A second mechanism is the carriers recombining spontaneously, eliciting in a decay of the number of carriers. The recombination rate, $R(N)$, can be written as the sum of three terms: a non-radiative term, AN, a spontaneous radiative recombination term, BN^2, and an Auger recombination rate, CN^3. We will approximate it by N/τ_s with τ_s the carrier lifetime.
- Diffusion of the carriers in the quantum well with diffusion strength, $\mathcal{D}$. This diffusion, however, will be neglected.
- The electric field stimulates the carriers to recombine.

Finally, when we make use of the slowly varying approximation around the cavity resonance, Ω, and we combine Eqs. (2.71)- (2.72) with Eqs. (2.69)- (2.70), we find:

$$\frac{dN}{dt} = \frac{J}{el} - \frac{N}{\tau_s} - \frac{2i}{\hbar}\left[\vec{P}\vec{E}^* - \vec{P}^*\vec{E}\right], \tag{2.73}$$

$$\frac{d\vec{P_p}}{dt} = -(\gamma_\perp + i(\omega_t - \Omega))\vec{P_p} - \frac{i}{\hbar}\left\|\mu\right\|^2 N\vec{E}, \tag{2.74}$$

with ω_t the transition frequency.

2.5 Adiabatic Elimination of the Polarisation Field

Combining the previous sections, we find the following set of rate equations:

$$\frac{dE_{cw}}{dT} = \left(-\frac{\Sigma}{\tau_R} - \frac{\rho L\sigma}{2cn\tau_R}\right)E_{cw} + i\frac{\rho L\mu_0\omega_0 c}{2n\tau_R}P_{cw} + \frac{k}{\tau_R}E_{ccw}, \tag{2.75}$$

$$\frac{dE_{ccw}}{dT} = \left(-\frac{\Sigma}{\tau_R} - \frac{\rho L\sigma}{2cn\tau_R}\right)E_{ccw} + i\frac{\rho L\mu_0\omega_0 c}{2n\tau_R}P_{ccw} + \frac{k}{\tau_R}E_{cw}, \tag{2.76}$$

$$\frac{dN}{dt} = \frac{J}{el} - \frac{N}{\tau_s} - \frac{2i}{\hbar}\left[\vec{P}\vec{E}^* - \vec{P}^*\vec{E}\right], \tag{2.77}$$

$$\frac{d\vec{P_p}}{dt} = -(\gamma_\perp + i(\omega_t - \Omega))\vec{P_p} - \frac{i}{\hbar}\left\|\mu\right\|^2 N\vec{E}. \tag{2.78}$$

In the above equations, every laser variable has its own time scale. For the electric field the decay rate is given by $\left(-\frac{\Sigma}{\tau_R} - \frac{\rho L\sigma}{2cn\tau_R}\right)$, for the carriers it can be found by taking $R(N)$ and dividing it by N and for the polarisation it is the dephasing rate, $\gamma_\perp$. Arecchi *et al.* [31] have proposed to divide lasers into different classes, based on the relative magnitude of these damping rates. Here we deal with a class B laser, in which $\gamma_\perp$, in the polarisation equation, is orders of magnitude larger than its equivalents in the other two equations. As a result, Eq. (2.78) can be adiabatically eliminated. This can be intuitively understood by considering that the electric field and the carriers are much slower than the polarisation, such that in Eq. (2.78), they can be taken constant. Whenever a perturbation in the the polarisation is present, from the point of view of E and N it will disappear immediately. The derivative of P will be so high that P almost instantly returns to its stationary value and once this stationary value is reached, the derivative turns to zero. If $\frac{\partial\vec{P}_p}{\partial t} = 0$, $\vec{P}_p$ can be eliminated in the other two equations. We find that

$$\vec{P}_p = -\frac{i}{\hbar}\left\|\mu\right\|^2 \frac{N}{\gamma_\perp + i(\omega_t - \Omega)}\vec{E}, \tag{2.79}$$

so if we split this up again into a clockwise and a counter-clockwise equation:

$$P_{cw} = -\frac{i}{\hbar}\left\|\mu\right\|^2 \frac{N}{\gamma_\perp + i(\omega_t - \Omega)}E_{cw}, \tag{2.80}$$

$$P_{ccw} = -\frac{i}{\hbar}\left\|\mu\right\|^2 \frac{N}{\gamma_\perp + i(\omega_t - \Omega)}E_{ccw}. \tag{2.81}$$

Eq. (2.80) allows to find the susceptibility, χ:

$$\chi = -\frac{i}{\epsilon_0\hbar}\left\|\mu\right\|^2 \frac{N}{\gamma_\perp + i(\omega_t - \Omega)}. \tag{2.82}$$

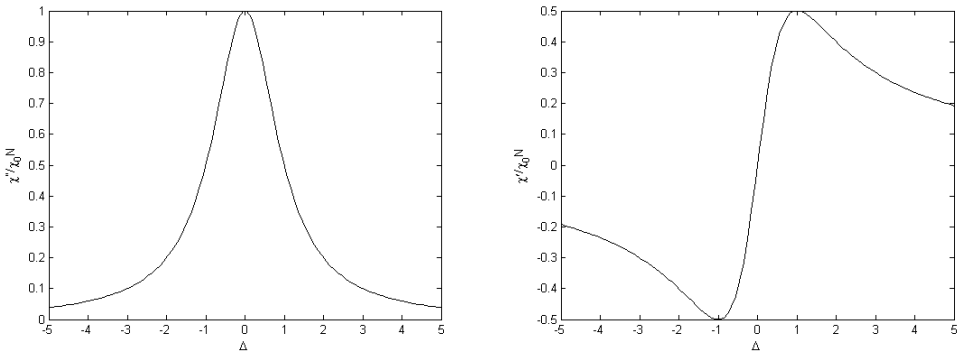

(a) Renormalized gain (b) Refractive index change

Figure 2.3: Spectral characteristics of the renormalized gain and refractive index change of a two-level system

This equation can be simplified to

$$\chi = -i\chi_0 \frac{N}{1 - i\Delta}, \tag{2.83}$$

with

$$\chi_0 = \frac{\|\mu\|^2}{\epsilon_0 \hbar \gamma_\perp}, \tag{2.84}$$

$$\Delta = \frac{(\Omega - \omega_t)}{\gamma_\perp}. \tag{2.85}$$

Furthermore, one has to keep in mind that the susceptibility, χ, can be divided into a real and an imaginary part, $\chi = \chi\prime - i\chi\prime\prime$, leading to:

$$\chi' = \chi_0 N \frac{\Delta}{1 + \Delta^2}, \tag{2.86}$$

$$\chi'' = \chi_0 N \frac{1}{1 + \Delta^2}. \tag{2.87}$$

It is from this equation that the often used linewidth enhancement factor α can be found [32]:

$$\alpha = \frac{\partial \chi'/\partial N}{\partial \chi''/\partial N} = \Delta. \tag{2.88}$$

It is necessary to mention that in reality, due to the large energy spread of the transitions, the gain spectrum does not look as it does in Figure 2.3. In a more complete model, you have to sum over all the transitions and the spectrum becomes asymmetric, with the

α-factor not crossing zero. The rate equations become:

$$\frac{dE_{cw}}{dT} = \left(-\frac{\Sigma}{\tau_R} - \frac{\rho L\sigma}{2cn\tau_R}\right)E_{cw} + \frac{\rho L\omega_0}{2cn\tau_R}\chi''(1+i\alpha)E_{cw} + \frac{k}{\tau_R}E_{ccw}, \tag{2.89}$$

$$\frac{dE_{ccw}}{dT} = \left(-\frac{\Sigma}{\tau_R} - \frac{\rho L\sigma}{2cn\tau_R}\right)E_{ccw} + \frac{\rho L\omega_0}{2cn\tau_R}\chi''(1+i\alpha)E_{ccw} + \frac{k}{\tau_R}E_{cw}, \tag{2.90}$$

$$\frac{dN}{dt} = \frac{J}{el} - \frac{N}{\tau_s} - \frac{4\epsilon_0}{\hbar}\chi''\left(|E_{cw}|^2 + |E_{ccw}|^2\right). \tag{2.91}$$

If we then define

$$G_n(N-N_0) = \frac{\rho L\omega_0}{cn\tau_R}\chi'', \tag{2.92}$$

$$\frac{1}{\tau_p} = \frac{2\Sigma}{\tau_R} - \frac{\rho L\sigma}{cn\tau_R}, \tag{2.93}$$

$$\mathcal{K} = \frac{k}{\tau_R}, \tag{2.94}$$

with G_n the semiconductor material gain, N_0 the carrier density at transparency and τ_p the photon lifetime. We obtain:

$$\frac{dE_{cw}}{dT} = \frac{1}{2}(1+i\alpha)G_{cw}E_{cw} - \frac{1}{2\tau_p}E_{cw} - \mathcal{K}E_{ccw}, \tag{2.95}$$

$$\frac{dE_{ccw}}{dT} = \frac{1}{2}(1+i\alpha)G_{ccw}E_{cw} - \frac{1}{2\tau_p}E_{ccw} - \mathcal{K}E_{cw}, \tag{2.96}$$

$$\frac{dN}{dT} = \frac{J}{el} - \frac{N}{\tau_s} - G_{cw}\,|E_{cw}|^2 - G_{ccw}\,|E_{ccw}|^2\,. \tag{2.97}$$

with

$$G_{cw} = G_n(N-N_0)(1-\epsilon_s\,|E_{cw}|^2 - \epsilon_c\,|E_{ccw}|^2), \tag{2.98}$$

$$G_{ccw} = G_n(N-N_0)(1-\epsilon_s\,|E_{ccw}|^2 - \epsilon_c)\,|E_{cw}|^2). \tag{2.99}$$

In the above equations, some effects were added phenomenologically. The fields are coupled to each other through nonlinear saturation effects. This saturation is accounted for in the terms $\epsilon_s\,|\mathcal{E}_i|^2$ and $\epsilon_c\left|\mathcal{E}_{1,2}\right|^2$ in which ϵ_s and ϵ_c are the saturation coefficients. ϵ_s is called the self-saturation coefficient and expresses how much a mode saturates itself. Furthermore, we know that a mode is also saturated by its counter-propagating counterpart, hence the cross-saturation coefficient ϵ_c is defined. The α-factor will lead to a frequency shift, which can be cancelled by adding an extra phase term to the electric field,

$$E_{cw,ccw} \rightarrow E_{cw,ccw}e^{\frac{i\alpha}{2\tau_p}T}. \tag{2.100}$$

The equations become

$$\frac{dE_{cw}}{dT}e^{\frac{i\alpha}{2\tau_p}T} + \frac{i\alpha}{2\tau_p}E_{cw}e^{\frac{i\alpha}{2\tau_p}T} = \frac{1}{2}(1+i\alpha)G_{cw}E_{cw}e^{\frac{i\alpha}{2\tau_p}T} - \frac{1}{2\tau_p}E_{cw}e^{\frac{i\alpha}{2\tau_p}T} - \mathcal{K}E_{ccw}e^{\frac{i\alpha}{2\tau_p}T}, \quad (2.101)$$

$$\frac{dE_{ccw}}{dT}e^{\frac{i\alpha}{2\tau_p}T} + \frac{i\alpha}{2\tau_p}E_{ccw}e^{\frac{i\alpha}{2\tau_p}T} = \frac{1}{2}(1+i\alpha)G_{ccw}E_{ccw}e^{\frac{i\alpha}{2\tau_p}T} - \frac{1}{2\tau_p}E_{ccw}e^{\frac{i\alpha}{2\tau_p}T} - \mathcal{K}E_{cw}e^{\frac{i\alpha}{2\tau_p}T}, \quad (2.102)$$

$$\frac{dN}{dT} = \frac{J}{el} - \frac{N}{\tau_s} - G_{cw}\left|E_{cw}\right|^2 - G_{ccw}\left|E_{ccw}\right|^2. \quad (2.103)$$

Omitting the phase factors in both the left and right segments, results in

$$\frac{dE_{cw}}{dT} = \frac{1}{2}(1+i\alpha)\left(G_{cw} - \frac{1}{\tau_p}\right)E_{cw} - \mathcal{K}E_{ccw}, \quad (2.104)$$

$$\frac{dE_{ccw}}{dT} = \frac{1}{2}(1+i\alpha)\left(G_{ccw} - \frac{1}{\tau_p}\right)E_{ccw} - \mathcal{K}E_{cw}, \quad (2.105)$$

$$\frac{dN}{dT} = \frac{J}{el} - \frac{N}{\tau_s} - G_{cw}\left|E_{cw}\right|^2 - G_{ccw}\left|E_{ccw}\right|^2. \quad (2.106)$$

The term $\frac{1}{\tau_p}$ represents the losses in the cavity. The last parameter that needs explaining is $\mathcal{K}$, the backscattering coefficient. The reflection can introduce a phase shift and hence it is required to take a complex number for $\mathcal{K}$, which we will note as $\mathcal{K}_d + i\mathcal{K}_c$. $\mathcal{K}_d$ is called the dissipative coupling and $\mathcal{K}_c$ the conservative coupling. If two counter-propagating waves are present in the cavity, a standing wave pattern will be formed and this can induce a grating in the carrier density. However, if the spatial period of the standing wave pattern is comparable to the carrier diffusion length, we note that its much smaller. In other words, the carrier diffusion will destroy the grating and, as a result, the carrier density, N, can be assumed uniform over the cavity.

2.6 Multimode Equations

The purpose of this thesis work is to study a system with two longitudinal modes present in the ring cavity. Eqs. (2.104)- (2.106) can be generalised for multimode semiconductor ring lasers on condition that the two frequencies are only slightly different. When the energy difference between the considered optical transitions is negligible, one can assume that the same carrier reservoir is used for both longitudinal modes. To have a better understanding of the effects that take place in a multimode ring laser, it is a good idea to follow a similar approach as explained in the case of a single mode ring laser. Inside a circular resonator the electric field can be written as the sum of the two longitudinal modes, each with two counter-propagating modes. The direction of propagation is again chosen along the z-coordinate and assumed positive in counter-

clockwise direction,

$$\vec{E}(\vec{r},t) = E(z,t)\,\vec{1_x}, \tag{2.107}$$

$$\begin{aligned} E(z,t) = {} & E_{1cw}(z)e^{i(k_1 z-\omega_1 t)} + E_{1ccw}(z)e^{-i(k_1 z+\omega_1 t)} + c.c. \\ & + E_{2cw}(z)e^{i(k_2 z-\omega_2 t)} + E_{2ccw}(z)e^{-i(k_2 z+\omega_2 t)} + c.c.. \end{aligned} \tag{2.108}$$

Again, the evolution of the electric fields and the carrier density can be described by differential equations.

$$\frac{dE_{1cw}}{dT} = \frac{1}{2}(1+i\alpha)\left[G_{1cw} - \frac{1}{\tau_p}\right]E_{1cw} - \mathcal{K}_1 E_{1ccw}, \tag{2.109}$$

$$\frac{dE_{1ccw}}{dT} = \frac{1}{2}(1+i\alpha)\left[G_{1ccw} - \frac{1}{\tau_p}\right]E_{1ccw} - \mathcal{K}_1 E_{1cw}, \tag{2.110}$$

$$\frac{dE_{2cw}}{dT} = \frac{1}{2}(1+i\alpha)\left[G_{2cw} - \frac{1}{\tau_p}\right]E_{2cw} - \mathcal{K}_2 E_{2ccw}, \tag{2.111}$$

$$\frac{dE_{2ccw}}{dT} = \frac{1}{2}(1+i\alpha)\left[G_{2ccw} - \frac{1}{\tau_p}\right]E_{2ccw} - \mathcal{K}_2 E_{2cw}, \tag{2.112}$$

$$\begin{aligned} \frac{dN}{dT} = {} & \frac{J}{el} - \frac{N}{\tau_s} - G_{1cw}\left|E_{1cw}\right|^2 - G_{1ccw}\left|E_{1ccw}\right|^2 \\ & - G_{2cw}\left|E_{2cw}\right|^2 - G_{2ccw}\left|E_{2ccw}\right|^2. \end{aligned} \tag{2.113}$$

with

$$\begin{aligned} G_{1cw} = {} & G_{n1}(N-N_0)\cdot \\ & (1-\epsilon_{s0}\left|E_{1cw}\right|^2 - \epsilon_{c0}\left|E_{1ccw}\right|^2 - \epsilon_{s1}\left|E_{2cw}\right|^2 - \epsilon_{c1}\left|E_{2ccw}\right|^2), \end{aligned} \tag{2.114}$$

$$\begin{aligned} G_{1ccw} = {} & G_{n1}(N-N_0)\cdot \\ & (1-\epsilon_{s0}\left|E_{1ccw}\right|^2 - \epsilon_{c0}\left|E_{1cw}\right|^2 - \epsilon_{s1}\left|E_{2ccw}\right|^2 - \epsilon_{c1}\left|E_{2cw}\right|^2), \end{aligned} \tag{2.115}$$

$$\begin{aligned} G_{2cw} = {} & G_{n2}(N-N_0)\cdot \\ & (1-\epsilon_{s0}\left|E_{2cw}\right|^2 - \epsilon_{c0}\left|E_{2ccw}\right|^2 - \tilde{\epsilon}_{s1}\left|E_{1cw}\right|^2 - \tilde{\epsilon}_{c1}\left|E_{1ccw}\right|^2), \end{aligned} \tag{2.116}$$

$$\begin{aligned} G_{2ccw} = {} & G_{n2}(N-N_0)\cdot \\ & (1-\epsilon_{s0}\left|E_{2ccw}\right|^2 - \epsilon_{c0}\left|E_{2cw}\right|^2 - \tilde{\epsilon}_{s1}\left|E_{1ccw}\right|^2 - \tilde{\epsilon}_{c1}\left|E_{1cw}\right|^2). \end{aligned} \tag{2.117}$$

This multimode rate equations exhibit some essential variations on the single mode model. From the beginning it becomes clear that just one self-saturation and one cross-saturation coefficient will not suffice to describe the situation accurately. It is already discussed that every mode will saturate the other to a certain amount and hence will provide a nonlinear coupling. This means that every mode is saturated by every other mode, with a corresponding saturation coefficient. First of all, every mode gets saturated by itself with a self-saturation coefficient ϵ_{s0} and by it's counter-propagating counterpart of the same longitudinal mode with a cross-saturation coefficient ϵ_{c0}. Somewhat more complicated is the choice of the saturation coefficients that establish the link between

the fields of the different longitudinal modes. If takes into account the symmetry in the cavity, it seems reasonable to assume that two counter-propagating modes of one longitudinal frequency are equally saturated by the fields with corresponding direction of propagation of another longitudinal mode. That is why in Eqs. (2.109) and (2.110) both of the equations contain ϵ_{s1}. With a similar reasoning one sees that also the ϵ_{c1} factor is the same for both directions. In the second longitudinal mode the situation is similar, but there the intermodal cross-saturation coefficients are different from the ones in the first two equations, because of the asymmetry of the gain curve, depicted in Figure 2.4. The reader should keep in mind that in spite of the notation only ϵ_{s0} is a self-saturation coefficient, while all the others, including ϵ_{s1} en $\tilde{\epsilon}_{s1}$, are cross-saturation coefficients. G_{n1} and G_{n2} are the semiconductor gain coefficients at the two considered frequencies.

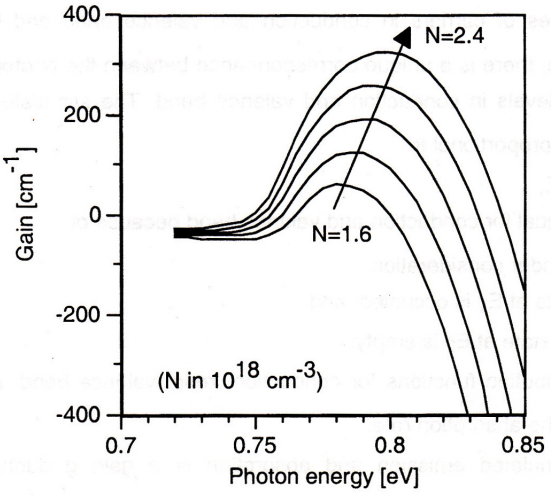

Figure 2.4: Gain vs photon energy in InGaAsP bulk material (Picture from Morthier *et al.* [33]).

2.7 Nondimensionalisation of the Equations

The method applied in this section is based on what was done by Sorel *et al.* [18]. They considered a single mode semiconductor ring laser and subsequently nondimensionalised the rate equation model, while in this case, we implement similar techniques for the multimode model. By rescaling Eqs. (2.109)- (2.113) it becomes possible to find a dimensionless set of equations. A new time t is defined,

$$t = \frac{T}{2\tau_p}, \tag{2.118}$$

and the electric fields and carrier density are redefined as

$$\mathcal{E}_{1cw} = \sqrt{\frac{G_{n1}+G_{n2}}{2}\tau_s}E_{1cw} \qquad \mathcal{E}_{2cw} = \sqrt{\frac{G_{n1}+G_{n2}}{2}\tau_s}E_{2cw}, \tag{2.119}$$

$$\mathcal{E}_{1ccw} = \sqrt{\frac{G_{n1}+G_{n2}}{2}\tau_s}E_{1ccw} \qquad \mathcal{E}_{2ccw} = \sqrt{\frac{G_{n1}+G_{n2}}{2}\tau_s}E_{2ccw}, \tag{2.120}$$

$$n = \frac{G_{n1}+G_{n2}}{2}\tau_p(N-N_0). \tag{2.121}$$

The saturation and gain coefficients are reformulated,

$$s_0 = \frac{\epsilon_{s0}}{\frac{G_{n1}+G_{n2}}{2}\tau_s} \qquad c_0 = \frac{\epsilon_{c0}}{\frac{G_{n1}+G_{n2}}{2}\tau_s}, \tag{2.122}$$

$$s_1 = \frac{\epsilon_{s1}}{\frac{G_{n1}+G_{n2}}{2}\tau_s} \qquad \tilde{s}_1 = \frac{\tilde{\epsilon}_{s1}}{\frac{G_{n1}+G_{n2}}{2}\tau_s}, \tag{2.123}$$

$$c_1 = \frac{\epsilon_{c1}}{\frac{G_{n1}+G_{n2}}{2}\tau_s} \qquad \tilde{c}_1 = \frac{\tilde{\epsilon}_{c1}}{\frac{G_{n1}+G_{n2}}{2}\tau_s}, \tag{2.124}$$

$$g_1 = \frac{2G_{n1}}{G_{n1}+G_{n2}} \qquad g_2 = \frac{2G_{n2}}{G_{n1}+G_{n2}}. \tag{2.125}$$

For the backscattering, one can explicitly write the backscattering coefficient as the sum of a real and an imaginary number:

$$\mathcal{K}_1 = \mathcal{K}_{d1} + i\mathcal{K}_{c1} \qquad \mathcal{K}_2 = \mathcal{K}_{d2} + i\mathcal{K}_{c2}. \tag{2.126}$$

These coefficients are also rescaled

$$\tilde{k}_{d1} = 2\tau_p\mathcal{K}_{d1} \qquad \tilde{k}_{d2} = 2\tau_p\mathcal{K}_{d2}, \tag{2.127}$$

$$\tilde{k}_{c1} = 2\tau_p\mathcal{K}_{c1} \qquad \tilde{k}_{c2} = 2\tau_p\mathcal{K}_{c2}. \tag{2.128}$$

For comfortableness we define two new variables:

$$\frac{\gamma}{\kappa} = \frac{2\tau_p}{\tau_s}, \tag{2.129}$$

$$\mu = \frac{(G_{n1}+G_{n2})\tau_p N_0}{2}\left(\frac{J\tau_s}{N_0 el}-1\right), \tag{2.130}$$

with This normalisation of the variables and parameters transforms Eqs. (2.109)- (2.113) into a new dimensionless set:

$$\frac{d\mathcal{E}_{1cw}}{dt} = (1+i\alpha)\left[g_1 n\left(1 - s_0\left|\mathcal{E}_{1cw}\right|^2 - c_0\left|\mathcal{E}_{1ccw}\right|^2 - s_1\left|\mathcal{E}_{2cw}\right|^2 - c_1\left|\mathcal{E}_{2ccw}\right|^2\right) - 1\right]\mathcal{E}_{1cw} - \left(\tilde{k}_{d1} + i\,\tilde{k}_{c1}\right)\mathcal{E}_{1ccw}, \tag{2.131}$$

$$\frac{d\mathcal{E}_{1ccw}}{dt} = (1+i\alpha)\left[g_1 n\left(1 - s_0\left|\mathcal{E}_{1ccw}\right|^2 - c_0\left|\mathcal{E}_{1cw}\right|^2 - s_1\left|\mathcal{E}_{2ccw}\right|^2 - c_1\left|\mathcal{E}_{2cw}\right|^2\right) - 1\right]\mathcal{E}_{1ccw} - \left(\tilde{k}_{d1} + i\,\tilde{k}_{c1}\right)\mathcal{E}_{1cw}, \tag{2.132}$$

$$\frac{d\mathcal{E}_{2cw}}{dt} = (1+i\alpha)\left[g_2 n\left(1 - s_0\left|\mathcal{E}_{2cw}\right|^2 - c_0\left|\mathcal{E}_{2ccw}\right|^2 - \tilde{s}_1\left|\mathcal{E}_{1cw}\right|^2 - \tilde{c}_1\left|\mathcal{E}_{1ccw}\right|^2\right) - 1\right]\mathcal{E}_{2cw} - \left(\tilde{k}_{d2} + i\,\tilde{k}_{c2}\right)\mathcal{E}_{2ccw}, \tag{2.133}$$

$$\frac{d\mathcal{E}_{2ccw}}{dt} = (1+i\alpha)\left[g_2 n\left(1 - s_0\left|\mathcal{E}_{2ccw}\right|^2 - c_0\left|\mathcal{E}_{2cw}\right|^2 - \tilde{s}_1\left|\mathcal{E}_{1ccw}\right|^2 - \tilde{c}_1\left|\mathcal{E}_{1cw}\right|^2\right) - 1\right]\mathcal{E}_{2ccw} - \left(\tilde{k}_{d2} + i\,\tilde{k}_{c2}\right)\mathcal{E}_{2cw}, \tag{2.134}$$

$$\begin{aligned}\frac{dn}{dt} = \frac{\gamma}{\kappa}\Big[&\mu - n - g_1 n\left(1 - s_0\left|\mathcal{E}_{1cw}\right|^2 - c_0\left|\mathcal{E}_{1ccw}\right|^2 - s_1\left|\mathcal{E}_{2cw}\right|^2 - c_1\left|\mathcal{E}_{2ccw}\right|^2\right)\\ &- g_1 n\left(1 - s_0\left|\mathcal{E}_{1ccw}\right|^2 - c_0\left|\mathcal{E}_{1cw}\right|^2 - s_1\left|\mathcal{E}_{2ccw}\right|^2 - c_1\left|\mathcal{E}_{2cw}\right|^2\right)\\ &- g_2 n\left(1 - s_0\left|\mathcal{E}_{2cw}\right|^2 - c_0\left|\mathcal{E}_{2ccw}\right|^2 - \tilde{s}_1\left|\mathcal{E}_{1cw}\right|^2 - \tilde{c}_1\left|\mathcal{E}_{1ccw}\right|^2\right)\\ &- g_2 n\left(1 - s_0\left|\mathcal{E}_{2ccw}\right|^2 - c_0\left|\mathcal{E}_{2cw}\right|^2 - \tilde{s}_1\left|\mathcal{E}_{1ccw}\right|^2 - \tilde{c}_1\left|\mathcal{E}_{1cw}\right|^2\right)\Big].\end{aligned} \tag{2.135}$$

$\mu = 1$ corresponds to the threshold condition of the laser. Later we will use a different time scaling, hence it is more appropriate to restore the dimension of the time t. That is why we will use the following set of equations as a starting point in chapter 3:

$$\frac{d\mathcal{E}_{1cw}}{dt} = \kappa(1+i\alpha)\left[N g_1\left(1 - s_0\left|\mathcal{E}_{1cw}\right|^2 - c_0\left|\mathcal{E}_{1ccw}\right|^2 - s_1\left|\mathcal{E}_{2cw}\right|^2 - c_1\left|\mathcal{E}_{2ccw}\right|^2\right) - 1\right]\mathcal{E}_{1cw} - (k_{d1} + i\,k_{c1})\,\mathcal{E}_{1ccw}, \tag{2.136}$$

$$\frac{d\mathcal{E}_{1ccw}}{dt} = \kappa(1+i\alpha)\left[N g_1\left(1 - s_0\left|\mathcal{E}_{1ccw}\right|^2 - c_0\left|\mathcal{E}_{1cw}\right|^2 - s_1\left|\mathcal{E}_{2ccw}\right|^2 - c_1\left|\mathcal{E}_{2cw}\right|^2\right) - 1\right]\mathcal{E}_{1ccw} - (k_{d1} + i\,k_{c1})\,\mathcal{E}_{1cw}, \tag{2.137}$$

$$\frac{d\mathcal{E}_{2cw}}{dt} = \kappa(1+i\alpha)\left[N g_2\left(1 - s_0\left|\mathcal{E}_{2cw}\right|^2 - c_0\left|\mathcal{E}_{2ccw}\right|^2 - \tilde{s}_1\left|\mathcal{E}_{1cw}\right|^2 - \tilde{c}_1\left|\mathcal{E}_{1ccw}\right|^2\right) - 1\right]\mathcal{E}_{2cw} - (k_{d2} + i\,k_{c2})\,\mathcal{E}_{2ccw}, \tag{2.138}$$

$$\frac{d\mathcal{E}_{2ccw}}{dt} = \kappa(1+i\alpha)\left[N g_2\left(1 - s_0\left|\mathcal{E}_{2ccw}\right|^2 - c_0\left|\mathcal{E}_{2cw}\right|^2 - \tilde{s}_1\left|\mathcal{E}_{1ccw}\right|^2 - \tilde{c}_1\left|\mathcal{E}_{1cw}\right|^2\right) - 1\right]\mathcal{E}_{2ccw} - (k_{d2} + i\,k_{c2})\,\mathcal{E}_{2cw}, \tag{2.139}$$

$$\begin{aligned}\frac{dN}{dt} = \gamma \Big[& \mu - N - N g_1 \left(1 - s_0 \left|\mathcal{E}_{1cw}\right|^2 - c_0 \left|\mathcal{E}_{1ccw}\right|^2 - s_1 \left|\mathcal{E}_{2cw}\right|^2 - c_1 \left|\mathcal{E}_{2ccw}\right|^2\right) \left|\mathcal{E}_{1cw}\right|^2 \\ & - N g_1 \left(1 - s_0 \left|\mathcal{E}_{1ccw}\right|^2 - c_0 \left|\mathcal{E}_{1cw}\right|^2 - s_1 \left|\mathcal{E}_{2ccw}\right|^2 - c_1 \left|\mathcal{E}_{2cw}\right|^2\right) \left|\mathcal{E}_{1ccw}\right|^2 \\ & - N g_2 \left(1 - s_0 \left|\mathcal{E}_{2cw}\right|^2 - c_0 \left|\mathcal{E}_{2ccw}\right|^2 - \tilde{s}_1 \left|\mathcal{E}_{1cw}\right|^2 - \tilde{c}_1 \left|\mathcal{E}_{1ccw}\right|^2\right) \left|\mathcal{E}_{2cw}\right|^2 \\ & - N g_2 \left(1 - s_0 \left|\mathcal{E}_{2ccw}\right|^2 - c_0 \left|\mathcal{E}_{2cw}\right|^2 - \tilde{s}_1 \left|\mathcal{E}_{1ccw}\right|^2 - \tilde{c}_1 \left|\mathcal{E}_{1cw}\right|^2\right) \left|\mathcal{E}_{2ccw}\right|^2 \Big], \end{aligned} \tag{2.140}$$

with $\kappa = \frac{1}{\tau_p}$ and N representing the carrier number.

Chapter 3

The Reduced Model for a Semiconductor Ring Laser with Two Longitudinal Modes

In this chapter, we go more into depth about the operation of a multimode system. Using some asymptotic methods similar to the ones used by Van der Sande *et al.* [34], we reduce the set of rate equations that we obtained in the previous chapter from 9 to 5 real equations. A multiple time scale analysis allows us to eliminate all but the slowest time scales. We determine the steady-state solutions and present some simulation results.

3.1 Operation of a Multimode Semiconductor Ring Laser

In a circular resonator, it is very likely that multiple wavelengths are stable. Similar to a Fabry-Pérot laser cavity, a whole series of wavelengths satisfies the phase condition that a roundtrip equals a phase shift of 2π. Normally, the factor that selects one of these wavelengths is the gain spectrum. One of the longitudinal modes will experience the largest gain and suppress the others. However, it is possible that the peak of the gain spectrum is very wide and that several wavelengths 'see' more or less the same gain. As a consequence a set of modes will lase, each with a slightly different threshold value, because of very small gain differences. The fact that more than one longitudinal mode is present has some serious implications on the operation of the ring laser. Not only interaction between two counter-propagating modes of the same frequency has to be taken into account, but also inter-frequency interactions. Every mode will get saturated by itself, by its counter-propagating equivalent and also by the two counter-propagating modes of the other frequencies. It gets even more complicated if one takes a look at the saturation coefficients, because it is perfectly possible that one frequency is

less saturated by the others than vice versa. In the following study of the problem, we assume that the backscattering process will not couple energy from one longitudinal mode into another. This can be excepted as a reasonable assumption, keeping in mind that it is a linear coupling between two modes. It is just a reflection that sends a wave in the opposite direction, so no frequency changes can take place there.
As mentioned before, the gain curve is not a perfectly flat curve. Although some wavelengths experience enough gain to make lasing possible, there will be small differences. These differences in gain will have their part in shaping the P-I curve, e.g. different longitudinal modes will have different thresholds. Also, the gain can vary with the pump current. As the current increases, the gain spectrum will shift slightly, but that shift can be sufficient to introduce another longitudinal mode or change the mode with the highest gain. Another problem when changing the pump current is that it cannot be avoided that the device's temperature will rise with increasing current. The ring laser is mounted on a heatsink, but this will not prevent the device from getting warmer. An increase in temperature results in an expansion of the device and therefore, the cavity. It is clear that this is an important problem, since other wavelengths will now fulfill the 2π condition. In chapter 2, we have found that the model in case of two longitudinal modes can be described by the following set of rate equations:

$$\begin{aligned}
\dot{\mathcal{E}}_{1cw} &= \kappa(1+i\alpha)\left[Ng_1\left(1-s_0\left|\mathcal{E}_{1cw}\right|^2-c_0\left|\mathcal{E}_{1ccw}\right|^2-s_1\left|\mathcal{E}_{2cw}\right|^2-c_1\left|\mathcal{E}_{2ccw}\right|^2\right)-1\right]\mathcal{E}_{1cw} \\
&\quad -(k_{d1}+i\,k_{c1})\,\mathcal{E}_{1ccw} \qquad (3.1)\\
\dot{\mathcal{E}}_{1ccw} &= \kappa(1+i\alpha)\left[Ng_1\left(1-s_0\left|\mathcal{E}_{1ccw}\right|^2-c_0\left|\mathcal{E}_{1cw}\right|^2-s_1\left|\mathcal{E}_{2ccw}\right|^2-c_1\left|\mathcal{E}_{2cw}\right|^2\right)-1\right]\mathcal{E}_{1ccw} \\
&\quad -(k_{d1}+i\,k_{c1})\,\mathcal{E}_{1cw} \qquad (3.2)\\
\dot{\mathcal{E}}_{2cw} &= \kappa(1+i\alpha)\left[Ng_2\left(1-s_0\left|\mathcal{E}_{2cw}\right|^2-c_0\left|\mathcal{E}_{2ccw}\right|^2-\tilde{s}_1\left|\mathcal{E}_{1cw}\right|^2-\tilde{c}_1\left|\mathcal{E}_{1ccw}\right|^2\right)-1\right]\mathcal{E}_{2cw} \\
&\quad -(k_{d2}+i\,k_{c2})\,\mathcal{E}_{2ccw} \qquad (3.3)\\
\dot{\mathcal{E}}_{2ccw} &= \kappa(1+i\alpha)\left[Ng_2\left(1-s_0\left|\mathcal{E}_{2ccw}\right|^2-c_0\left|\mathcal{E}_{2cw}\right|^2-\tilde{s}_1\left|\mathcal{E}_{1ccw}\right|^2-\tilde{c}_1\left|\mathcal{E}_{1cw}\right|^2\right)-1\right]\mathcal{E}_{2ccw} \\
&\quad -(k_{d2}+i\,k_{c2})\,\mathcal{E}_{2cw} \qquad (3.4)\\
\dot{N} &= \gamma\Big[\mu-N-Ng_1\left(1-s_0\left|\mathcal{E}_{1cw}\right|^2-c_0\left|\mathcal{E}_{1ccw}\right|^2-s_1\left|\mathcal{E}_{2cw}\right|^2-c_1\left|\mathcal{E}_{2ccw}\right|^2\right)\left|\mathcal{E}_{1cw}\right|^2 \\
&\quad -Ng_1\left(1-s_0\left|\mathcal{E}_{1ccw}\right|^2-c_0\left|\mathcal{E}_{1cw}\right|^2-s_1\left|\mathcal{E}_{2ccw}\right|^2-c_1\left|\mathcal{E}_{2cw}\right|^2\right)\left|\mathcal{E}_{1ccw}\right|^2 \\
&\quad -Ng_2\left(1-s_0\left|\mathcal{E}_{2cw}\right|^2-c_0\left|\mathcal{E}_{2ccw}\right|^2-\tilde{s}_1\left|\mathcal{E}_{1cw}\right|^2-\tilde{c}_1\left|\mathcal{E}_{1ccw}\right|^2\right)\left|\mathcal{E}_{2cw}\right|^2 \\
&\quad -Ng_2\left(1-s_0\left|\mathcal{E}_{2ccw}\right|^2-c_0\left|\mathcal{E}_{2cw}\right|^2-\tilde{s}_1\left|\mathcal{E}_{1ccw}\right|^2-\tilde{c}_1\left|\mathcal{E}_{1cw}\right|^2\right)\left|\mathcal{E}_{2ccw}\right|^2 \qquad (3.5)
\end{aligned}$$

The dots here represent the derivative with respect to T. κ is the field decay rate, while γ denotes the decay rate of the carrier population. α is the linewidth enhancement factor and μ is the renormalised injection current, which is defined such that $\mu = 1$ at lasing threshold. N is the current density, rescaled, such that is 0 at transparency. The linear coupling between two counter-propagating modes with the same frequency is provided by the backscattering coefficients k_{d1}, k_{c1}, k_{d2} en k_{c2} and the nonlinear coupling is present in the form of saturation coefficients. Remark that there is no backscattering

from one frequency to another. Also the possibility for the different longitudinal modes to 'feel' another differential gain is foreseen by using g_1 and g_2. These factors can be current dependent and are vital for this model, even a difference of a few promille may cause one mode to be completely suppressed by the other.

3.2 Amplitude-Phase Decomposition

Since the electrical field is a complex variable, Eqs. (3.1)-(3.4) can all four of them be split up in real and imaginary parts. In principle there are eight real field equations plus a real carrier equation. A possible way to separate the real and imaginary parts is to apply what is called an amplitude-phase decomposition. This means that the electric field variable E must explicitly be written as the product of a real amplitude and a complex exponent representing the phase. This should be done for all four electric fields present in the cavity.

$$\mathcal{E}_{1ccw} = Q_{1ccw} e^{i\phi_{1ccw}}, \tag{3.6}$$
$$\mathcal{E}_{1cw} = Q_{1cw} e^{i\phi_{1cw}}, \tag{3.7}$$
$$\mathcal{E}_{2ccw} = Q_{2ccw} e^{i\phi_{2ccw}}, \tag{3.8}$$
$$\mathcal{E}_{2cw} = Q_{2cw} e^{i\phi_{2cw}}. \tag{3.9}$$

In the left segment of each equation a derivative with respect to time is found. If we take the derivatives of Eqs. (3.6)- (3.9), we get

$$\dot{\mathcal{E}}_{1ccw} = \dot{Q}_{1ccw} e^{i\phi_{1ccw}} + Q_{1ccw} e^{i\phi_{1ccw}} \dot{\phi}_{1ccw}, \tag{3.10}$$
$$\dot{\mathcal{E}}_{1cw} = \dot{Q}_{1cw} e^{i\phi_{1cw}} + Q_{1cw} e^{i\phi_{1cw}} \dot{\phi}_{1cw}, \tag{3.11}$$
$$\dot{\mathcal{E}}_{2ccw} = \dot{Q}_{2ccw} e^{i\phi_{2ccw}} + Q_{2ccw} e^{i\phi_{2ccw}} \dot{\phi}_{2ccw}, \tag{3.12}$$
$$\dot{\mathcal{E}}_{2cw} = \dot{Q}_{2cw} e^{i\phi_{2cw}} + Q_{2cw} e^{i\phi_{2cw}} \dot{\phi}_{2cw}. \tag{3.13}$$

One notices instantly that in each of the Eqs. (3.10)-(3.13) the original phase terms are still present in every term. If we substitute Eqs. (3.10)-(3.13) in Eqs. (3.1)-(3.4) and then divide both segments of the equation by this phase term, only the phase difference between two phases of the same longitudinal mode will remain. If we introduce a new substitution

$$\psi_1 = \phi_{1ccw} - \phi_{1cw}, \tag{3.14}$$
$$\psi_2 = \phi_{2ccw} - \phi_{2cw}, \tag{3.15}$$

with $\psi_i \in [0, 2\pi[$, all single phase terms can be eliminated. Because only the difference appears in the other equations, the phase equations we found from the imaginary part can be subtracted to form a phase difference. This means we already have two

equations less. Another substitution we will carry through involves the backscattering coefficients. The sum $k_{d1,2} + i\,k_{c1,2}$ can be rewritten as $k_{1,2}\,e^{i\phi_{k1,2}}$. Later it will become clear why this is a more elegant way of writing down the backscattering. Eqs. (3.10)- (3.15) can now be formulated as:

$$\begin{aligned}
\dot{Q}_{1cw} &= \kappa(1+i\alpha)\left[Ng_1\left(1 - s_0Q_{1cw}^2 - c_0Q_{1ccw}^2 - s_1Q_{2cw}^2 - c_1Q_{2ccw}^2\right) - 1\right]Q_{1cw} \\
&\quad - k_1\left(cos(\phi_{k1} + \psi_1)\right)Q_{1ccw}, \qquad (3.16)\\
\dot{Q}_{1ccw} &= \kappa(1+i\alpha)\left[Ng_1\left(1 - s_0Q_{1ccw}^2 - c_0Q_{1cw}^2 - s_1Q_{2ccw}^2 - c_1Q_{2cw}^2\right) - 1\right]Q_{1ccw} \\
&\quad - k_1\left(cos(\phi_{k1} - \psi_1)\right)Q_{1cw}, \qquad (3.17)\\
\dot{Q}_{2cw} &= \kappa(1+i\alpha)\left[Ng_2\left(1 - s_0Q_{2cw}^2 - c_0Q_{2ccw}^2 - \tilde{s}_1Q_{1cw}^2 - \tilde{c}_1Q_{1ccw}^2\right) - 1\right]Q_{2cw} \\
&\quad - k_2\left(cos(\phi_{k2} + \psi_2)\right)Q_{2ccw}, \qquad (3.18)\\
\dot{Q}_{2ccw} &= \kappa(1+i\alpha)\left[Ng_2\left(1 - s_0Q_{2ccw}^2 - c_0Q_{2cw}^2 - \tilde{s}_1Q_{1ccw}^2 - \tilde{c}_1Q_{1cw}^2\right) - 1\right]Q_{2ccw} \\
&\quad - k_2\left(cos(\phi_{k2} - \psi_2)\right)Q_{2cw}, \qquad (3.19)\\
\dot{\psi}_1 &= \kappa\alpha Ng_1\left[(s_0 - c_0)(Q_{1cw}^2 - Q_{1ccw}^2) + (s_1 - c_1)(Q_{2cw}^2 - Q_{2ccw}^2)\right] \\
&\quad - k_1\left[\sin(\phi_{k1} - \psi_1)\frac{Q_{1cw}}{Q_{1ccw}} - \sin(\phi_{k1} + \psi_1)\frac{Q_{1ccw}}{Q_{1cw}}\right], \qquad (3.20)\\
\dot{\psi}_2 &= \kappa\alpha Ng_2\left[(s_0 - c_0)(Q_{2cw}^2 - Q_{2ccw}^2) + (s_2 - c_2)(Q_{1cw}^2 - Q_{1ccw}^2)\right] \\
&\quad - k_2\left[\sin(\phi_{k2} - \psi_2)\frac{Q_{2cw}}{Q_{2ccw}} - \sin(\phi_{k2} + \psi_2)\frac{Q_{2ccw}}{Q_{2cw}}\right], \qquad (3.21)
\end{aligned}$$

$$\begin{aligned}
\dot{N} &= \gamma\Big[\mu - N - Ng_1\left(1 - s_0Q_{1cw}^2 - c_0Q_{1ccw}^2 - s_1Q_{2cw}^2 - c_1Q_{2ccw}^2\right)Q_{1cw}^2 \\
&\quad - Ng_1\left(1 - s_0Q_{1ccw}^2 - c_0Q_{1cw}^2 - s_1Q_{2ccw}^2 - c_1Q_{2cw}^2\right)Q_{1ccw}^2 \\
&\quad - Ng_2\left(1 - s_0Q_{2cw}^2 - c_0Q_{2ccw}^2 - \tilde{s}_1Q_{1cw}^2 - \tilde{c}_1Q_{1ccw}^2\right)Q_{2cw}^2 \\
&\quad - Ng_2\left(1 - s_0Q_{2ccw}^2 - c_0Q_{2cw}^2 - \tilde{s}_1Q_{1ccw}^2 - \tilde{c}_1Q_{1cw}^2\right)Q_{2ccw}^2\Big]. \qquad (3.22)
\end{aligned}$$

3.3 Multiple Scales Analysis

It can be remarked that in the model used to describe the multimode situation, the values of the parameters span a range of several orders of magnitude. This provides the opportunity for a first reduction step. From numerical simulations done by Van der Sande *et al.* [34] we know that the backscattering coefficients $k_{d1,2}$ and $k_{c1,2}$ are an order of magnitude smaller than the parameter κ. They have also found that N, which is a dynamical variable, has a value near to 1. The saturation coefficients have small values compared 1. What is more, g_1 and g_2 have values very close to 1, due

to the nondimensionalisation of the original model. Two new parameters need to be constructed. First, we introduce a dimensionless time τ,

$$\tau = \gamma T, \tag{3.23}$$

thus the original time is scaled with the carrier life time. Next, the smallness parameter ρ will allow us to describe mathematically what are small parameter values,

$$\rho = \frac{\gamma}{\kappa}. \tag{3.24}$$

Furthermore, we express that the carrier density will be approximately 1:

$$N = 1 + \rho n, \tag{3.25}$$

with n of $O(1)$. We know that the saturation and backscattering coefficients are very small, of $O(\rho)$. To express this we put

$$s_0 = \rho S_0 \qquad c_0 = \rho C_0, \tag{3.26}$$
$$s_1 = \rho S_1 \qquad c_1 = \rho C_1, \tag{3.27}$$
$$\tilde{s}_1 = \rho \tilde{S}_1 \qquad \tilde{c}_1 = \rho \tilde{C}_1, \tag{3.28}$$
$$k_{d1} = \kappa\rho K_{d1} \qquad k_{c1} = \kappa\rho K_{c1}, \tag{3.29}$$
$$k_{d2} = \kappa\rho K_{d2} \qquad k_{c2} = \kappa\rho K_{c2}. \tag{3.30}$$

Also the differential gain factors can be written in a more useful way for further reduction of the model. The two gain factors are almost 1. For use at a later stage of the reduction, we define the gain factors in a symmetric way:

$$g_1 = 1 - \frac{\rho G}{2}, \tag{3.31}$$
$$g_2 = 1 + \frac{\rho G}{2}. \tag{3.32}$$

A new symbol appears, G, or the difference in differential gain between the two longitudinal modes. G is again of $O(1)$ and expresses which of the two modes experiences the largest differential gain. If one wishes to favour the other mode, the sign of the gain simply has to be reversed. The next step is to substitute the new parameters in the rate equations. From the numerical simulations we know that ρ is of the order of 10^{-3}. Hence, it becomes acceptable to neglect all the terms of $O(\rho^2)$. Finally, a reduced model

can be proposed:

$$Q'_{1cw} = \left[n - \frac{G}{2} - S_0 Q_{1cw}^2 - C_0 Q_{1ccw}^2 - S_1 Q_{2cw}^2 - C_1 Q_{2ccw}^2\right] Q_{1cw} - K_1 \cos(\psi_1 + \phi_{k1}) Q_{1ccw}, \tag{3.33}$$

$$Q'_{1ccw} = \left[n - \frac{G}{2} - S_0 Q_{1ccw}^2 - C_0 Q_{1cw}^2 - S_1 Q_{2ccw}^2 - C_1 Q_{2cw}^2\right] Q_{1ccw} - K_1 \cos(-\psi_1 + \phi_{k1}) Q_{1cw}, \tag{3.34}$$

$$Q'_{2cw} = \left[n + \frac{G}{2} - S_0 Q_{2cw}^2 - C_0 Q_{2ccw}^2 - \tilde{S}_1 Q_{1cw}^2 - \tilde{C}_1 Q_{1ccw}^2\right] Q_{2cw} - K_2 \cos(\psi_2 + \phi_{k2}) Q_{2ccw}, \tag{3.35}$$

$$Q'_{2ccw} = \left[n + \frac{G}{2} - S_0 Q_{2ccw}^2 - C_0 Q_{2cw}^2 - \tilde{S}_1 Q_{1ccw}^2 - \tilde{c}_1 Q_{1cw}^2\right] Q_{2ccw} - K_2 \cos(-\psi_2 + \phi_{k2}) Q_{2cw}, \tag{3.36}$$

$$\psi'_1 = \alpha\left[(S_0 - C_0)\left(Q_{1cw}^2 - Q_{1ccw}^2\right) + (S_1 - C_1)\left(Q_{2cw}^2 - Q_{2ccw}^2\right)\right] - K_1\left[\sin(-\psi_1 + \phi_{k1})\frac{Q_{1cw}}{Q_{1ccw}} - \sin(\psi_1 + \phi_{k1})\frac{Q_{1ccw}}{Q_{1cw}}\right], \tag{3.37}$$

$$\psi'_2 = \alpha\left[(S_0 - C_0)\left(Q_{2cw}^2 - Q_{2ccw}^2\right) + \left(\tilde{S}_1 - \tilde{C}_1\right)\left(Q_{1cw}^2 - Q_{1ccw}^2\right)\right] - K_2\left[\sin(-\psi_2 + \phi_{k2})\frac{Q_{2cw}}{Q_{2ccw}} - \sin(\psi_2 + \phi_{k2})\frac{Q_{2ccw}}{Q_{2cw}}\right], \tag{3.38}$$

$$n = \frac{1}{\mu - 1}\left[S_0\left(Q_{1cw}^4 + Q_{1ccw}^4 + Q_{2cw}^4 + Q_{2ccw}^4\right) + 2C_0\left(Q_{1cw}^2 Q_{1ccw}^2 + Q_{2cw}^2 Q_{2ccw}^2\right) + \left(S_1 + \tilde{S}_1\right)\left(Q_{1cw}^2 Q_{2cw}^2 + Q_{1ccw}^2 Q_{2ccw}^2\right) + \left(C_1 + \tilde{C}_1\right)\left(Q_{1cw}^2 Q_{2ccw}^2 + Q_{2cw}^2 Q_{1ccw}^2\right) + \frac{G}{2}\left(Q_{1cw}^2 + Q_{1ccw}^2 - Q_{2cw}^2 - Q_{2ccw}^2\right) + 2K_1 \cos\psi_1 \cos\phi_{k1} Q_{1cw} Q_{1ccw} + 2K_2 \cos\psi_2 \cos\phi_{k2} Q_{2cw} Q_{2ccw}\right], \tag{3.39}$$

$$\mu - 1 = Q_{1cw}^2 + Q_{1ccw}^2 + Q_{2cw}^2 + Q_{2ccw}^2. \tag{3.40}$$

In the above set of equations, Eq. (3.39) is no longer a real rate equation. It is just an equation that gives the value of n to be substituted in Eqs. (3.33)- (3.36). The multiple scales analysis and the subsequent neglecting of terms of $O(\rho^2)$ has transformed the equation for $\dot{N}$ into Eq. (3.40). Basically, this is a conservation law, pointing out that the sum of the intensities should always equal $\mu - 1$.

The system is fully determined. It consists of six independent equations and six variables ($Q_{1cw}, Q_{1ccw}, Q_{2cw}, Q_{2ccw}, \psi_1, \psi_2$). Although the model is correct for time scales slower than the damping rate of the relaxation oscillations, in the order of GHz, it is not completely satisfying. The equations cannot be easily interpreted. Even more, in the numerical simulations of Eqs. (3.33)- (3.40), we could not find a stable algorithm to solve these equations. After analysis of the diverging time series, we found that for

each current, all the intensities tend to go to infinity. In other words, the conservation law is violated. This numerical instability is probably due to the fact that our integration algorithm is not suitable for differential-algebraic equations. We have tried different numerical algorithms developed especially for this situation, such as those included in the mathematical packages Matlab and Mathematica, but without satisfying results. Since we attribute the numerical instability to the presence of the algebraic conservation law, we can try to have the equations satisfy the law automatically. A possible way to achieve this is by using a similar approach as in [34]. If a transformation, which represents the intensities as the product of sines and cosines, is applied, the problem mentioned above will disappear. Indeed, it is possible to define the intensities, such that the conservation law will be expressed by the sum of a square sine and a square cosine. We will clarify this approach in the following section.

3.4 Angular Representation of Intensities

Three angles are used for a complete representation of the energy distribution. θ_1 indicates the distribution of energy between the two counter-propagating modes of the first longitudinal mode, while θ_2 has the same function but for the second longitudinal mode. θ_3 indicates the distribution of energy between the two different frequencies. The coordinate transformation looks as follows

$$Q_{1cw}^2 = (\mu - 1)\cos^2\left(\frac{\theta_3 + \pi/2}{2}\right)\cos^2\left(\frac{\theta_1 + \pi/2}{2}\right), \tag{3.41}$$

$$Q_{1ccw}^2 = (\mu - 1)\cos^2\left(\frac{\theta_3 + \pi/2}{2}\right)\sin^2\left(\frac{\theta_1 + \pi/2}{2}\right), \tag{3.42}$$

$$Q_{2cw}^2 = (\mu - 1)\sin^2\left(\frac{\theta_3 + \pi/2}{2}\right)\cos^2\left(\frac{\theta_2 + \pi/2}{2}\right), \tag{3.43}$$

$$Q_{2ccw}^2 = (\mu - 1)\sin^2\left(\frac{\theta_3 + \pi/2}{2}\right)\sin^2\left(\frac{\theta_2 + \pi/2}{2}\right), \tag{3.44}$$

with $\theta_i \in [-\frac{\pi}{2}, \frac{\pi}{2}]$. Applying some simple trigonometric rules allows us to write

$$Q_{1cw}^2 = \frac{\mu - 1}{4}(1 - \sin\theta_3)(1 - \sin\theta_1), \tag{3.45}$$

$$Q_{1ccw}^2 = \frac{\mu - 1}{4}(1 - \sin\theta_3)(1 + \sin\theta_1), \tag{3.46}$$

$$Q_{2cw}^2 = \frac{\mu - 1}{4}(1 + \sin\theta_3)(1 - \sin\theta_2), \tag{3.47}$$

$$Q_{2ccw}^2 = \frac{\mu - 1}{4}(1 + \sin\theta_3)(1 + \sin\theta_2). \tag{3.48}$$

The angle variables can be interpreted as follows. If $\theta_1 = 0$, the energy is equally distributed over the two counter-propagating modes of longitudinal mode 1. A value

of $\pi/2$ or $-\pi/2$ denotes concentrating all the energy in only one of the two counter-propagating modes. θ_2 has a similar interpretation, but for the second longitudinal mode. When $\theta_2 = 0$, all energy is equally distributed over the two counter-propagating modes of longitudinal mode 2. For θ_3 a similar reasoning can be applied, only it does not consider the counter-propagating modes but the longitudinal modes. The use of angles makes it possible to represent the solutions of one longitudinal mode of the system on a sphere, as depicted in Figure 3.1.

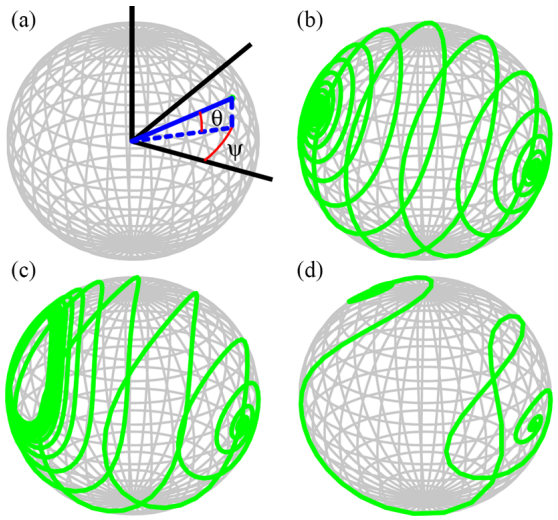

Figure 3.1: Phase-space portraits in the spherical phase space of one longitudinal mode. (a) Definition of the angles. (b) Time evolution from an unstable In-Phase Symmetric Solution to a stable Out-of-Phase Symmetric Solution. (c) Time evolution from an unstable In-Phase Symmetric Solution to stable oscillations. (d) Time evolution from an unstable In-Phase Symmetric Solution to a stable Out-of-Phase Antisymmetric Solution. Picture from Van der Sande *et al.* [34].

Keeping in mind that $\cos^2(\alpha) + \sin^2(\alpha) = 1$ for every α, one understands immediately that the sum of the four intensities equals $\mu - 1$,

$$\begin{aligned}
&Q_{1cw}^2 + Q_{1ccw}^2 + Q_{2cw}^2 + Q_{2ccw}^2 \\
&= (\mu-1)\left[\cos^2\left(\frac{\theta_3+\pi/2}{2}\right)\left(\cos^2\left(\frac{\theta_1+\pi/2}{2}\right)+\sin^2\left(\frac{\theta_1+\pi/2}{2}\right)\right)\right. \\
&\left.+\sin^2\left(\frac{\theta_3+\pi/2}{2}\right)\left(\cos^2\left(\frac{\theta_2+\pi/2}{2}\right)+\sin^2\left(\frac{\theta_2+\pi/2}{2}\right)\right)\right] \\
&= (\mu-1)\left[\cos^2\left(\frac{\theta_3+\pi/2}{2}\right)+\sin^2\left(\frac{\theta_3+\pi/2}{2}\right)\right] \\
&= \mu - 1, \qquad (3.49)
\end{aligned}$$

no matter what the angles might be. In other words, the conservation law is respected in any case, resulting in a model that can be numerically simulated without problems.

When substituted in the reduced model, one finds

$$\theta_1' = \left(\frac{\mu-1}{2}\right)\cos\theta_1\left[(C_0-S_0)\sin\theta_1(1-\sin\theta_3)+(C_1-S_1)\sin\theta_2(1+\sin\theta_3)\right] + 2K_1\left[\sin\theta_1\cos\psi_1\cos\phi_{k1}-\sin\phi_{k1}\sin\psi_1\right], \tag{3.50}$$

$$\theta_2' = \left(\frac{\mu-1}{2}\right)\cos\theta_2\left[(C_0-S_0)\sin\theta_2(1+\sin\theta_3)+(\tilde{C}_1-\tilde{S}_1)\sin\theta_1(1-\sin\theta_3)\right] + 2K_2\left[\sin\theta_2\cos\psi_2\cos\phi_{k2}-\sin\phi_{k2}\sin\psi_2\right], \tag{3.51}$$

$$\theta_3' = \frac{1-\sin\theta_3}{\cos\theta_3}\left[\frac{1-\sin\theta_1}{\cos\theta_1}\left[\theta_1'+2K_1\cos(-\psi_1+\phi_{k1})\right] - 2\left[-\frac{G}{2}+n-S_0\frac{\mu-1}{4}(1-\sin\theta_3)(1+\sin\theta_1)-C_0\frac{\mu-1}{4}(1-\sin\theta_3)(1-\sin\theta_1) -S_1\frac{\mu-1}{4}(1+\sin\theta_3)(1+\sin\theta_2)-C_1\frac{\mu-1}{4}(1+\sin\theta_3)(1-\sin\theta_2)\right]\right], \tag{3.52}$$

$$\psi_1' = \alpha\left(\frac{\mu-1}{2}\right)\left[(C_0-S_0)(1-\sin\theta_3)\sin\theta_1+(C_1-S_1)(1+\sin\theta_3)\sin\theta_2\right] + \frac{2K_1}{\cos\theta_1}\left[\cos\phi_{k1}\sin(-\psi_1)+\sin\theta_1\sin\phi_{k1}\cos\psi_1\right], \tag{3.53}$$

$$\psi_2' = \alpha\left(\frac{\mu-1}{2}\right)\left[(C_0-S_0)(1+\sin\theta_3)\sin\theta_2+\left(\tilde{C}_1-\tilde{S}_1\right)(1-\sin\theta_3)\sin\theta_1\right] + \frac{2K_2}{\cos\theta_2}\left[\cos\phi_{k2}\sin(-\psi_2)+\sin\theta_2\sin\phi_{k2}\cos\psi_2\right]. \tag{3.54}$$

with

$$\begin{aligned} n = {} & \frac{S_0}{8}(\mu-1)\left((1-\sin\theta_3)^2(1+\sin^2\theta_1)+(1+\sin\theta_3)^2(1+\sin^2\theta_2)\right) \\ & + \frac{C_0}{8}(\mu-1)\left((1-\sin\theta_3)^2\cos^2\theta_1+(1+\sin\theta_3)^2\cos^2\theta_2\right) \\ & + \frac{S_1+\tilde{S}_1}{8}(\mu-1)\cos^2\theta_3(1+\sin\theta_1\sin\theta_2) \\ & + \frac{C_1+\tilde{C}_1}{8}(\mu-1)\cos^2\theta_3(1-\sin\theta_1\sin\theta_2) \\ & - \frac{G}{2}\sin\theta_3 \\ & + \frac{K_1}{2}\cos\psi_1\cos\phi_{k1}(1-\sin\theta_3)\cos\theta_1+\frac{K_2}{2}\cos\psi_2\cos\phi_{k2}(1+\sin\theta_3)\cos\theta_2. \end{aligned} \tag{3.55}$$

When we now solve the equations numerically, the violation of the conservation law has disappeared. Although the reduction has some significant benefits concerning the numerical simulation, the primary goal, namely having equations that can easily be

interpreted, has not been achieved yet. At first glance the equations seem enormous, but with only a few assumptions they simplify considerably. We first consider

$$K_1 = K_2 \equiv K, \tag{3.56}$$

then, all the equations are divided by a common factor K, the backscattering magnitude. A new time is defined

$$\tau_{new} = K\tau_{old}, \tag{3.57}$$

along with some new variables.

$$J = \frac{(C_0 - S_0)(\mu - 1)}{2K}, \tag{3.58}$$

$$\Gamma = \frac{G}{K}. \tag{3.59}$$

These last two definitions make the equations more readable and change nothing to the actual model. Furthermore, some of the different saturation coefficients can be taken equal. A possible combination is $S_1 = C_1 = \tilde{S}_1 = \tilde{C}_1 \equiv S$. In other words, the inter-frequency saturation coefficients are equal. Every mode is in the same way saturated by the modes of another frequency. This assumption leads to a synoptic set of equations:

$$\theta_1' = J\cos\theta_1 \sin\theta_1(1 - \sin\theta_3) + 2\left(\sin\theta_1\cos\psi_1\cos\phi_{k1} - \sin\phi_{k1}\sin\psi_1\right), \tag{3.60}$$

$$\theta_2' = J\cos\theta_2 \sin\theta_2(1 + \sin\theta_3) + 2\left(\sin\theta_2\cos\psi_2\cos\phi_{k2} - \sin\phi_{k2}\sin\psi_2\right), \tag{3.61}$$

$$\begin{aligned}\theta_3' = {} & \frac{J\cos\theta_3}{2}\left[(\sin\theta_3 - 1)\sin^2\theta_1 + (\sin\theta_3 + 1)\sin^2\theta_2 + \sin\theta_3\sigma\right] \\ & + \Gamma\cos\theta_3 + \cos\theta_3\left[\cos\theta_1\cos\psi_1\cos\phi_{k1} - \cos\theta_2\cos\psi_2\cos\phi_{k2}\right],\end{aligned} \tag{3.62}$$

$$\psi_1' = J\alpha(1 - \sin\theta_3)\sin\theta_1 + \frac{2}{\cos\theta_1}\left[\cos\phi_{k1}\sin\psi_1 + \sin\theta_1\sin\phi_{k1}\cos\psi_1\right], \tag{3.63}$$

$$\psi_2' = J\alpha(1 + \sin\theta_3)\sin\theta_2 + \frac{2}{\cos\theta_2}\left[\cos\phi_{k2}\sin\psi_2 + \sin\theta_2\sin\phi_{k2}\cos\psi_2\right]. \tag{3.64}$$

In the above equations, the effect of saturation can be described by a single variable:

$$\sigma = \frac{4S - 2(S_0 + C_0)}{C_0 - S_0}, \tag{3.65}$$

Although the differences between these coefficients will be extremely small, we will continue the study of this model assuming that $S_1 = C_1$ and $\tilde{S}_1 = \tilde{C}_1$, but not $S_1 = \tilde{S}_1$. This means that within one longitudinal mode, a mode gets equally saturated by both modes with another frequency. However, there still is a difference in saturation strength

between the two longitudinal modes. If we do this, we get

$$\theta_1^{'} = J\cos\theta_1\sin\theta_1(1-\sin\theta_3) + 2\Big(\sin\theta_1\cos\psi_1\cos\phi_{k1} - \sin\phi_{k1}\sin\psi_1\Big), \tag{3.66}$$

$$\theta_2^{'} = J\cos\theta_2\sin\theta_2(1+\sin\theta_3) + 2\Big(\sin\theta_2\cos\psi_2\cos\phi_{k2} - \sin\phi_{k2}\sin\psi_2\Big), \tag{3.67}$$

$$\begin{aligned}\theta_3^{'} = {} & \frac{J\cos\theta_3}{2}\Big[(\sin\theta_3-1)\sin^2\theta_1 + (\sin\theta_3+1)\sin^2\theta_2 + \sigma_1 + \sin\theta_3\sigma_2\Big] \\ & + \Gamma\cos\theta_3 + \cos\theta_3\Big[\cos\theta_1\cos\psi_1\cos\phi_{k1} - \cos\theta_2\cos\psi_2\cos\phi_{k2}\Big],\end{aligned} \tag{3.68}$$

$$\psi_1^{'} = J\alpha(1-\sin\theta_3)\sin\theta_1 + \frac{2}{\cos\theta_1}\Big[\cos\phi_{k1}\sin\psi_1 + \sin\theta_1\sin\phi_{k1}\cos\psi_1\Big], \tag{3.69}$$

$$\psi_2^{'} = J\alpha(1+\sin\theta_3)\sin\theta_2 + \frac{2}{\cos\theta_2}\Big[\cos\phi_{k2}\sin\psi_2 + \sin\theta_2\sin\phi_{k2}\cos\psi_2\Big]. \tag{3.70}$$

Now, the saturation is described by two independent variables, σ_1 and σ_2.

$$\sigma_1 = 2\left(\frac{S_1 - \tilde{S}_1}{C_0 - S_0}\right), \tag{3.71}$$

$$\sigma_2 = 2\left(\frac{(S_1 + \tilde{S}_1) - (S_0 + C_0)}{C_0 - S_0}\right). \tag{3.72}$$

It is obvious that if one sets $S_1 = \tilde{S}_1$ the Eqs. (3.66)- (3.70) reduce to Eqs. (3.60)- (3.64) with $\sigma_1 = 0$ and $\sigma_2 = \sigma$.

3.5 Validation of the Model

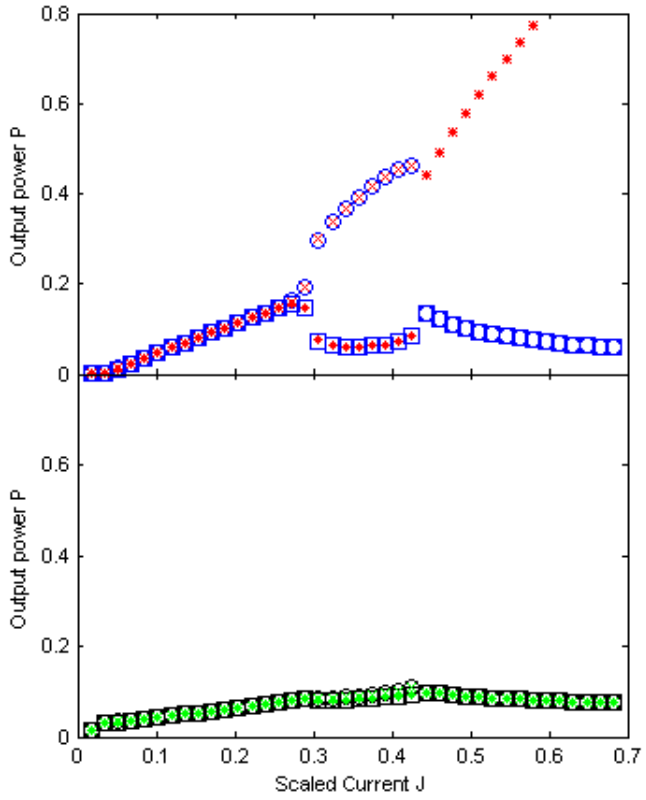

Figure 3.2: Numerically calculated P-I curve, using the full model, Eqs. (3.1)- (3.5). The parameters are: $\gamma = 0.002 s_0 = 0.01$, $c_0 = 0.02$, $s_1 = 0$, $c_1 = 0$, $\tilde{s}_1 = 0.01$, $\tilde{c}_1 = 0.01$, $k_{d1} = k_{d2} = 3.2616 \times 10^{-4}$, $k_{c1} = k_{c2} = 0.0044$, $\alpha = 3.5$, $\phi_{k1} = \phi_{k2} = 1.4966$, $g_1 = 0.9996$ and $g_2 = 1.0004$. The maxima and minima of $|E_{1cw}|^2$ ($|E_{1ccw}|^2$) are denoted by open blue squares and circles (red crosses and dots), respectively. For the second longitudinal mode, the maxima and minima of $|E_{2cw}|^2$ ($|E_{2ccw}|^2$) are denoted by open black squares and circles (green crosses and dots), respectively.

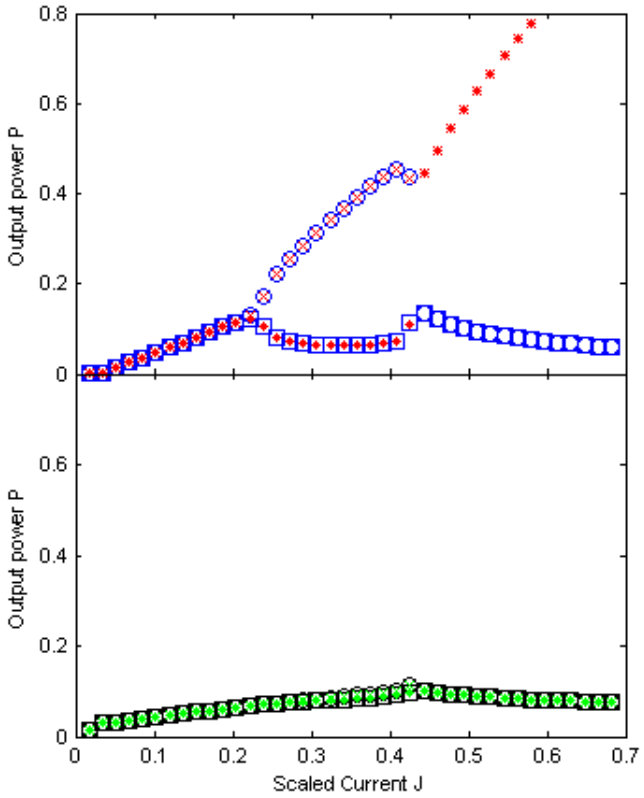

Figure 3.3: The intensities of the numerically calculated P-I curve, defined the same way as in Figure 3.2, using the reduced model, Eqs. (3.66)- (3.70). $\sigma_1 = -2$, $\sigma_2 = -4$, $\alpha = 3.5$, $\phi_{k1} = \phi_{k2} = 1.4966$ and $\Gamma = 0.0909$.

In Figure 3.2, the P-I curve using the equations of the full model is depicted, for intelligibility vs. the scaled current of the reduced model. When we compare this with the result we obtain from reduced model, Figure 3.3, we find that the curves are similar. One notices that in the proximity of the first bifurcation point, there is a slight difference. In the full model, the bifurcation starts somewhat later, but is more abrupt. Hence, the intensities in the two models converge to the same value if we go to currents, a bit higher than the bifurcation current. In Figure 3.4 the angles corresponding to the situation in Figure 3.3 are depicted as a function of the pump current.

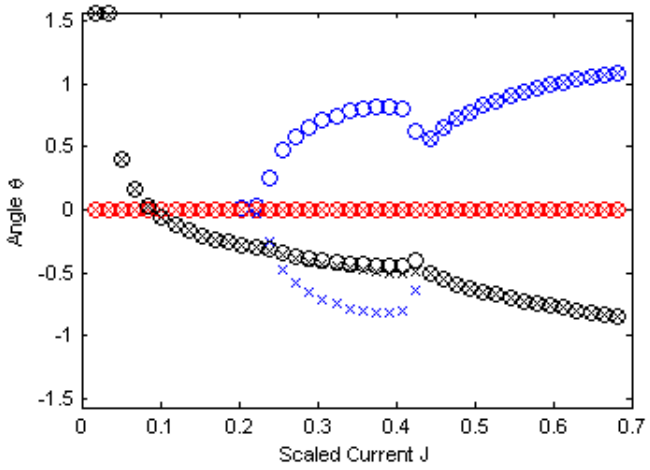

Figure 3.4: The values of the angles used to indicate the energy distribution between the modes. θ_1 (blue), θ_2 (red) and θ_3 (black).

When we compare the time traces at corresponding currents, we find Figure 3.5(a) for the full model and Figure 3.5(b) for the reduced model. In this comparison it becomes clear that in the reduced model the fast dynamics have been eliminated. The figure depicts a current step from 1.1 to 1.2 at time $t = 0$. In the full model, fast dynamics make sure that the steady-state values are almost immediately reached. In the reduced model, only slow dynamics are present, resulting in a significantly longer time to reach the steady-state value. However, the steady-state value itself is equal in both models.

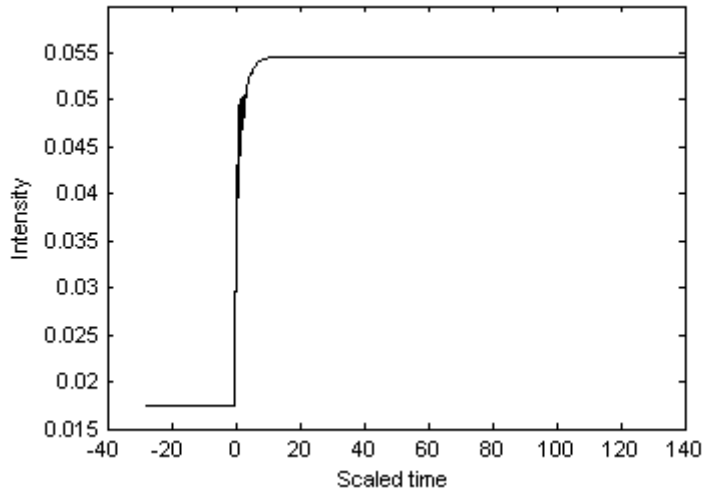

(a)

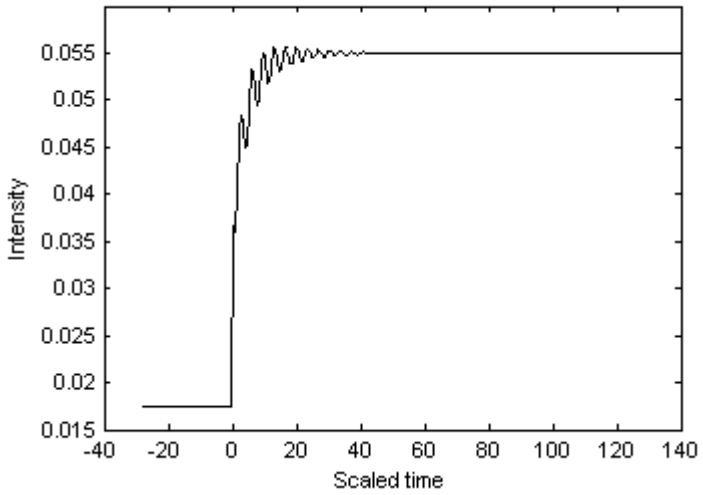

(b)

Figure 3.5: (a) Timetrace of the intensity for the full model, with identical parameters as in Figure 3.2. (b) Timetrace of the intensity for the reduced model, with identical parameters as in Figure 3.3. It becomes clear that in the full model, fast dynamical processes are not yet eliminated, resulting in fast convergence to the steady state. In the reduced model, it takes longer to reach the steady state, since only slow dynamics are accounted for.

3.6 Steady-State Solutions of the Reduced Model

- A first case we will consider is the case in which $\theta_1 = \theta_2 = 0$ and $\theta_3 = \frac{\pi}{2}$. In other words, the system behaves as if single mode and bidirectional. From Eqs. (3.45)- (3.48) it is clear that for $\theta_3 = \frac{\pi}{2}$ all the energy is concentrated in the second longitudinal mode. The fact $\theta_1 = \theta_2 = 0$ means that each mode, if present, will be in its bidirectional regime with the amount of energy in the clockwise mode equal to the amount of energy in the counter-clockwise mode. The steady-state solutions for this case are

$$\theta_1 = 0, \qquad \psi_1 = k\pi, \tag{3.73}$$
$$\theta_2 = 0, \qquad \psi_2 = l\pi, \tag{3.74}$$
$$\theta_3 = \frac{\pi}{2}. \tag{3.75}$$

- Another situation that is worth investigating is the one in which two different longitudinal modes are lasing, both of them bidirectional. This is the case when $\theta_1 = \theta_2 = 0$, but θ_3 is left free. By substituting the values of θ_1 and θ_2 into Eqs. (3.66)- (3.70), the steady-state solutions can be found:

$$\theta_1 = 0, \qquad \psi_1 = k\pi, \tag{3.76}$$
$$\theta_2 = 0, \qquad \psi_2 = l\pi, \tag{3.77}$$

$$\theta_3 = \arcsin\left(\frac{-2\Gamma - J\sigma_1 - 2\cos\phi_{k1}\cos\psi_1 + 2\cos\phi_{k2}\cos\psi_2}{J\sigma_2}\right). \tag{3.78}$$

Remark that if the argument of the arcsine equals 1, Eqs. (3.76)- (3.78) become the same as Eqs. (3.73)- (3.75).

- We propose a third steady-state solution, namely the one with two longitudinal modes lasing, one in its bidirectional regime and one in its unidirectional regime. Translating this into angles is a fairly complicated job. We assume that, for example, mode one is the longitudinal mode residing in the bidirectional regime. This gives the first expressions:

$$\theta_1 = 0, \tag{3.79}$$
$$\psi_1 = k\pi. \tag{3.80}$$

To calculate the steady-state solution for θ_2, ψ_2 and θ_3, we found our inspiration in [34]. From there we know that in the unidirectional case it possible to find a solution for θ_2 and J, using ψ_2 as a parameter. If we define a new parameter:

$$\Xi = J(1 + \sin\theta_3), \tag{3.81}$$

we can use their solution:

$$\theta_2(\psi_2) = \arcsin\left(\frac{\alpha\sin\phi_{k2} + \cos\phi_{k2}}{\alpha\cos\phi_{k2} - \sin\phi_{k2}}\tan\psi_2\right), \tag{3.82}$$

$$\Xi(\theta_3, \psi_2) = 2\csc\theta_2(\psi_2)\sec\theta_2(\psi_2)\left[\sin\phi_{k2}\sin\psi_2 - \cos\phi_{k2}\cos\psi_2\sin\theta_2(\psi_2)\right]. \tag{3.83}$$

As a result, θ_3 , which is a function of the other variables, that are all parametrised in ψ_2, can also be parametrised. Solving Eq. (3.68) to θ_3 results in

$$\theta_3 = -\arcsin\left(\frac{\frac{\Xi}{2}(\sigma_1 + \sin^2\theta_2) + \Gamma + \cos\theta_1\cos\psi_1\cos\phi_{k1} - \cos\theta_2\cos\psi_2\cos\phi_{k2}}{\sigma_2 + \frac{\Xi}{2}\sin^2\theta_2 + \Gamma + \cos\theta_1\cos\psi_1\cos\phi_{k1} - \cos\theta_2\cos\psi_2\cos\phi_{k2}}\right). \tag{3.84}$$

- Finally, we can use a similar approach to derive the solution of the most general situation. Once more, we use the parametrisation, now for both $\overline{\theta}_1$ and $\overline{\theta}_2$ with parameters ψ_1 and ψ_2. For the first longitudinal mode we get:

$$\theta_1(\psi_1) = \arcsin\left(\frac{\alpha\sin\phi_{k1} + \cos\phi_{k1}}{\alpha\cos\phi_{k1} - \sin\phi_{k1}}\tan\psi_1\right), \tag{3.85}$$

$$J(1 - \sin\theta_3) = 2\csc\theta_1(\psi_1)\sec\theta_1(\psi_1)\left[\sin\phi_{k1}\sin\psi_1 - \cos\phi_{k1}\cos\psi_1\sin\theta_1(\psi_1)\right]. \tag{3.86}$$

For the second one we find:

$$\theta_2(\psi_2) = \arcsin\left(\frac{\alpha\sin\phi_{k2} + \cos\phi_{k2}}{\alpha\cos\phi_{k2} - \sin\phi_{k2}}\tan\psi_2\right), \tag{3.87}$$

$$J(1 + \sin\theta_3) = 2\csc\theta_2(\psi_2)\sec\theta_2(\psi_2)\left[\sin\phi_{k2}\sin\psi_2 - \cos\phi_{k2}\cos\psi_2\sin\theta_2(\psi_2)\right]. \tag{3.88}$$

In short notation, this looks like

$$\theta_1 = \theta_1(\psi_1), \tag{3.89}$$

$$J = \frac{1}{1 - \sin\theta_3} f(\psi_1), \tag{3.90}$$

$$\theta_2 = \theta_2(\psi_2), \tag{3.91}$$

$$J = \frac{1}{1 + \sin\theta_3} f(\psi_2), \tag{3.92}$$

$$\sin\theta_3 = g(\theta_1, \theta_2, \psi_1, \psi_2). \tag{3.93}$$

We have found an analytical expression of all the angles θ as a function of the parameters ψ_1 and ψ_2. To find a relation between ψ_1 and ψ_2, we express that Eqs. (3.90) and (3.92) are equal, what leads to

$$\begin{aligned}(1 - \sin\theta_3)f(\psi_2) &= (1 + \sin\theta_3)f(\psi_1)\\ \Leftrightarrow \sin\theta_3\left[f(\psi_2) + f(\psi_1)\right] - f(\psi_2) + f(\psi_1) &= 0.\end{aligned} \tag{3.94}$$

Since it is considered too hard to find an analytical solution for Eq. (3.94), a numerical solution is presented in Figure 3.6.

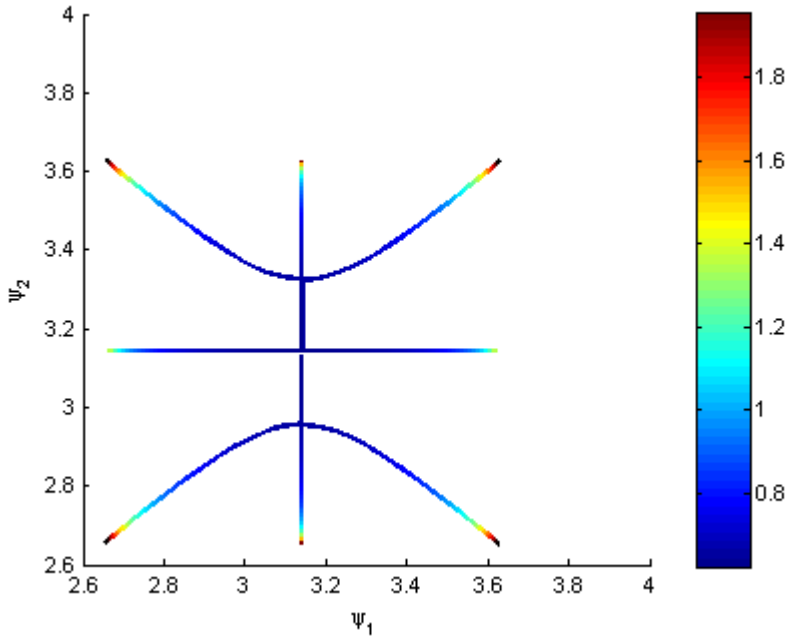

Figure 3.6: Numerically calculated solution of Eqs. (3.66) (3.70) as a function of parameters ψ_1 and ψ_2 and the current J. The current is depicted by using the colour code on the right hand side of the figure. The parameters are: $\alpha = 3.5$, $\phi_{k1} = \phi_{k2} = 0.8$, $\Gamma = 0.0455$, $\sigma_1 = 0$ and $\sigma_2 = -4$.

In this figure, three different cases are depicted. The horizontal and vertical lines through the centre represent the case in which one of the ψ-parameters equals π, the third steady-state solution. The curved lines depict the solution from Eq. (3.94). The minimum and maximum values for ψ_1 and ψ_2 are determined by Eqs. (3.85) and (3.87).

Chapter 4

Stability Analysis

A lot of information on dynamical systems can be obtained from the stability of its stationary solutions. In this chapter, we start with a discussion of the method of linear stability analysis, which is subsequently applied to the stationary solutions that were derived in chapter 3. In this way, we can determine for arbitrary parameter values if one or both longitudinal modes will be lasing, and what will be their mode of operation: bidirectional, unidirectional or oscillating.

4.1 Linear Stability Analysis

We start from the stationary solution derived in chapter 3. These solutions are represented by fixed points in the phase space spanned by the variables θ_1, θ_2, θ_3, ψ_1 and ψ_2. To study stability properties. We consider just small perturbations that can be generated either internally, e.g., spontaneous emission, or externally. If we assume x^* to be a fixed point and $\eta(t) = x(t) - x^*$ to be a small perturbation away from it, we derive an expression for the perturbation η by a linearisation around the fixed point. If we differentiate $\eta(t)$ and keep in mind that x^* is a constant, we find that

$$\dot{\eta} = \frac{d}{dt}(x - x^*) = \dot{x}, \tag{4.1}$$

or

$$\dot{\eta} = \dot{x} = f(x) = f(x^* + \eta). \tag{4.2}$$

By using a Taylor expansion we obtain

$$f(x^* + \eta) = f(x^*) + \eta f'(x^*) + O(\eta^2), \tag{4.3}$$

where $O(\eta^2)$ is a quadratically small term in η. However, for a fixed point, $f(x^* = \dot{x}^* = 0)$. This means that Eq. (4.1) reduces to

$$\dot{\eta} = \eta f'(x^*) + O(\eta^2). \tag{4.4}$$

If $f'(x^*) \neq 0$, we can safely neglect the $O(\eta^2)$ terms and the expression becomes

$$\dot{\eta} = \eta f'(x^*). \tag{4.5}$$

Eq. (4.5) shows that the perturbation $\eta(t)$ grows exponentially if $f'(x^*) > 0$ and is damped if $f'(x^*) < 0$. In other words, it is the slope of the function f at the fixed point that determines its stability. Negative slopes correspond to stable fixed points, while positive slopes correspond to unstable fixed points. In case the derivative equals zero, the $O(\eta^2)$ terms are no longer negligible one must perform a nonlinear stability analysis.
In our case, we will have to deal with more than one equation, we have a five-dimensional linear system:

$$\theta_1' = f_1(\theta_1, \psi_1, \theta_3) \qquad \theta_2' = f_3(\theta_2, \psi_2, \theta_3), \tag{4.6}$$
$$\psi_1' = f_2(\theta_1, \psi_1, \theta_3) \qquad \psi_2' = f_4(\theta_2, \psi_2, \theta_3), \tag{4.7}$$
$$\tag{4.8}$$
$$\theta_3' = f_5(\theta_1, \psi_1, \theta_2, \psi_2, \theta_3). \tag{4.9}$$

This system can be reformulated as

$$\mathbf{x}' = \mathrm{A}\mathbf{x}, \tag{4.10}$$

with

$$\mathbf{x}' = \begin{pmatrix} \theta_1' \\ \psi_1' \\ \theta_2' \\ \psi_2' \\ \theta_3' \end{pmatrix}, \qquad \mathbf{x} = \begin{pmatrix} \theta_1 \\ \psi_1 \\ \theta_2 \\ \psi_2 \\ \theta_3 \end{pmatrix}. \tag{4.11}$$

For each parameter θ_i or ψ_i, small deviations from the steady state value are introduced. The notation is as follows

$$\theta_1 \to \overline{\theta}_1 + u_1, \qquad \theta_2 \to \overline{\theta}_2 + u_3, \tag{4.12}$$
$$\psi_1 \to \overline{\psi}_1 + u_2, \qquad \psi_2 \to \overline{\psi}_2 + u_4, \tag{4.13}$$
$$\tag{4.14}$$
$$\theta_3 \to \overline{\theta}_3 + u_5. \tag{4.15}$$

The overbar denotes steady-state values. The new formulations for the $\theta's$ and the $\psi's$ are then substituted into the rate equations. All that is left are terms originating from the introduced perturbations. The new set of equations can, in first order, be formulated as a Jacobian matrix evaluated at the equilibrium point. First order indicates approximations such as:

$$\sin u_i \approx u_i, \tag{4.16}$$
$$\cos u_i \approx 1. \tag{4.17}$$

The expression becomes

$$\begin{pmatrix} u_1' \\ u_2' \\ u_3' \\ u_4' \\ u_5' \end{pmatrix} = \begin{pmatrix} J_{11} & J_{12} & J_{13} & J_{14} & J_{15} \\ J_{21} & J_{22} & J_{23} & J_{24} & J_{25} \\ J_{31} & J_{32} & J_{33} & J_{34} & J_{35} \\ J_{41} & J_{42} & J_{43} & J_{44} & J_{45} \\ J_{51} & J_{52} & J_{53} & J_{54} & J_{55} \end{pmatrix} \begin{pmatrix} u_1 \\ u_2 \\ u_3 \\ u_4 \\ u_5 \end{pmatrix}, \tag{4.18}$$

with

$$J_{kl} = \left. \frac{\partial f_k}{\partial x_l} \right|_{\theta_1=\overline{\theta}_1,\theta_2=\overline{\theta}_2,\theta_3=\overline{\theta}_3,\psi_1=\overline{\psi}_1,\psi_2=\overline{\psi}_2} . \tag{4.19}$$

This Jacobian contains expressions that depend on constant parameters and steady-state values and not on the dynamic variables. Eq. (4.18) thus becomes a set of linear differential equations. The solutions of such linear differential equations are given by a superposition of terms of the form $e^{\lambda_j t}$ with $\{\lambda_j\}$ a set of eigenvalues of the Jacobian. Since every eigenvalue is in general a complex number, every λ_j can be split up in real and imaginary parts:

$$\lambda_j = \lambda_{j_{Re}} + i\lambda_{j_{Im}}. \tag{4.20}$$

This allows to rewrite the exponential terms in the solution as:

$$e^{\lambda_{j_{Re}} t} e^{i\lambda_{j_{Im}} t}. \tag{4.21}$$

The last of the two exponents can in turn be written as

$$e^{i\lambda_{j_{Im}} t} = \cos \lambda_{j_{Im}} t + i \sin \lambda_{j_{Im}} t, \tag{4.22}$$

so it becomes obvious that this is no more than an oscillatory term. This term will not make the system diverge, however, the real part can. Indeed, if $\lambda_{j_{Re}} > 0$, this factor will grow exponentially in time, indicating an unstable fixed point. We now calculate the full Jacobian for the ODE system given by Eqs. (3.66) (3.70). The full expression of the

linear system looks as follows:

$$
\begin{aligned}
u_1^{'} &= \left[J(1-\sin\overline{\theta}_3)(\cos^2\overline{\theta}_1-\sin^2\overline{\theta_1})+2\cos\overline{\theta}_1\cos\overline{\psi}_1\cos\phi_{k1}\right]\ u_1\\
&+\left[-2\sin\overline{\theta}_1\sin\overline{\psi}_1\cos\phi_{k1}-2\cos\overline{\psi}_1\sin\phi_{k1}\right]\ u_2\\
&+\left[-J\cos\overline{\theta}_1\sin\overline{\theta}_1\cos\overline{\theta}_3\right]\ u_5,\\
\\
u_2^{'} &= \left[J\alpha(1-\sin\overline{\theta}_3)\cos\overline{\theta}_1+2\tan\overline{\theta}_1\sec\overline{\theta}_1\sin\overline{\psi}_1\cos\phi_{k1}+2\sec^2\overline{\theta}_1\cos\overline{\psi}_1\sin\phi_{k1}\right]\ u_1\\
&+\left[2\sec\overline{\theta}_1\cos\overline{\psi}_1\cos\phi_{k1}-2\tan\overline{\theta}_1\sin\overline{\psi}_1\sin\phi_{k1}\right]\ u_2\\
&+\left[-J\alpha\sin\overline{\theta}_1\cos\overline{\theta}_3\right]\ u_5,\\
\\
u_3^{'} &= \left[J(1+\sin\overline{\theta}_3)(\cos^2\overline{\theta}_2-\sin^2\overline{\theta_2})+2\cos\overline{\theta}_2\cos\overline{\psi}_2\cos\phi_{k2}\right]\ u_3\\
&+\left[-2\sin\overline{\theta}_2\sin\overline{\psi}_2\cos\phi_{k2}-2\cos\overline{\psi}_2\sin\phi_{k2}\right]\ u_4\\
&+\left[J\cos\overline{\theta}_2\sin\overline{\theta}_2\cos\overline{\theta}_3\right]\ u_5, \qquad (4.23)\\
\\
u_4^{'} &= \left[J\alpha(1+\sin\overline{\theta}_3)\cos\overline{\theta}_2+2\tan\overline{\theta}_2\sec\overline{\theta}_2\sin\overline{\psi}_2\cos\phi_{k2}+2\sec^2\overline{\theta}_2\cos\overline{\psi}_2\sin\phi_{k2}\right]\ u_3\\
&+\left[2\sec\overline{\theta}_2\cos\overline{\psi}_2\cos\phi_{k2}-2\tan\overline{\theta}_2\sin\overline{\psi}_2\sin\phi_{k2}\right]\ u_4\\
&+\left[J\alpha\sin\overline{\theta}_2\cos\overline{\theta}_3\right]\ u_5,\\
\\
u_5^{'} &= \left[J\sin\overline{\theta}_1\cos\overline{\theta}_1\cos\overline{\theta}_3(\sin\overline{\theta}_3-1)-\sin\overline{\theta}_1\cos\overline{\theta}_3\cos\overline{\psi}_1\cos\phi_{k1}\right]\ u_1\\
&+\left[-\cos\overline{\theta}_1\cos\overline{\theta}_3\sin\overline{\psi}_1\cos\phi_{k1}\right]\ u_2\\
&+\left[J\sin\overline{\theta}_2\cos\overline{\theta}_2\cos\overline{\theta}_3(\sin\overline{\theta}_3+1)+\sin\overline{\theta}_2\cos\overline{\theta}_3\cos\overline{\psi}_2\cos\phi_{k2}\right]\ u_3\\
&+\left[\cos\overline{\theta}_2\cos\overline{\theta}_3\sin\overline{\psi}_2\cos\phi_{k2}\right]\ u_4\\
&+[\frac{J}{2}(\sin^2\overline{\theta}_1\left(\cos^2\overline{\theta}_3-\sin\overline{\theta}_3\left(\sin\overline{\theta}_3-1\right)\right)+\sin^2\overline{\theta}_2\left(\cos^2\overline{\theta}_3-\sin\overline{\theta}_3\left(\sin\overline{\theta}_3+1\right)\right)\\
&-\sin\overline{\theta}_3\sigma_1+\cos 2\overline{\theta}_3\sigma_2)-\Gamma\sin\overline{\theta}_3-\sin\overline{\theta}_3\left(\cos\overline{\theta}_1\cos\overline{\psi}_1\cos\overline{\phi}_{k1}-\cos\overline{\theta}_2\cos\overline{\psi}_2\cos\overline{\phi}_{k2}\right)]\ u_5.\\
& \qquad (4.24)
\end{aligned}
$$

In general, there is no simple interpretation of the eigenvalues of this system. In the previous chapter, different types of steady-state solutions have been discussed. First, we have found a solution, describing the case where only one longitudinal mode is lasing and it is lasing bidirectionally. A second solution is the one where two longitudinal modes are lasing, both of them bidirectionally. The third steady-state situation is the one in which two longitudinal modes are lasing, but only one of the bidirectionally. Here, we have found expressions parameterised in ψ_1 or ψ_2. Finally, again by using a

parameterisation, the most general case has been solved, the one in which all variables left free. If these solutions are implemented in the Jacobian, we find that in some cases the characteristic polynomial is suitable for analytical interpretation.

4.2 Stability of Steady-State Solution 1: $\overline{\theta}_1 = \overline{\theta}_2 = 0,\ \overline{\theta}_3 = \frac{\pi}{2}$

4.2.1 Analytical Expressions

From our simulations, we have seen that the device is always lasing in a single mode that is bidirectional for sufficiently low pump current. To express that we are in the bidirectional regime, we take $\overline{\theta}_1 = \overline{\theta}_2 = 0$. Besides, we assume that only the second longitudinal mode has reached its threshold and is lasing, which implies that $\overline{\theta}_3 = \frac{\pi}{2}$. In this case, the Jacobian simplifies significantly:

$$\begin{pmatrix} J_{11} & J_{12} & 0 & 0 & 0 \\ J_{21} & J_{22} & 0 & 0 & 0 \\ 0 & 0 & J_{33} & J_{34} & 0 \\ 0 & 0 & J_{43} & J_{44} & 0 \\ 0 & 0 & 0 & 0 & J_{55} \end{pmatrix}, \tag{4.25}$$

with

$$J_{11} = 2\cos\phi_{k1}\cos\overline{\psi}_1, \tag{4.26}$$
$$J_{12} = -2\sin\phi_{k1}\cos\overline{\psi}_1, \tag{4.27}$$
$$J_{21} = 2\sin\phi_{k1}\cos\overline{\psi}_1, \tag{4.28}$$
$$J_{22} = 2\cos\phi_{k1}\cos\overline{\psi}_1, \tag{4.29}$$

$$J_{33} = 2J + 2\cos\phi_{k2}\cos\overline{\psi_2}, \tag{4.30}$$
$$J_{34} = -2\cos\overline{\psi_2}\sin\phi_{k2}, \tag{4.31}$$
$$J_{43} = 2\alpha J + 2\cos\overline{\psi_2}\sin\phi_{k2}, \tag{4.32}$$
$$J_{44} = 2\cos\phi_{k2}\cos\overline{\psi_2}, \tag{4.33}$$

$$J_{55} = -\Gamma - \frac{J(\sigma_1+\sigma_2)}{2} - \cos\phi_{k1}\cos\overline{\psi}_1 + \cos\phi_{k2}\cos\overline{\psi_2}. \tag{4.34}$$

Note that the Jacobian splits up into several independent blocks. This means that, in the neighbourhood of the fixed point in phase space, the evolution of (θ_1, ψ_1), (θ_2, ψ_2) and θ_3 is decoupled, what greatly signifies the stability analysis. In fact, the eigenvalues deducted from the first two blocks indicate when $\overline{\theta}_1$ or $\overline{\theta}_2$ will bifurcate. J_{55}, on the

other hand, informs us when $\overline{\theta}_3 = \frac{\pi}{2}$ is no longer stable, hence when the laser will no longer operate in its single mode regime. To calculate the exact stability criteria of this solution, the eigenvalues are needed. The eigenvalues from the first block are:

$$\lambda_{1,2} = 2\cos\overline{\psi}_1\left(\cos\phi_k \pm i\sin\phi_{k1}\right). \tag{4.35}$$

To extract the stability information, we need to express that the real part of $\lambda_{1,2}$ is smaller than zero. Since the current J is not present in the expression of the eigenvalues, the stability information we find here does not depend on the current. Indeed, the real part of expression (4.35) is smaller than zero when:

$$2\cos\overline{\psi}_1\cos\phi_{k1} < 0, \tag{4.36}$$

We know that for small current values, the device will always operate bidirectional, so the solution that we are discussing should be stable. Remember that the bidirectional operation, implies that $\overline{\psi}_1 = k\pi$, with $k = 0$ or $k = 1$. From Eq. (4.36), we find that ϕ_{k1} determines which of the two solutions of $\overline{\psi}_1$ is stable. When ϕ_{k1} is located in the first quadrant, we find:

$$\begin{aligned} &\cos\phi_{k1} > 0, \\ &\Rightarrow \cos\overline{\psi}_1 < 0, \\ &\Rightarrow \overline{\psi}_1 = \pi. \end{aligned} \tag{4.37}$$

If we had chosen ϕ_{k1} to be in the second quadrant, we would have found, $\overline{\psi}_1 = 0$. For more information about the stability of steady-state solution 1, the eigenvalues $\lambda_{3,4}$ need to be investigated as well:

$$\lambda_{3,4} = J + 2\cos\phi_{k2}\cos\overline{\psi}_2 \pm \sqrt{J^2 - 4\alpha J\cos\overline{\psi}_2\sin\phi_{k2} - 4\cos^2\overline{\psi}_2\sin^2\phi_{k2}}. \tag{4.38}$$

This eigenvalue allows to determine which solution for $\overline{\psi}_2$ is stable. We know that for small pump currents, $\lambda_{3,4}$ should have negative real parts, such that the regime with only one longitudinal mode in its bidirectional regime is stable. If we equate J to 0, we find

$$\lambda_{3,4} = 2\cos\phi_{k2}\cos\overline{\psi}_2 \pm \sqrt{-4\cos^2\overline{\psi}_2\sin^2\phi_{k2}}. \tag{4.39}$$

The argument of the square root is negative or zero, hence the root will not contribute to the real part of the eigenvalue. With a deduction analogous to the one for $\overline{\psi}_1$, we find that if ϕ_{k2} is situated in the first quadrant, $\cos\phi_{k2} > 0$ and we can conclude that $\overline{\psi_2} = \pi$. When ϕ_{k2} is situated in the second quadrant, $\overline{\psi_2} = 0$. From now on, we will always consider ϕ_{k1} and ϕ_{k2} to be in the first quadrant. The expression for $\lambda_{3,4}$ becomes:

$$\lambda_{3,4} = J - 2\cos\phi_{k2} \pm \sqrt{J^2 + 4\alpha J\sin\phi_{k2} - 4\sin^2\phi_{k2}}. \tag{4.40}$$

In this eigenvalue, the current J appears and there is no explicit imaginary part. However, for certain current values, it is possible that the square root is a purely imaginary value. As long as the current, J, is smaller than

$$J_{Im} = 2\sin\phi_{k2}\left(-\alpha + \sqrt{1+\alpha^2}\right), \tag{4.41}$$

the argument of the square root is negative, hence the eigenvalues are complex conjugates with a non-zero imaginary part. The study of the eigenvalues can be split up into two parts. The eigenvalues are of the following form:

$$\lambda_{3,4} = a \pm \sqrt{b}. \tag{4.42}$$

First, we assume $J > J_{Im}$ or $b > 0$. In this case, the square root of b is real-valued and, as a consequence, the eigenvalues have no imaginary part. Expressing that $\Re(\lambda_{3,4}) < 0$ is exactly the same as expressing that $\lambda_{3,4} < 0$. The bifurcation current we find is

$$J_{PF} = \frac{1}{\cos\phi_{k2} + \alpha\sin\phi_{k2}}. \tag{4.43}$$

At this pump current, both the real and imaginary parts of the eigenvalue are zero and the eigenvalues cross the real axis, toward the right half plane when the current increases. This is called a pitchfork bifurcation [21].
Second, we consider the case in which $J < J_{Im}$ or $b < 0$. If so, the square root of b equals a purely imaginary number after substitution of the parameter values. This means that for finding the bifurcation current, we can ignore the square root. Equating the real part to zero gives the current,

$$J_H = 2\cos\phi_{k2}. \tag{4.44}$$

The bifurcation we encounter here is a Hopf bifurcation [21]. A Hopf bifurcation is a bifurcation in which a fixed point loses stability as a pair of complex conjugate eigenvalues crosses the imaginary axis in the complex plane. This results in a limit cycle branching from the fixed point. In other words, harmonic amplitude oscillations will occur, with frequency

$$\Omega_H = \left\| \sqrt{J_H^2 + 4\alpha J_H \sin\phi_{k2} - 4\sin^2\phi_{k2}} \right\| \tag{4.45}$$

$$= \left\| \sqrt{4\cos^2\phi_{k2} + 8\alpha\cos\phi_{k2}\sin\phi_{k2} - 4\sin^2\phi_{k2}} \right\| \tag{4.46}$$

$$= 2\left\| \sqrt{\cos 2\phi_{k2} + \alpha\sin 2\phi_{k2}} \right\|. \tag{4.47}$$

The last eigenvalue is more straightforward. It contains the current and has no square root or imaginary parts in it. The eigenvalue λ_5 equals the Jacobian element J_{55},

$$\lambda_5 = -\Gamma - \frac{J(\sigma_1+\sigma_2)}{2} - \cos\phi_{k1}\cos\overline{\psi}_1 + \cos\phi_{k2}\cos\overline{\psi_2}. \tag{4.48}$$

Because of the assumption that ϕ_{k1} and ϕ_{k2} are in the first quadrant, we know that $\overline{\psi}_1 = \overline{\psi}_2 = \pi$, resulting in

$$\lambda_5 = -\Gamma - \frac{J(\sigma_1 + \sigma_2)}{2} + \cos\phi_{k1} - \cos\phi_{k2}. \tag{4.49}$$

The bifurcation current we find is

$$J_{2mode} = \frac{2\left(\Gamma - \cos\phi_{k1} + \cos\phi_{k2}\right)}{-\sigma_1 - \sigma_2}. \tag{4.50}$$

This last bifurcation is called a supercritcal pitchfork bifurcation. This can be seen when we write down the Jacobian up to the third order. We then obtain a normal form that allows us to classify the problem. A supercritical pitchfork implicates that, at the bifurcation point, one fixed point solution loses stability, while two new, stable solutions arise. We will confirm this later in this chapter. Three bifurcation currents have been found for this first steady state solution: J_{2mode}, J_H and J_{PF}. All three of them indicate a pump current for which one or more eigenvalues cross the imaginary axis in the complex plane. In the phase space, constructed by θ_1, θ_2, θ_3, ψ_1 and ψ_2, they indicate bifurcations originating from the steady-state solution with one longitudinal mode lasing and with its energy equally distributed over the two counter-propagating modes. However, we note that not all currents will indicate a special point in this curve, since on a P-I curve only the stable solutions are depicted. The smallest bifurcation current indicates the point where the studied solution is no longer stable. Bifurcation currents larger than this first current are no longer situated in a region where their solution is stable and do not correspond to visual bifurcations.

4.2.2 Numerical Validation

These results can be numerically validated. Depending on the values of the parameters, different eigenvalues will be the first ones to cross the imaginary axis and move on to the right half plane. Once the real part of one of the eigenvalues becomes positive, the solution with one longitudinal mode in its bidirectional regime becomes unstable and is no longer visible on a P-I curve. However, the solution still exists in phase space. The other eigenvalues are still negative and the current values where they reach the imaginary axis, will no longer correspond to a visual bifurcation point in the P-I curve. In Figure 4.1, we find a first scenario. The parameters are chosen as $\sigma_1 = 0$, $\sigma_2 = -4$, $\alpha = 3.5$, $\phi_{k1} = \phi_{k2} = 1.4966$ and $\Gamma = 0.0909$. We see that one mode starts lasing bidirectionally, i.e., the behaviour we have just studied, until the second longitudinal mode reaches threshold. If we calculate the bifurcation currents from Eqs. (4.43), (4.44) and (4.50), we find that the one in Eq. (4.50), J_{2mode}, is the smallest one. In other words, once this current is reached (black vertical line), the bifurcation occurs and the considered regime loses stability. While this current indicates the point at which the second mode reaches its threshold and starts lasing, the other currents indicate other

kinds of bifurcations. In Figure 4.2, we have changed the parameters to $\sigma_1 = -2$, $\sigma_2 = 4$, $\alpha = 3.5$, $\phi_{k1} = \phi_{k2} = 1.4966$ and $\Gamma = 0.0909$. Now, the first bifurcation that occurs is the one in which the dominant mode reaches the oscillatory-regime. Note that this time, the current J_H (red vertical line),found in Eq. (4.44), is the smallest positive one. The current from Eq. (4.50) has now become negative, with all positive values situated in the stable area. Earlier we have derived that the current from Eq. (4.44) corresponds to a Hopf bifurcation, hence a transition from a stable fixed point to a stable limit cycle. The P-I curve confirms this, since mode two starts to oscillate, once the bifurcation current is surpassed. This a visualisation of the limit cycle, the stable solution is closed trajectory around an unstable fixed point.

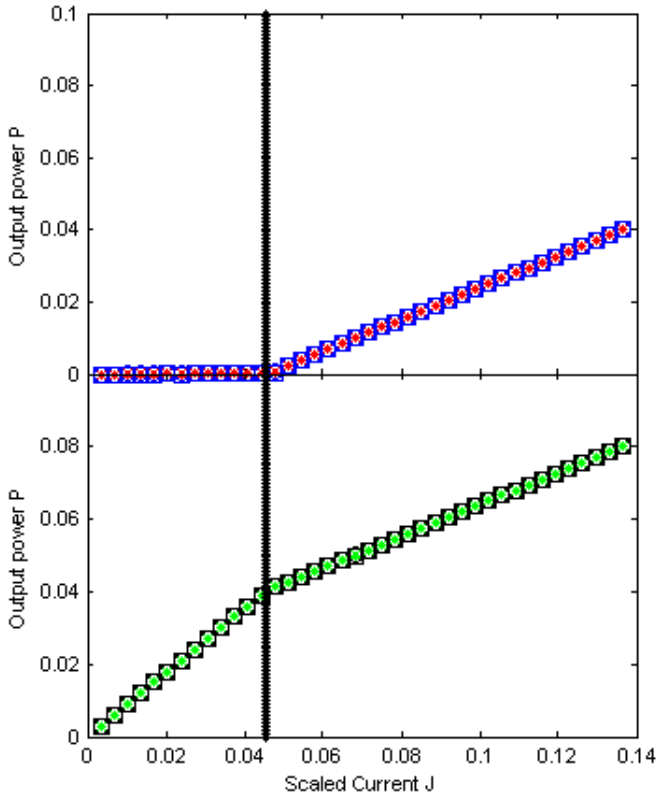

(a)

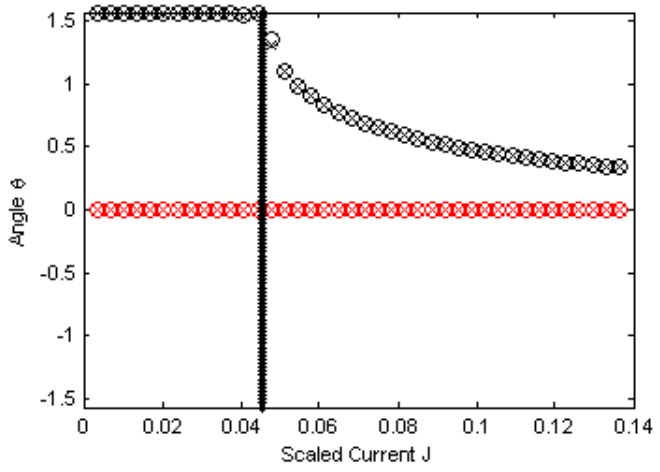

(b)

Figure 4.1: (a) Simulated P-I curve of a multi mode SRL with two longitudinal modes, $\sigma_1 = 0$, $\sigma_2 = -4$, $\alpha = 3.5$, $\phi_{k1} = \phi_{k2} = 1.4966$ and $\Gamma = 0.0909$. The black vertical line corresponds to the current from Eq. 4.50 and indicates point where the solution with only one longitudinal mode, lasing bidirectionally, becomes unstable. The maxima and minima of $|E_{1cw}|$ ($|E_{1ccw}|$) are denoted by open blue squares and circles (red crosses and dots), respectively. For the second longitudinal mode, the maxima and minima of $|E_{2cw}|$ ($|E_{2ccw}|$) are denoted by open black squares and circles (green crosses and dots), respectively. (b) Angles as a function of the scaled pump current, $\overline{\theta}_1$ (blue), $\overline{\theta}_2$ (red) and $\overline{\theta}_3$ (black).

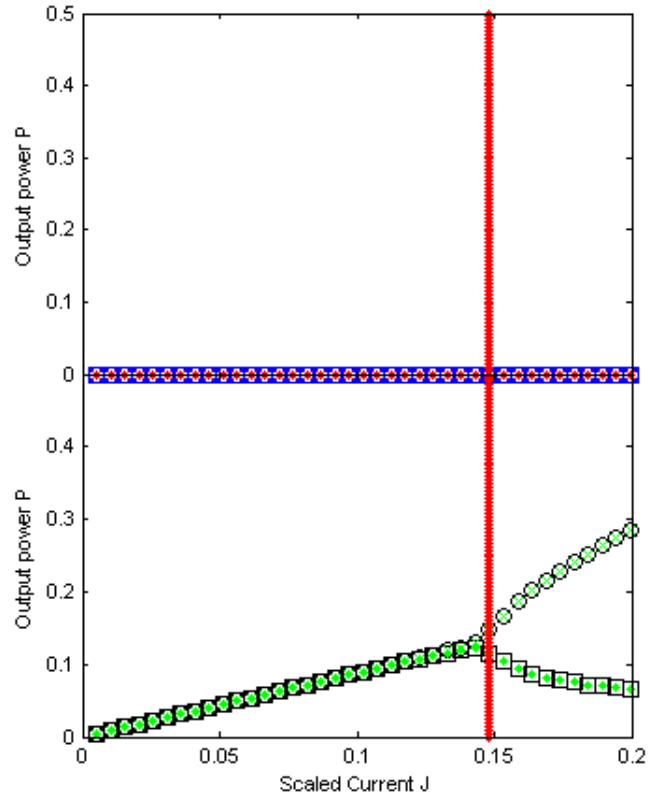

(a)

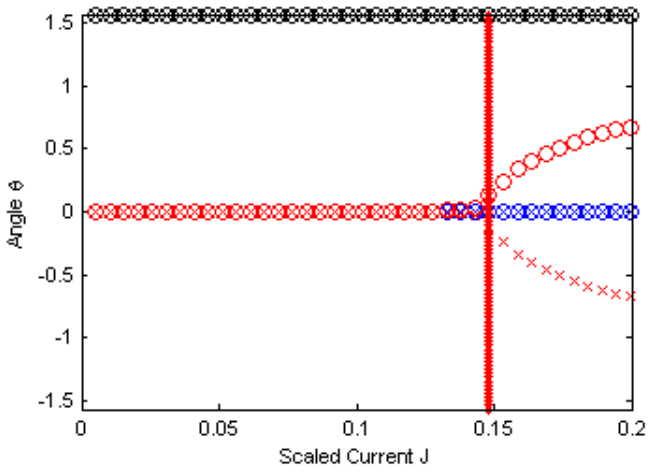

(b)

Figure 4.2: (a) Simulated P-I curve of a multi mode SRL with two longitudinal modes, $\sigma_1 = -2$, $\sigma_2 = 4$, $\alpha = 3.5$, $\phi_{k1} = \phi_{k2} = 1.4966$ and $\Gamma = 0.0909$. The red vertical line corresponds to the current J_H from Eq. 4.44 and indicates point where the solution with only one longitudinal mode, lasing bidirectionally, becomes unstable in favour of a solution with oscillations. The intensities are depicted with the same legend as in Figure 4.1. (b) Angles as a function of the scaled pump current, $\overline{\theta}_1$ (blue), $\overline{\theta}_2$ (red) and $\overline{\theta}_3$ (black).

4.3 Stability of Steady-State Solution 2: $\overline{\theta}_1 = \overline{\theta}_2 = 0$, $\overline{\theta}_3 = free$

4.3.1 Analytical expressions

As shown in chapter 3, there exists a solution with $\overline{\theta}_1 = \overline{\theta}_2 = 0$, but with $\overline{\theta}_3$ left free. Physically, this means that both longitudinal modes reside in the bidirectional regime, but that the energy is no longer equally distributed over the two longitudinal modes. This leads to the following steady-state expressions:

$$\overline{\theta}_1 = 0, \qquad \overline{\psi}_1 = k\pi, \tag{4.51}$$

$$\overline{\theta}_2 = 0, \qquad \overline{\psi}_2 = l\pi, \tag{4.52}$$

$$\overline{\theta}_3 = \arcsin\left(\frac{-2\Gamma - J\sigma_1 - 2\cos\phi_{k1}\cos\overline{\psi}_1 + 2\cos\phi_{k2}\cos\overline{\psi}_2}{J\sigma_2}\right). \tag{4.53}$$

Once again, the Jacobian has the same form as in Eq. (4.25), because $\sin k\pi = \sin l\pi = 0$, even if we do not know whether k and l are even or odd. This time the elements of the matrix look like

$$J_{11} = \frac{2\Gamma + J(\sigma_1 + \sigma_2) + 2(1+\sigma_2)\cos\phi_{k1}\cos\overline{\psi}_1 - 2\cos\phi_{k2}\cos\overline{\psi}_2}{\sigma_2} \tag{4.54}$$

$$J_{12} = -2\sin\phi_{k1}\cos\overline{\psi}_1 \tag{4.55}$$

$$J_{21} = \frac{2\alpha\Gamma + \alpha J(\sigma_1 + \sigma_2) + 2\alpha\cos\phi_{k1}\cos\overline{\psi}_1 - 2\alpha\cos\phi_{k2}\cos\overline{\psi}_2}{\sigma_2} + 2\sin\phi_{k1}\cos\overline{\psi}_1 \tag{4.56}$$

$$J_{22} = 2\cos\phi_{k1}\cos\overline{\psi}_1 \tag{4.57}$$

$$J_{33} = \frac{-2\Gamma - J(\sigma_1 - \sigma_2) - 2\cos\phi_{k1}\cos\overline{\psi}_1 + 2(1+\sigma_2)\cos\phi_{k2}\cos\overline{\psi}_2}{\sigma_2} \tag{4.58}$$

$$J_{34} = -2\sin\phi_{k2}\cos\overline{\psi}_2 \tag{4.59}$$

$$J_{43} = \frac{\alpha\left(-2\Gamma - J(\sigma_1 - \sigma_2) - 2\cos\phi_{k1}\cos\overline{\psi}_1 + 2\cos\phi_{k2}\cos\overline{\psi}_2\right)}{\sigma_2} + 2\sin\phi_{k2}\cos\overline{\psi}_2 \tag{4.60}$$

$$J_{44} = 2\cos\phi_{k2}\cos\overline{\psi}_2 \tag{4.61}$$

$$J_{55} = \frac{1}{2J\sigma_2}\Big[-\cos\phi_{k1}\left(\cos\phi_{k1} + 8\Gamma\cos\overline{\psi}_1 + 4J\sigma_1\cos\overline{\psi}_1 + 2\cos\phi_{k1}\cos 2\overline{\psi}_1\right) - 2 - (2\Gamma + J\sigma_1)^2 + J^2\sigma_2^2 + 4\cos\phi_{k2}\left(2\Gamma + J\sigma_1 + 2\cos\phi_{k1}\cos\overline{\psi}_1\right)\cos\overline{\psi}_2 - \cos^2\phi_{k2}\left(1 + 2\cos 2\overline{\psi}_2\right) + \sin^2\phi_{k1} + \sin^2\phi_{k2}\Big] \tag{4.62}$$

The eigenvalues can again be calculated, although, the expressions become somewhat more complicated. For the the first eigenvalues, we find again something of the form

$$\lambda_{1,2} = a \pm \sqrt{b}, \tag{4.63}$$

with

$$a = \frac{1}{2\sigma_2}\left[2\Gamma + J(\sigma_1 + \sigma_2) + 2(1 + 2\sigma 2)\cos\phi_{k1}\cos\overline{\psi}_1 - 2\cos\phi_{k2}\cos\overline{\psi}_2\right] \tag{4.64}$$

$$\begin{aligned} b = \frac{1}{4\sigma_2^2}\Big[&3/2 + 4\Gamma^2 - 6\sigma_2^2 + 4\Gamma J(\sigma_1 + \sigma_2) + J^2(\sigma_1 + \sigma_2)^2 + \cos 2\phi_{k2} \\ &+ 2(1 + 4\sigma_2^2)\cos\phi_{k1}{}^2\cos\overline{\psi}_1{}^2 + (1 + 4\sigma_2^2)\cos 2\phi_{k1}\cos\overline{\psi}_1{}^2 \\ &+ 1/2\cos 2\overline{\psi}_1 - 6\sigma_2^2\cos 2\overline{\psi}_1 - 4(2\Gamma + J(\sigma_1 + \sigma_2))\cos\phi_{k2}\cos\overline{\psi}_2 \\ &+ 4\cos\phi_{k1}\cos\overline{\psi}_1(2\Gamma + J(\sigma_1 + \sigma_2) - 2\cos\phi_{k2}\cos\overline{\psi}_2) + 2\cos\phi_{k2}{}^2\cos 2\overline{\psi}_2 \\ &-8\alpha\sigma_2\cos\overline{\psi}_1(2\Gamma + J(\sigma_1 + \sigma_2) + 2\cos\phi_{k1}\cos\overline{\psi}_1 - 2\cos\phi_{k2}\cos\overline{\psi}_2)\sin\phi_{k1}\Big]. \end{aligned} \tag{4.65}$$

For reasons similar those in section 4.2, two different analyses must be made, depending on the sign of b. If the pump current is chosen such that $b > 0$, the square root equals a real number and the bifurcation current is found by equating the entire eigenvalue $\lambda_{1,2}$ to zero:

$$J_{PF1} = \frac{-1}{(\sigma_1 + \sigma_2)\left(\cos\phi_{k1} + \alpha\sin\phi_{k1}\right)}\Big[\cos^2\phi_{k1}\cos\overline{\psi}_1 + 2\left(\cos\phi_{k1} + \alpha\sin\phi_{k1}\right)\left(\Gamma - \cos\phi_{k2}\cos\overline{\psi}_2\right) + \cos\overline{\psi}_1\left(1 + 2\sigma_2 - \sin^2\phi_{k2} + \alpha\sin 2\phi_{k1}\right)\Big]. \tag{4.66}$$

Since at this current, two real eigenvalues cross the imaginary axis toward the right half plane, this is a pitchfork bifurcation, indicating that one of the modes becomes unidirectional.

If the pump current has a value leading to $b < 0$, the square root equals an imaginary number and the bifurcation point is found by equating only the real part, a, to zero:

$$J_{H1} = \frac{-2\Gamma - 2(1 + 2\sigma_2)\cos\phi_{k1}\cos\overline{\psi}_1 + 2\cos\phi_{k2}\cos\overline{\psi}_2}{\sigma_1 + \sigma_2} \tag{4.67}$$

This is a Hopf bifurcation in the first longitudinal mode, with Hopf frequency

$$\begin{aligned}\Omega_{H1} &= \left\| \sqrt{b(J_{H1})} \right\| \\ &= \left\| \sqrt{16\sigma_2^2 \cos^2\psi_1(\cos 2\phi_{k1} + \alpha \sin 2\phi_{k1})} \right\| \\ &= 4 \left\| \sigma_2 \cos\psi_1 \sqrt{\cos 2\phi_{k1} + \alpha \sin 2\phi_{k1}} \right\|. \end{aligned} \tag{4.68}$$

The next two eigenvalues, which have the form

$$\lambda_{1,2} = c \pm \sqrt{d}, \tag{4.69}$$

with

$$c = \frac{1}{2\sigma_2}\left[-2\Gamma - J\sigma_1 + J\sigma_2 - 2\cos\phi_{k1}\cos\overline{\psi}_1 + 2(1+2\sigma_2)\cos\phi_{k2}\cos\overline{\psi}_2\right] \tag{4.70}$$

$$\begin{aligned} d = \frac{1}{4\sigma_2^2}\Big[&2 + (2\Gamma + J\sigma_1 + 2\sigma_2 - J\sigma_2)(2\Gamma + J\sigma_1 - (2+J)\sigma_2) + \cos 2\phi_{k1} \\ &+ (1+4\sigma_2^2)\cos 2\phi_{k2} + 2\cos\phi_{k1}(2(2\Gamma + J\sigma_1 - J\sigma_2)\cos\overline{\psi}_1 + \cos\phi_{k1}\cos 2\overline{\psi}_1) \\ &+ 4(2\Gamma + J\sigma_1 - J\sigma_2 + 2\cos\phi_{k1}\cos\overline{\psi}_1)\cos\overline{\psi}_2(-\cos\phi_{k2} + 2\alpha\sigma_2\sin\phi_{k2}) \\ &-4\alpha\sigma_2\sin 2\phi_{k2} + \cos 2\overline{\psi}_2(1 - 4\sigma_2^2 + (1+4\sigma_2^2)\cos 2\phi_{k2} - 4\alpha\sigma_2\sin 2\phi_{k2})\Big] \end{aligned} \tag{4.71}$$

can be treated similarly. Once more, two different cases must be considered, depending on the value of the pump current. If $d > 0$, the square root equals a real number and the bifurcation current is found by equating the entire eigenvalue $\lambda_{3,4}$ to zero. We find the pitchfork bifurcation current to be

$$J_{PF2} = \frac{-2(\Gamma + \cos\phi_{k1}\cos\overline{\psi}_1)(\cos\phi_{k2} + \alpha\sin\phi_{k2}) + \cos\overline{\psi}_2(1 + 2\sigma_2 + \cos 2\phi_{k2} + \alpha\sin 2\phi_{k2})}{(\sigma_1 - \sigma_2)(\cos\phi_{k2} + \alpha\sin\phi_{k2})} \tag{4.72}$$

When $d < 0$, the square root equals an imaginary number and a Hopf bifurcation is found by equating only the real part, c, to zero:

$$J_{H2} = \frac{2\Gamma + 2\cos\phi_{k1}\cos\overline{\psi}_1 - 2(1+2\sigma_2)\cos\phi_{k2}\cos\overline{\psi}_2}{-\sigma_1 + \sigma_2}. \tag{4.73}$$

The Hopf frequency is

$$\Omega_{H2} = \left\| \sqrt{d(J_{H2})} \right\|, \tag{4.74}$$

being an elaborate expression.
Eventually, the last eigenvalue is the easiest to calculate, since it is just element J_{55} in

the Jacobian :

$$\begin{aligned}\lambda_5 = \frac{1}{2J\sigma_2}\Big[&-\cos\phi_{k1}\left(\cos\phi_{k1} + 8\Gamma\cos\overline{\psi}_1 + 4J\sigma_1\cos\overline{\psi}_1 + 2\cos\phi_{k1}\cos 2\overline{\psi}_1\right)\\ &- 2 - (2\Gamma + J\sigma_1)^2 + J^2\sigma_2^2 + 4\cos\phi_{k2}\left(2\Gamma + J\sigma_1 + 2\cos\phi_{k1}\cos\overline{\psi}_1\right)\cos\overline{\psi}_2\\ &- \cos^2\phi_{k2}\left(1 + 2\cos 2\overline{\psi}_2\right) + \sin^2\phi_{k1} + \sin^2\phi_{k2},\end{aligned} \tag{4.75}$$

leading to the currents,

$$J_{2mode} = \frac{2}{\sigma_1^2 - \sigma_2^2}\left[(-\sigma_1 \pm \sigma_2)\left(\Gamma + \cos\phi_{k1}\cos\overline{\psi}_1 - \cos\phi_{k2}\cos\overline{\psi}_2\right)\right] \tag{4.76}$$

Because of reasons similar to case 1, this denotes a supercritical bifurcation.

4.3.2 Numerical Validation

In Figure 4.3, three of the five found bifurcation currents are depicted. The first one we find is represented by the vertical black line. This corresponds to the current J_{2mode} from Eq. (4.76) and is equal to the one from the first case in Eq. (4.50). Hence, we find that the solution with only one longitudinal mode loses stability and that the two-mode solution becomes stable at the same point. In fact, this is what we predicted in the previous section. For currents lower than J_{2mode}, there exists only one fixed point. At the supercritical pitchfork it loses stability, in favour of two new, stable solutions. Figure 4.3 depicts only one of these solutions, namely the one where θ_3 decays to zero. The second one was intentionally left out, because of the definition of the variables of the model, but it does exist. The second solution is the one where θ_3 grows to values larger than $\frac{\pi}{2}$. When the current is further increased, we encounter the first Hopf bifurcation, the green line at J_{H2}, given by Eq. (4.73). Here mode 2 is no longer purely bidirectional, the oscillations appear. In fact, this is where the studied situation is no longer stable, so we cannot expect the other bifurcation currents to represent bifurcations, visible on the P-I graph. However, as we already noticed before, the Jacobian split up into two independent blocks. $\overline{\theta}_2$ is no longer zero, but this has no effect on the solution and stability of $\overline{\theta}_1$. That is why the red line in Figure. 4.3, at J_{H1}, denotes the correct value for the start of the oscillatory regime of mode 1. The two currents that do not appear on the P-I curve are the ones from Eqs. (4.66), J_{PF1}, and (4.72), J_{PF2}. They correspond to pitchfork bifurcations, denoting the change from the bidirectional to the unidirectional regime, respectively for mode 1 and mode 2. In Figure 4.4 such a situation is depicted.

4.3.3 Remark

A feature that immediately catches the eye in Figure 4.3(a) is that both the Hopf bifurcations seem to occur at the same intensity. Both longitudinal modes enter the oscillatory regime around intensity levels of about 0.13. Using the results found in the stability

analysis, it is possible to analytically check whether this is indeed the same intensity value for both longitudinal modes. Remember that the solution of the situation with two longitudinal modes, each of them lasing bidirectionally is given by

$$\overline{\theta}_1 = 0 \qquad \overline{\psi}_1 = k\pi, \tag{4.77}$$

$$\overline{\theta}_2 = 0 \qquad \overline{\psi}_2 = l\pi, \tag{4.78}$$

$$\overline{\theta}_3 = \arcsin\left(\frac{-2\Gamma - J\sigma_1 - 2\cos\phi_{k1}\cos\overline{\psi}_1 + 2\cos\phi_{k2}\cos\overline{\psi}_2}{J\sigma_2}\right). \tag{4.79}$$

The current of the first Hopf bifurcation, the one in mode 1, is given by

$$J_{H1} = \frac{-2\Gamma - 2\,(1+2\sigma_2)\cos\phi_{k1}\cos\overline{\psi}_1 + 2\cos\phi_{k2}\cos\overline{\psi}_2}{\sigma_1 + \sigma_2}. \tag{4.80}$$

The second Hopf bifurcation current is given by

$$J_{H2} = \frac{2\Gamma + 2\cos\phi_{k1}\cos\overline{\psi}_1 - 2(1+2\sigma_2)\cos\phi_{k2}\cos\overline{\psi}_2}{-\sigma_1 + \sigma_2}. \tag{4.81}$$

Since we have the solutions for every angle $\overline{\theta}$ and we have the currents at which the bifurcations occur, we are capable of analytically calculating the intensity at the bifurcation point. The intensities of the two longitudinal modes are given by

$$Q^2_{1cw} = Q^2_{1ccw} = \frac{\mu_1 - 1}{4}\left(1 - \sin\overline{\theta}_3(J_1)\right), \tag{4.82}$$

$$Q^2_{2cw} = Q^2_{2ccw} = \frac{\mu_2 - 1}{4}\left(1 + \sin\overline{\theta}_3(J_2)\right), \tag{4.83}$$

where we already took into account that $\overline{\theta}_1 = \overline{\theta}_2 = 0$. In both expressions, $\overline{\theta}_3$ should be evaluated at the correct current, J_i. Also μ_i depends on J_i, since

$$\mu_i = \frac{2KJ_i}{C_0 - S_0} + 1. \tag{4.84}$$

If we substitute Eqs. (4.84), (4.80) and (4.81) in Eqs. (4.82)- (4.83), we find that both intensities are indeed the same and equal to $\frac{2K\cos\phi_k}{C_0 - S_0} = 0.130466$, on the condition that $\phi_{k1} = \phi_{k2} = \phi_k$. This last condition has indeed been used in the case of Figure 4.3(a).

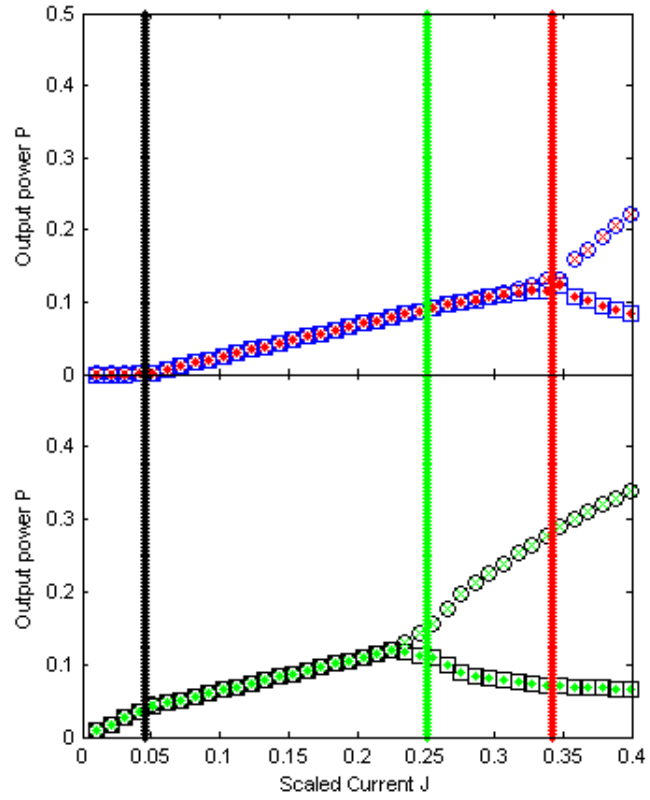

(a)

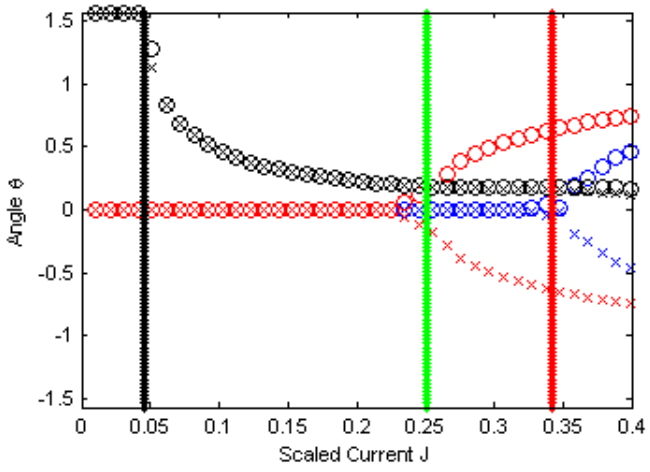

(b)

Figure 4.3: (a) P-I curve of a multi mode SRL with two longitudinal modes, $\sigma_1 = 0$, $\sigma_2 = -4$, $\alpha = 3.5$, $\phi_{k1} = \phi_{k2} = 1.4966$ and $\Gamma = 0.0909$. The black vertical line corresponds to the current from Eq. 4.76 and indicates point where the solution with two longitudinal modes, each lasing bidirectionally, becomes stable. The red and green vertical lines correspond to the bifurcation points where a Hopf bifurcation takes place, the currents J_{H1} and J_{H2} found in, respectively, Eq. 4.67 and Eq. 4.73. The intensities are depicted with the same legend as in Figure 4.1. (b) Angles as a function of the scaled pump current, $\overline{\theta}_1$ (blue), $\overline{\theta}_2$ (red) and $\overline{\theta}_3$ (black).

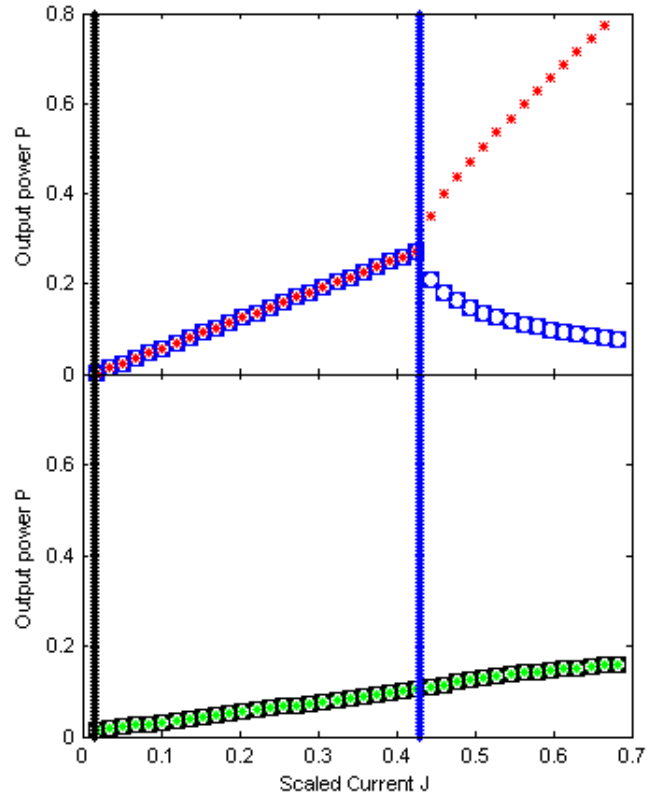

(a)

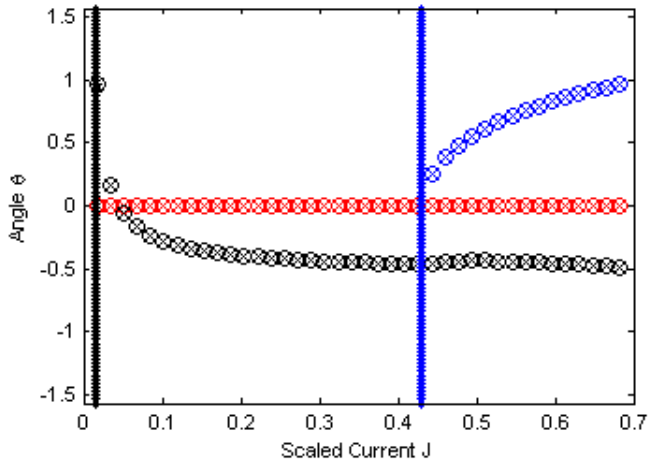

(b)

Figure 4.4: (a) P-I curve of a multi mode SRL with two longitudinal modes, $\sigma_1 = -2$, $\sigma_2 = -4$, $\alpha = 3.5$, $\phi_{k1} = \phi_{k2} = 0.8$ and $\Gamma = 0.0455$. The vertical black line indicates where the solution with two longitudinally modes, each lasing bidirectionally, becomes stable, while the vertical blue line indicates the analytically predicted current for the pitchfork bifurcation from Eq. (4.66). This is the point where the solution with two longitudinal modes, each lasing bidirectionally, becomes unstable in favour of the situation with one bidirectional longitudinal mode and one unidirectional longitudinal mode. The intensities are depicted with the same legend as in Figure 4.1. (b) Angles as a function of the scaled pump current, $\overline{\theta}_1$ (blue), $\overline{\theta}_2$ (red) and $\overline{\theta}_3$ (black).

4.4 Stability of Steady-State Solution 3: $\overline{\theta}_1 = 0,\ \overline{\theta}_2 = free,\ \overline{\theta}_3 = free$

In this section we will study the stability of the third steady-state solution, the one in which one longitudinal mode lases bidirectionally, while the other lases unidirectionally. In the previous chapter we have deduced a parametrised form of this solution, using ψ_2 as a parameter.

$$\overline{\theta}_1 = 0, \tag{4.85}$$

$$\overline{\psi}_1 = k\pi, \tag{4.86}$$

$$\overline{\theta}_2(\psi_2) = \arcsin\left(\frac{\alpha \sin\phi_{k2} + \cos\phi_{k2}}{\alpha\cos\phi_{k2} - \sin\phi_{k2}} \tan\psi_2\right), \tag{4.87}$$

$$\overline{\theta}_3 = -\arcsin\left(\frac{\frac{\Xi}{2}(\sigma_1 + \sin^2\overline{\theta}_2) + \Gamma + \cos\overline{\theta}_1\cos\overline{\psi}_1\cos\phi_{k1} - \cos\overline{\theta}_2\cos\psi_2\cos\phi_{k2}}{\sigma_2 + \frac{\Xi}{2}\sin^2\overline{\theta}_2 + \Gamma + \cos\overline{\theta}_1\cos\overline{\psi}_1\cos\phi_{k1} - \cos\overline{\theta}_2\cos\psi_2\cos\phi_{k2}}\right). \tag{4.88}$$

with

$$\Xi(\overline{\theta}_3, \psi_2) = 2\csc\overline{\theta}_2(\psi_2)\sec\overline{\theta}_2(\psi_2)\left[\sin\phi_{k2}\sin\psi_2 - \cos\phi_{k2}\cos\psi_2\sin\overline{\theta}_2(\psi_2)\right]. \tag{4.89}$$

When we fill in these values in the Jacobian, it splits up in a 2×2-matrix and a 3×3-matrix:

$$\begin{pmatrix} J_{11} & J_{12} & 0 & 0 & 0 \\ J_{21} & J_{22} & 0 & 0 & 0 \\ 0 & 0 & J_{33} & J_{34} & J_{35} \\ 0 & 0 & J_{43} & J_{44} & J_{45} \\ 0 & 0 & J_{53} & J_{54} & J_{55}. \end{pmatrix}, \tag{4.90}$$

with the expressions for J_{kl} being very elaborate. The first two eigenvalues can easily be found by calculating the 2×2-determinant corresponding to the first longitudinal mode. Their expressions are given by

$$\lambda_{1,2} = \frac{1}{2}\left(J_{11} + J_{22} \pm \sqrt{J_{11}^2 + 4J_{12}J_{22} + J_{22}^2}\right) \tag{4.91}$$

The eigenvalues of the 3×3-matrix are more difficult to find and therefore we will invoke the Routh-Hurwitz method [35–37]. This method allows, given the characteristic polynomial, to calculate the parameters for which the system becomes unstable. If the characteristic equation is given by

$$\lambda^n + b_1\lambda^{n-1} + ... + b_{n-1}\lambda + b_n = 0, \tag{4.92}$$

with λ the eigenvalues of an $n\times n$-matrix A, in our case the Jacobian, then the eigenvalues λ all have negative real parts if

$$\Delta_1 > 0,\ \Delta_2 > 0, ..., \Delta_n > 0, \tag{4.93}$$

where

$$\Delta_k = \begin{vmatrix} b_1 & 1 & 0 & 0 & 0 & 0 & \dots & 0 \\ b_3 & b_2 & b_1 & 1 & 0 & 0 & \dots & 0 \\ b_5 & b_4 & b_3 & b_2 & b_1 & 1 & \dots & 0 \\ \vdots & \vdots & \vdots & \vdots & \vdots & \vdots & \ddots & \vdots \\ b_{2k-1} & b_{2k-2} & b_{2k-3} & b_{2k-4} & b_{2k-5} & b_{2k-6} & \dots & b_k \end{vmatrix}. \tag{4.94}$$

In our case the characteristic polynomial, P, is given by

$$\begin{aligned} P = &-J_{35}J_{44}J_{53} + J_{34}J_{45}J_{53} + J_{35}J_{43}J_{54} - J_{33}J_{45}J_{54} - J_{34}J_{43}J_{55} + J_{33}J_{44}J_{55} \\ &+ (J_{34}J_{43} - J_{33}J_{44} + J_{35}J_{53} + J_{45}J_{54} - J_{33}J_{55} - J_{44}J_{55})\lambda + (J_{33} + J_{44} + J_{55})\lambda^2 - \lambda^3. \end{aligned} \tag{4.95}$$

Since this is a third order polynomial, we have to construct three determinants. The determinants are given by

$$\begin{aligned} \Delta_1 &= b_1 \\ &= -J_{33} - J_{44} - J_{55}, \end{aligned} \tag{4.96}$$

$$\begin{aligned} \Delta_2 &= \begin{vmatrix} b_1 & 1 \\ b_3 & b_2 \end{vmatrix} \\ &= J_{33}J_{34}J_{43} - J_{33}^2J_{44} + J_{34}J_{43}J_{44} - J_{33}J_{44}^2 + J_{33}J_{35}J_{53} + J_{34}J_{45}J_{53} + J_{35}J_{43}J_{54} + J_{44}J_{45}J_{54} \\ &\quad - J_{33}^2J_{55} - 2J_{33}J_{44}J_{55} - J_{44}^2J_{55} + J_{35}J_{53}J_{55} + J_{45}J_{54}J_{55} - J_{33}J_{55}^2 - J_{44}J_{55}^2, \end{aligned} \tag{4.97}$$

$$\begin{aligned} \Delta_3 &= \begin{vmatrix} b_1 & 1 & 0 \\ b_3 & b_2 & b_1 \\ b_5 & b_4 & b_3 \end{vmatrix} \\ &= (J_{35}J_{44}J_{53} - J_{34}J_{45}J_{53} - J_{35}J_{43}J_{54} + J_{33}J_{45}J_{54} + J_{34}J_{43}J_{55} - J_{33}J_{44}J_{55})\Big(J_{33}J_{34}J_{43} - J_{33}^2J_{44} \\ &\quad + J_{34}J_{43}J_{44} - J_{33}J_{44}^2 + J_{33}J_{35}J_{53} + J_{34}J_{45}J_{53} + J_{35}J_{43}J_{54} + J_{44}J_{45}J_{54} - J_{33}^2J_{55} - 2J_{33}J_{44}J_{55} \\ &\quad - J_{44}^2J_{55} + J_{35}J_{53}J_{55} + J_{45}J_{54}J_{55} - J_{33}J_{55}^2 - J_{44}J_{55}^2\Big). \end{aligned} \tag{4.98}$$

In principle, it would be enough to solve $\Delta_k = 0$ for $k = \{1, 2, 3\}$ to ψ_2. With the knowledge of ψ_2 we are able to calculate the currents for which the solution becomes unstable. However, these expression are far to tedious to write down here. The analytical form of the solutions is so complex that there is no easy interpretation possible. As an alternative, the stability will be checked numerically. Results are given in the next section, combined with a study of the most general case.

4.5 Stability of Steady-State Solution 4: $\overline{\theta}_1 = free$, $\overline{\theta}_2 = free$, $\overline{\theta}_3 = free$

In the previous chapter we have succeeded in writing down a general solution of the reduced multi mode model, using ψ_1 and ψ_2 as parameters. The expressions we found

were:

$$\overline{\theta}_1(\psi_1) = \arcsin\left(\frac{\alpha \sin\phi_{k1} + \cos\phi_{k1}}{\alpha\cos\phi_{k1} - \sin\phi_{k1}} \tan\psi_1\right), \tag{4.99}$$

$$\overline{\theta}_2(\psi_2) = \arcsin\left(\frac{\alpha \sin\phi_{k2} + \cos\phi_{k2}}{\alpha\cos\phi_{k2} - \sin\phi_{k2}} \tan\psi_2\right), \tag{4.100}$$

$$\sin\overline{\theta}_3 = g(\overline{\theta}_1, \overline{\theta}_2, \psi_1, \psi_2), \tag{4.101}$$

and

$$\sin\overline{\theta}_3 \left[f(\psi_2) + f(\psi_1)\right] - f(\psi_2) + f(\psi_1) = 0. \tag{4.102}$$

Since we have found an analytical expression for the Jacobian, Eq. (4.23), we can find numerically the values of ψ_1 and ψ_2 that fulfill Eq. (4.102). Once the ψ's are known, the numerical values of the $\overline{\theta}$'s are also known and the Jacobian and its eigenvalues can be calculated. If for every ψ_1-ψ_2 combination, every eigenvalue is checked, we can determine whether the solution is stable or unstable. The result is depicted in Figure 4.5.

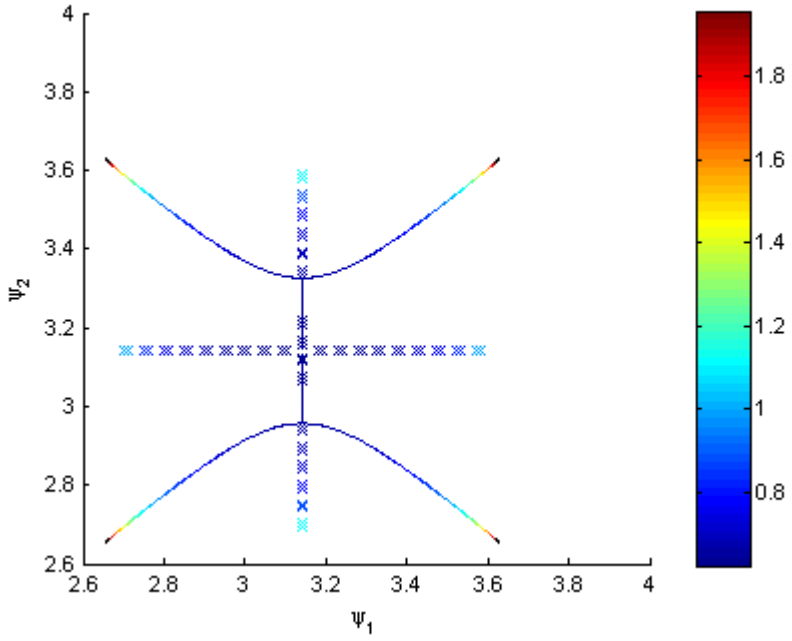

Figure 4.5: Numerically calculated solution of Eqs. (3.66) (3.70) as a function of parameters ψ_1 and ψ_2 and the current J. The current is depicted by using the colour code on the right hand side of the figure. The parameters are: $\alpha = 3.5$, $\phi_{k1} = \phi_{k2} = 0.8$, $\Gamma = 0.0455$, $\sigma_1 = 0$ and $\sigma_2 = -4$. Stable areas are denoted by a full line, while unstable areas are denotes by crosses.

In Figure 4.5, it is possible to predict the appearance of the P-I curve with corresponding parameters. At low currents, the bidirectional solutions are stable, with both psi_1 and ψ_2 equal to π. This solution is located in the origin of the ψ_1-ψ_2 plane. When we increase the current, we reach the oscillatory regime, which is not presented in this figure. At a certain point, mode 1 will return to the bidirectional solution, while mode 2 becomes unidirectional. This behaviour corresponds to the part of the vertical line that is full, hence stable. If the current is then even further increased, both modes become unidirectional, depicted in the form of the two branches.

Chapter 5

Conclusion and Outlook

In this work, we have studied semiconductor ring lasers. These devices consist of a circular cavity and a straight output coupler, implying that two counter-propagating modes can be present in the resonator simultaneously. These modes are linearly coupled due to backscattering and nonlinearly due to saturation effects. Moreover, there can be different longitudinal modes, which saturate each other's gain. Semiconductor ring lasers are suitable candidates for monolithic integration of photonic devices and they are particularly usable for optic switching.
We have described the construction and physical operation of the ring resonators and their output couplers. Rate equations have been deduced for the single mode case, using a combination of a classical and a quantum mechanical approach. Furthermore, we have applied the mean-field approximation, assuming that one roundtrip in the cavity hardly changes the electromagnetic fields. Because a semiconductor ring laser allows for more than one longitudinal mode in the cavity, a multimode representation is desired. Therefore, the equations have been extended to the multimode case, assuming that the longitudinal modes have frequencies close to one another. Subsequently, several processes have been added phenomenologically, such as the saturation of a mode by influence of its counter-propagating counterpart and by other longitudinal modes. Next, the equations have been nondimensionalised using an approach similar to the one used in Ref. [18]. This result contains the expressions that form the base of our study of the multimode model. Starting from nine real equations describing the model, we have succeeded in reducing this to only five. The obtained model no longer includes fast dynamics such as relaxation oscillations. A new representation has been invoked, making use of angles to describe the relative distribution of the power over the several modes. This new way of representing the intensities is not just for aesthetic reasons, but enables us to use a numerically stable integration procedure. Since the full description of this reduced model is somewhat complicated, we have continued the work with a simplified model, that describes all saturation effects with two coefficients.
Finally, a stability analysis has been performed, enabling us to describe analytically the majority of the bifurcation points found in the P-I curve of the multimode ring laser. The established analytical description can be used to describe switches between two

longitudinal modes and can thus be an important tool to study the control mechanisms of this behaviour.

A first important future perspective is establishing a link between the derived model and experimental results. Some results have been obtained in the meanwhile by Verschaffelt *et al.* [38] at the TONA department. In their experimental set-ups, it has been observed that when the laser switches from one longitudinal mode to another, sometimes not only the frequency of the dominant mode changes, but also the direction of propagation. Since the model is able to indicate which steady-state solution is stable at a given current range, it would in principle be possible to explain the observed phenomena. By performing a fit between experimental data and the model, certain parameters can be estimated and subsequently be used to predict the dynamical behaviour of the semiconductor ring laser.

There are several interesting properties and effects that still have to be investigated in the domain of ring lasers and especially in the multimode case. A first improvement of the model is to add more longitudinal modes to the cavity. It is known that the gain spectrum is asymmetric, i.e., when we have a central mode, one of its side modes will experience a higher gain than its equivalent mirrored around the centre frequency. When, due to a current change, the gain spectrum shifts for a small amount, other modes may become the dominant ones. The asymmetry of the gain spectrum makes predicting which mode would be the dominant one somewhat more complicated. To describe this effect accurately, four longitudinal modes should be taken into account, because whenever three different wavelengths interact, photons of a fourth wavelength are created due to scattering of the incident photons, because of four-wave mixing.
So far we have not included a carrier grating. When two counter-propagating modes are present in a cavity, a standing wave pattern is formed, such that in some places there is more recombination than in others. Since the carriers are used more intensively in some places, a carrier grating can be formed. In the single mode case, the two counter-propagating modes have the same frequency and the carrier grating is very fast in spatial terms. Because of diffusion, the carriers will immediately fill up the area where there is a shortage and the grating disappears. However, in the multimode situation, the counter-propagating modes do not have the same frequency and a slight frequency splitting exists. The spatial frequency of standing wave pattern will be of the order of the beat length, hence much smaller. This time the grating cannot be destroyed by diffusion and could have a significant effect on the ring laser dynamics.
Another effect is that in semiconductor ring lasers, the carriers tend to gather at the outer rim of the cavity. A possible way to force them to stay where they are, is by integrating quantum dots (QDs) into the structure. QDs are semiconductor nanostructures that confine the movement of the carriers in all three dimensions [39]. They are implanted into the quantum well of the semiconductor ring laser in one or multiple layers. The presence of the QDs can have a significant effect on the dynamics of the system [40–45]. Not only the dynamics described in this thesis work play a role in the system, but some extra processes then have to be taken into account. There will be a carrier exchange

between the wetting layer, a layer formed on top of the quantum well layer, and the dots. In the dots themselves, there are ground states and excited states, with extra dynamics as a consequence. In theory, all dots can be equal in size, but in reality, there will be groups or families with more or less the same shape and size. Because of the fact that in one laser there will be different families of dots, the laser will operate in multimode. Indeed, a certain dot geometry will provide certain energy states available for optical transitions. If we wish to implement QDs in the present multimode model, one equation will no longer be enough to describe the carrier density. Different families of dots means different carrier reservoirs, hence we need to describe the carrier evolution in each reservoir. It was already mentioned in chapter 3 that the differential gain factor in the rate equations can vary with the pump current. Hence, this is something that still has to be included in the model.

References

[1] A. Einstein, "Zur quantentheorie der strahlung," *Physik. Zeitschr.* **18**, p. 121, 1917.

[2] D. ter Haar, *The old quantum theory*, Pergamon Press, New York, 1967.

[3] N. Basov and A. Prokorov, "3-level gas oscillator," *Zh. Eksp. Teor. Fiz.* **27**, p. 431, 1954.

[4] A. Schwalow and C. Townes, "Infrared and optical masers," *Phys. Rev.* **112**, p. 1940, 1958.

[5] T. Maiman, "Stimulated optical radiation in ruby," *Nature* **187**, p. 493, 1960.

[6] Z. Alferov, "Nobel lecture: The double heterostructure concept and its applications in physics, electronics, and technology," *Rev. Mod. Phys.* **73**, p. 767, 2001.

[7] H. Kroemer, "A proposed class of heterojunction injection lasers," *Proc. IEEE* **51**, p. 1782, 1963.

[8] University of Cambridge, "Introduction to semiconductors." `http://www.doitpoms.ac.uk/tlplib/semiconductors/printall.php`, [cited at 2 April 2008]. *University of Cambridge [Online].*

[9] University of Cambridge, "Light-emitting diodes." `http://www.lightemittingdiodes.org`, [cited at 2 April 2008]. *University of Cambridge [Online].*

[10] G. Griffel, "Synthesis of optical filters using ring resonator arrays," *Photon. Technol. Lett.* **12**, p. 810, 2000.

[11] H. Han, D. Forbes, and J. Coleman, "InGaAs-AlGaAs-GaAs strained-layer quantum-well heterostructuresquare ring lasers," *IEEE J. Quantum Electron.* **31**, p. 1994, 1995.

[12] C. Ji, M. Leary, and J. Ballantyne, "Long-wavelength triangular ring laser," *Photon. Technol. Lett.* **9**, p. 1469, 1997.

[13] L. Bach, "Wavelength stabilized single-mode lasers by coupled micro-square resonators," *Photon. Technol. Lett.* **15**, p. 377, 2003.

[14] H. Cao and M. Osinski, "Large s-section-ring-cavity diode lasers: directional switching, electrical diagnostics, and mode beating spectra," *Photon. Technol. Lett.* **17**, p. 282, 2005.

[15] M. Hill, "A fast low-power optical memory based on coupled micro-ring lasers," *Nature* **432**, p. 206, 2004.

[16] A. Liao and S. Wang, "Semiconductor injection lasers with a circular resonator," *Appl. Phys. Lett.* **36**, p. 801, 1980.

[17] Z. Wang, G. Verschaffelt, Y. Shu, G. Mezosi, M. Sorel, J. Danckaert, and S. Yu, "Integrated small-sized semiconductor micro-ring laser with novel retro-reflector cavity," *Photon. Technol. Lett.* **20**, p. 99, 2008.

[18] M. Sorel, G. Giuliani, R. M. A. Scirè, S. Donati, and P. Laybourn, "Operating regimes of GaAs-AlGaAs semiconductor ring lasers: experiment and model," *IEEE J. Quantum Electron.* **39**, p. 1187, 2003.

[19] T. Krauss, R. D. L. Rue, P. Laybourn, B. Vogele, and C. Stanley, "Efficient semiconductor ring lasers made by a simple self-aligned fabrication process," *IEEE J. Quantum Electron.* **1**, p. 757, 1995.

[20] G. Griffel, J. Abeles, R. Menna, A. Braun, J. Connolly, and M. King, "Low threshold InGaAsP ring laser fabricated using bi-level dry etching," *Photon. Technol. Lett.* **12**, p. 146, 2000.

[21] S. H. Strogatz, *Nonlinear Dynamics and Chaos*, Perseus Books, Jackson (TN), 1994.

[22] L. A. Coldren and S. Corzine, *Diode Lasers and Photonic Integrated Circuits*, Wiley, New York, 1995.

[23] R. Lang and K. Kobayashi, "External optical feedback effects on semiconductor injection laser properties," *IEEE J. Quantum Electron.* **16**, p. 347, 1980.

[24] G. van Tartwijk, "Semiconductor lasers with optical injection and feedback," *Quantum Semiclass. Opt.* **7**, p. 87, 1995.

[25] G. Verschaffelt, Z. Wang, Y. Shu, G. Mezosi, J. Danckaert, M. Sorel, and S. Yu, "High-speed integrated semiconductor micro-ring lasers with efficient off-axis parabolic reflectors," in *Semiconductor Lasers and Laser Dynamics III*, **6997**, SPIE, 2008.

[26] M. Born and E. Wolf, *Principles of Optics*, Pergamon, Oxford, 1980.

[27] P. Tassin, "A Contribution to Nonlinear Optics with Left-Handed Materials," Master's thesis, Vrije Universiteit Brussel, Brussels, 2005.

[28] H. Haken and H. Sauermann, "Nonlinear interactions of laser modes," *Z. Phys.* **173**, p. 261, 1963.

[29] W. Lamb Jr., "Theory of an optical maser," *Phys. Rev.* **134**, p. A1429, 1964.

[30] M. Sargent III, M. Scully, and W. L. Jr., *Laser physics*, Addison-Wesley, Reading (Mass.), 1974.

[31] F. Arecchi, G. Lippi, G. Puccioni, and J. Tredicce, "Deterministic chaos in laser with injected signal," *Opt. Commun.* **51**, p. 308, 1984.

[32] M. S. Miguel, Q. Feng, and J. Moloney, "Light-polarization dynamics in surface-emitting semiconductor lasers," *Phys. Rev. A* **52**, p. 1728, 1995.

[33] G. Morthier, *High speed photonic components*, Ghent University, Ghent, 2007.

[34] G. Van der Sande, L. Gelens, P. Tassin, A. Scirè, and J. Danckaert, "Two-dimensional phase-space analysis and bifurcation study of the dynamical behavior of a semiconductor ring laser," *J. Phys. B: At. Mol. Opt. Phys.* **41**, p. 8, 2008.

[35] Wolfram Mathworld, "Routh-hurwitz theorem." `http://mathworld.wolfram.com/Routh-HurwitzTheorem.html`, [cited at 2 April 2008]. *Wolfram Mathworld [Online]*.

[36] F. Gantmacher, *Applications of the Theory of Matrices*, Wiley, New York, 1959.

[37] I. S. Gradshteyn and I. Ryzhik, *Tables of Integrals, Series, and Products, 6th ed.*, Academic Press, San Diego (CA), 2000.

[38] G. Verschaffelt, S. Beri, L. Gelens, G. Van der Sande, and J. Danckaert, "VUB activity report," 2008.

[39] D. Bimberg, M. Grundmann, and N. N. Ledentsov, *Quantum Dot Heterostructures*, Wiley, New York, 1999.

[40] A. Markus, J. X. Chen, O. Gauthier-Lafaye, J.-G. Provost, C. Paranthoën, and A. Fiore, "Impact if intraband relaxation on the performance of a quantum dot laser," *IEEE J. Quantum Electron.* **9**, p. 1308, 2003.

[41] H. Koskenvaara, J. Riikonen, J. Sormunen, M. Sopanen, and H. Lipsanen, "Carrier dynamics in strain-induced InGaAsP/InP quantum dots," *Physica E* **32**, p. 179, 2006.

[42] S. Anantathanasarn, R. Nötzel, P. van Veldhoven, F. van Otten, T. Eijkemans, and J. Wolter, "Stacking and polarization control of wavelength-tunable (1.55 μm region) InAs/InGaAsP/InP (100) quantum dots," *Appl. Phys. Lett.* **88**, 2006.

[43] Y. Tanguy, J. Houlihan, G. Huyet, E. A. Viktorov, and P. Mandel, "Synchronization and clustering in a multimode quantum dot laser," *Phys. Rev. Lett.* **96**, 2006.

[44] S. Melnik, G. Huyet, and A. V.Uskov, "The linewidth enhancement factor α of quantum dot semiconductor lasers," *Opt. Expr.* **14**, p. 2950, 2006.

[45] E. A. Viktorov, P. Mandel, I. O'Driscoll, O. Carrol, G. Huyet, J. Houlihan, and Y. Tanguy, "Low-frequency fluctuations in two-state quantum dot lasers," *Opt. Lett.* **31**, p. 2302, 2006.